A Thesis

entitled

"A STUDY OF SMALL PARTICLES IN THE

NEIGHBOURHOOD OF THE MELTING POINT"

by

Muhammad Sajedur Rahman

Submitted for the

Degree of Doctor of Philosophy

of the

University of London

Imperial College of Science and Technology

London

<u>1976</u>

ABSTRACT

The melting of small particles of bismuth and tin has been studied, in situ, in an electron microscope. A special technique has been used to measure the specimen temperatures accurately.

The melting of bismuth crystallites was investigated on amorphous carbon, and molybdenite substrates. A platelet form and a polyhedral form of crystallite obtained on the carbon substrates, both exhibited a time delay phenomenon before melting (as also observed by Peppiatt, 1973, 1975). The time delay of the polyhedral particles obtained in an initial solid deposit decreased to zero as the sizes of the particles increased beyond 1400 $\overset{o}{A}$. Under certain conditions, it was found that the characteristic time of melting of the polyhedral particles obtained by recrystallizing the liquid layers, varied inversely as the surface area of the particles. On the molybdenite substrates, needle-like platelets were obtained, which also exhibited the time delay phenomenon in melting. For the crystallites on both substrates, the time delay was found to be a well-defined function of temperature.

The melting of tin crystallites was investigated mainly using carbon substrates, but also in a few experiments using molybdenite and graphite substrates. The crystallites were in the form of thin platelets having a variety of shapes. In this case, no time delay for the melting of the platelets was observed. The melting point of the platelets was found to decrease with decreasing

ABSTRACT (Contd.)

platelet thickness.   By using a liquid skin melting model,
a value of 70 ± 7 ergs cm^{-2} has been obtained for the
solid/liquid interfacial energy $(\gamma_{s\ell})$ of tin.

Other properties of small particles of bismuth and
tin investigated were:

1. The amount of supercooling in the liquid droplets
of bismuth and tin on carbon, molybdenite and graphite
substrates.

2. An anomalous behaviour of tin platelets close to
the melting point;   these showed a sudden change of shape
though remaining solid - a phenomenon previously observed
for bismuth crystallites.

INDEX

INDEX   (contd.)

INDEX   (contd.)

INDEX (contd.)

INDEX (contd.)

INDEX (contd.)

CHAPTER 1

INTRODUCTION

1.1. Melting

1.1.1. Melting as a Surface Phenomenon,

The phenomenon of melting by which a substance changes from the solid to the liquid phase at a reproducible and well-defined temperature is one of the best known of phase transformations. The sharpness of the melting temperature for a pure substance has made its use invaluable in highly accurate standardisation of temperatures and also in chemistry as a test of purity of substances. This is in contrast to the reverse process of solidification which may occur at widely differing temperatures due to the phenomenon of supercooling. Although melting is a well-known occurrence, the actual mechanism of melting is far from being clearly understood. This apparently simple phenomenon has caused many theoreticians to postulate correspondingly simple mechanisms. The majority of these however, consider only the properties of the solid in determining the temperature at which the crystal lattice becomes absolutely unstable (see, for example, the theories of Lindemann, 1910; Born, 1939; Lennard-Jones and Devonshire, 1939; Kuhlmann-Wilsdorf, 1965; Vladimirov, 1969; Cotterill and Pederson, 1972; Jensen et al., 1973). While these models describe properties of melting which are either thermodynamic (such as volume change) or statistical (loss of long range order during the phase transformation), they do not consider either the kinetics of melting, that is, the mechanism by

which the melting interface moves into the solid, or the

importance of the initial nucleation of the liquid.

Experimental evidence (described below) indicates that melting

involves nucleation, in particular on crystal surfaces.

Above the melting point, the liquid phase has a lower free

energy than the solid. Therefore, once the liquid has

nucleated at suitable sites, the solid/liquid interface is

able to move through the remaining solid as this results in

a progressive lowering of the free energy of the system.

The importance of the crystal surface in melting

was recognised by Tammann (1909-10), who carried out

experiments on the rates of melting and crystallisation of

organic crystals. He suggested that melting and solidification

were reverse processes, and therefore that the properties of

the two should be very similar. Solidification is

essentially a surface phenomenon, the solid/liquid interface

moving into the melt; therefore melting should also be a

surface phenomenon. In his book "States of Aggregation"

Tammann (1925) states, "Melting takes place on the surface

of a crystal in a uniform manner..,..." His view that

melting process starts at the crystal surface has some

supporting evidence. For example, when a suitable impurity

is added to the melt of a solid/liquid system which is

in equilibrium, the solid immediately dissolves in the melt

(see, for example, Block et al., 1931).

Cormia et al. (1963) and Ainslie et al. (1961) showed

that bulk quartz and phosphorous pentoxide (P_2O_5) crystals could be superheated by 300 and 50K respectively, due to the slow propagation of the viscous molten interface into these solids. Melting was found to begin on the surface of the crystals, in particular at emerging dislocations or imperfections. The melt would then propagate into the bulk solid. In order to avoid nucleation of the melt at the surface, Khaikin and Benet (1939) heated the inside of a tin single crystal while keeping the surface cool. This resulted in the superheating of the solid core. They explained the results in terms of the absence of "centres of fusion" inside good crystals, which, they state are always present at the surface of a crystal. Volmer and Schmidt (1937) observed, during their melting experiments on carefully grown single crystals of gallium, that melting always started at isolated points on the surface. They interpreted this as being due to local impurities which had induced strains and become centres of defects, resulting in a lowering of melting point in these regions. They also found that well-formed crystal faces rarely produced these initial melting regions. Irregularities, especially edges along definite crystallographic directions were often observed where the liquid appeared. They state, "......melting is not disintegration of the lattice, but starts at favoured positions". Stranski et al. (1963) have taken the same view as Tammann (1909-10) and considered melting as the dissolution of a solid in its own melt. They consider melting as a

function of crystal surfaces; they postulate that melting
is initiated on high index crystallographic faces, the low
index faces being stable at all temperatures to the melting
point.

Burton et al.(1951) have calculated a "transition
temperature" of the order of one-half of the melting point,
for the surfaces of simple cubic crystals. This they
interpreted as a form of "surface melting". Stark (1965)
has postulated that "vacancy concentration" at the surface
builds up faster than in the bulk; when a critical
concentration of vacancies is reached, melting
is nucleated at the surface. A few workers have attempted
experimental observations of surface melting of crystals at
temperatures below the bulk melting point. However their
results are conflicting. Pavlovska and Nenow (1971) claim
to have observed surface melting (below the bulk melting
point) in diphenyl. However, low-energy electron diffraction
(LEED) studies of Goodman and Somorjai (1970) on the melting
of low-index faces of single crystals of bismuth, lead and
tin, they say indicated no surface melting. The different
surfaces seemed to disorder at the respective bulk melting
temperature. Henrion and Rhead (1972), in similar LEED
investigations of lead overlayers on copper, claimed to have
observed a order-disorder transformation in the layers at
temperatures close to, but below the bulk melting point,
While ascribing this as a two-dimensional order-disorder.

transformation, they also suggest it to be surface melting, by analogy with the behaviour of three dimensional crystals. However, the importance of the Henrion and Rhead work is not the reduction in melting point (which would be expected for a monolayer), but the fact that the solid diffraction pattern could be seen "through" the liquid, thus casting doubts on the conclusions of Goodman and Somorjai.

The conclusions arrived at in the present work do not come from a study of the surfaces of crystal (such as, for example, low- or high- energy electron diffraction), but from observations of the effects caused by the presence of the surface. A study has been made of small crystallites in the neighbourhood of the melting point. Small particles have large surface area relative to their volume, as compared to bulk specimens. The influence of this surface on the melting properties of the small particles has been investigated.

1.1.2. The Melting of Small Particles.

For small particles of a size suitable for viewing in the electron microscope, the amount of surface free energy associated with each partice is significant. As the volume terms are proportional to the cube of the linear dimension and the surface terms are proportional to the square, the influence of the surface is greater the smaller the particle. The significance of the surface energy for small

particles has been observed in several ways. For example,
it is well-known (see, for example, Hollomon and Turnbull,
1950) that liquids can be cooled considerably below the
melting point before solidification begins; in this the
formation of a small nucleus of the stable solid phase is
hindered by an energy barrier due to the surface energy. Also
Sambles (1971) in a test of the Kelvin equation which by
considering the effect of surface energy, relates the vapour
pressure of a particle to its size, found a substantial
increase in the vapour pressure for microscopic particles.

The dependence of the phase equilibrium of a one
component system on the size of one of the phases was first
suggested by Thomson (1888) with reference to the solubility
of small particles. Kürster (1906) predicted that the
melting point of a material is lowered with a reduction in
grain size, and, a few years later, Pawlow (1908-9, 1909)
obtained an equation relating this lowering of the melting
point to the radius of the solid particle which he assumed
to be spherical. His theoretical conception of the lowering
of melting point was later extended by Hanszen (1960).

The first experimental measurements on the melting
point of small particles were carried out by Takagi (1954).
She used an electron diffraction technique to determine when,
upon heating, layers of bismuth, tin and lead changed from
the solid to the liquid state; the melting point was
determined as the temperature at which the sharp crystalline

rings changed into the diffuse halos of the liquid. However, the particle sizes were deduced indirectly and are, therefore subject to large error. Blackman and Curzon (1959) (see also, Curzon, 1960) observed the melting point of small particles of tin by the electron diffraction technique which combined with a subsequent electron microscopic study of the particle sizes gave the variation of melting temperature with particle radius. A similar method was later used by Wronski (1967) again using particles of tin; Coombes (1969, 1972) with bismuth, lead and indium; Gladkich et al.(1966) with copper, silver, aluminium and germanium; and Boiko et al. (1969) with indium. The electron diffraction technique has the advantage that good diffraction patterns are more easily obtained than, for example, by x-ray diffraction. It also has an advantage over a direct electron microscope method, as the beam heating of the specimen is negligibly small. Another advantage is that as very small particles with correspondingly large changes in melting point are observed, the temperature control does not need to be highly accurate. This method can be used with particles ranging in size from a few tens, to upto, 1,000$\overset{o}{A}$.

However, the electron diffraction technique has several disadvantages. It necessarily involves an averaging of the particle size over an entire specimen; only the temperature at which a proportion of the number of particles present have melted could be determined. Clearly because the

particles were not of a uniform size the melting point is not
the same for all particles; the choice of a particle size to
correspond to the measured melting temperature was therefore
to some extent arbitrary.   Also, if there were an additional
effect, such as shape or strain effects in the particles
which may influence the melting point, these could not be
detected and the results would accordingly be in error.   To
obtain more information, it is therefore necessary to observe
the melting point of individual particles rather than complete
layers.

Pocza et al.(1969) seem to be the first to have
observed the melting of individual particles.   Using a
selected area diffraction pattern in an electron microscope,
they monitored the melting of a few particles of indium within
the area of the fine electron beam, in a residual vacuum
of 2×10^{-9} torr.   Their temperature measurements, however,
may be considerably more inaccurate than they suggest due to
the electron beam heating (see Gale and Hale, 1961).   Hanszen
(1966) observed, again using the diffraction pattern, the
melting of layers of bismuth in an electron microscope in
a residual vacuum of 10^{-4} torr.   His results, which were
purely qualitative, showed that each deposit melted over a
range of temperature.   Hanszen vaguely ascribed this to a
size effect.   Also his temperature measurements are again
greatly in error due to the heating effect of the electron
beam.   Stowell et al.(1970) also observed the melting by
diffraction pattern of thin layers of lead, evaporated

"in situ" in an electron microscope.   They state that 'the
deposits did not melt completely at one temperature, so a
dependence of the melting point on size may be inferred, but
there was not a good correlation of the melting point with
size'.

The experiments of Sambles (1971) on the melting of
small particles of gold in an electron microscope are the
first in which the problem of electron beam heating was
overcome.   While studying the rate of evaporation of gold
particles, he noticed that for some particles, the
evaporation rate altered abruptly, giving rise to a
discontinuity ('kink') in the particle radius versus time
graph.   He interpreted this as due to the melting of the
gold particle at this radius, the kink being caused by a
difference in the evaporation coefficients of the solid and
liquid.   As the temperature of the particle was known
accurately from the evaporation rate at a large radius, he
obtained a plot of particle size against melting point for
radii between 50Å and 400Å.

Although the above method could be applied successfully
to the melting of gold which has a high vapour pressure at
the melting point, it is, however, not applicable to materials
with a low vapour pressure at the melting point.   Clearly
for such materials the evaporation rate would not be appreciable
until the materials have melted.   Sambles (see Blackman et al,
1972) subsequently developed an ingenious method to study

the melting of small particles in an electron microscope

overcoming the problem of electron beam heating.   This method

employed the fact that small particles if uncontaminated can

in general be supercooled by over a hundred degrees.   In

this method a specimen layer was heated in the absence of

the electron beam, to a temperature at which some particles

are expected to melt.   The layer was then cooled by about

50K and the electron beam could then be switched on for

observation.   As the specimen temperature could be determined

by a carefully constructed heater/thermocouple arrangement

(while the electron beam is switched off), the experimental

temperature will be accurate within the accuracy ($\pm$ 1K) of the

thermocouple calibration.   This method has previously been

used by Peppiatt (1973, 1975) and Peppiatt and Sambles

(1975) to study the melting of individual particles of

bismuth and lead.   In the present work, it has been applied

to study the melting of small particles of bismuth and tin.

Various other methods have been used to investigate

the variation of melting point with size.   Fujiki and

Suganuma (1953) studied optical properties of thin films of

bismuth during heating and report a "structure loosening",

temperature for bismuth.   This was probably a rearrangement

of the solid film (see Lisgarten et al, 1974, see also,

Peppiatt, 1973), rather than melting.   Palatnik and Komnik

(1960) used a similar optical method to study the melting

point of thin layers of tin and bismuth.   However, no attempt

was made to examine the actual nature of the deposits using
a replica or stripping technique with electron microscopy;
rather the sizes of the crystallites were inferred from the
mean thickness of the deposit and certain doubtful assumptions
concerning the mode of growth of the films - see the comments
of Fisher (1967) and Fisher and Anderson (1968).   Petrov
(1965) investigated the melting of small particles of bismuth,
antimony and lead using an x-ray analogue of the electron
diffraction method.   The particles were suspended in varnish
for irradiation and therefore the results could be
influenced by contamination, and pressure effects (as the
melting is at constant volume).

1.2   The Melting of Small Particles of Bismuth

The melting of thin layers of bismuth was first
carried out by Takagi (1954), by using the electron
diffraction technique in reflection.   The bismuth layers
were deposited on the cleavage faces of single crystals of
zinc blende, galena, molybdenite and silicon carbide.   She
quotes a depression from the bulk melting point (544K) of
23K for a film of mean thickness 50Å with a corresponding
particle radius of 39Å.   The thickness was estimated from
the amount of material evaporated and the particle radius
from supercooling data, and therefore neither are very
accurate.   Also the shapes of the particles were not known.
Hanszen (1966) investigated the melting of thin layers of

bismuth, deposited on a thin carbon film "in situ" in an electron microscope. He observed the morphology of the layers between successive melting and recognised the melting point using the diffraction pattern. His results are mostly qualitative and his temperature measurements are probably greatly in error due to the effect of electron beam heating of the specimen.

Coombes (1969) performed detailed experiments on the melting of small particles of bismuth. He used the electron diffraction technique in transmission and obtained an estimate of the particle size from the transmission electron micrographs of the specimens. By using a carefully constructed furnace, he determined temperatures to within a degree. He found that the bismuth particles with radius between ~150$\overset{o}{A}$ and 250$\overset{o}{A}$ in the initial deposit could often be superheated upto 10K above the bulk melting point before melting was complete (figure 1.2.1.). He also found that particles of greater than 100$\overset{o}{A}$ radius formed by resolidifying liquid droplets, to melt close to, but not above the bulk melting point. In both cases, the melting point decreased with particle sizes below 100$\overset{o}{A}$ radius. Peppiatt (1973) repeated part of Coombes experiments by using the same electron diffraction technique, and confirmed the results obtained by Coombes.

Peppiatt (1973,1975)(see also, Peppiatt and Sambles, 1975) in addition to his work on lead, also carried out

Particle Radius (Å)
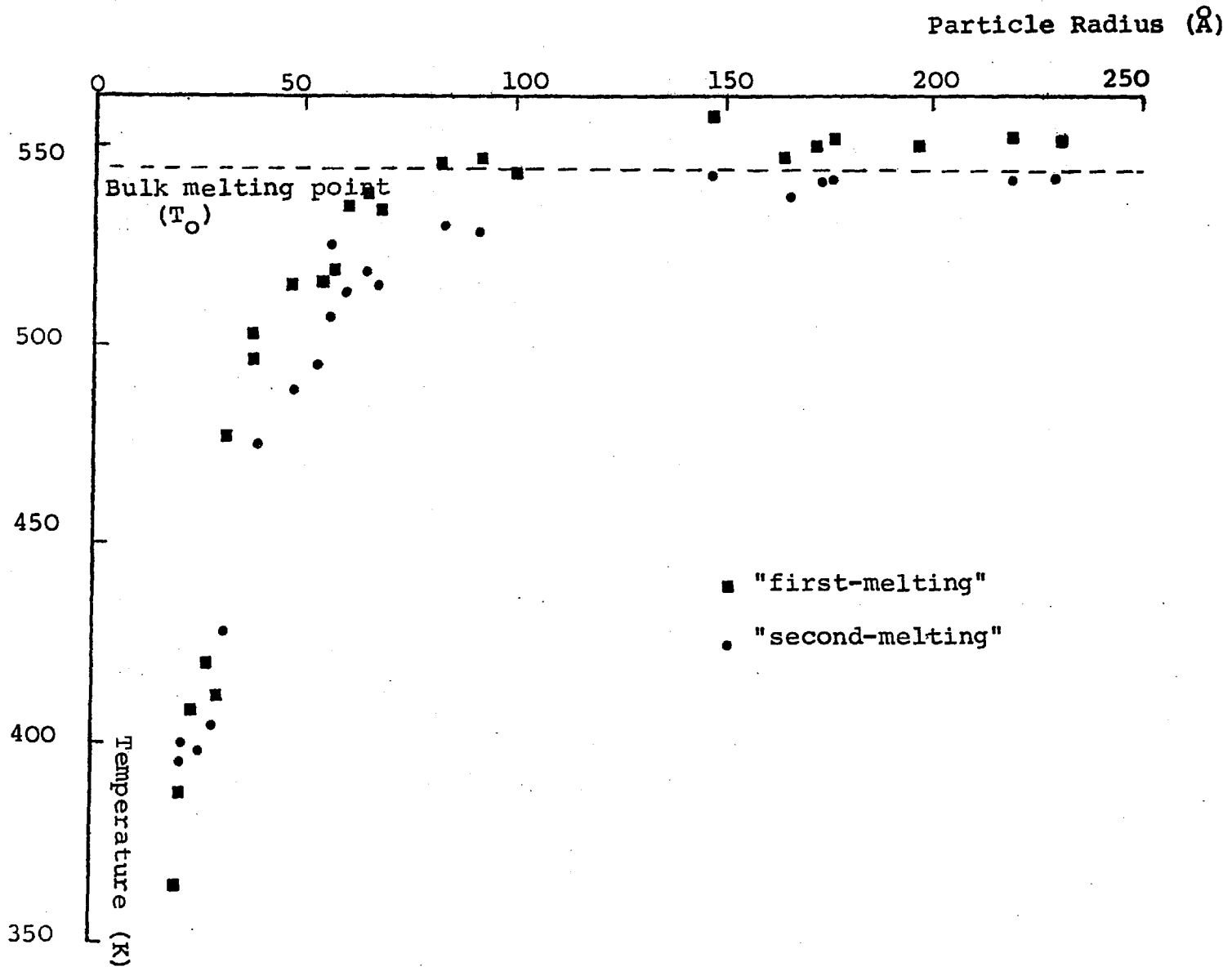
FIGURE 1.2.1.

The variation of melting point with size for small
particles of bismuth (Coombes, 1969).

experiments on the melting of individual particles of bismuth,
"in situ" in an electron microscope, in a residual vacuum
of $\sim 5 \times 10^{-7}$ torr.   Thin films of amorphous carbon were used
as substrates.   The specimen temperatures were measured by
the method devised by Sambles, as described previously.   He
obtained three types of bismuth particles and classified them
according to their morphology and origin as follows.

(i) Platelet (Type I) particles:

These were thin crystallites, formed by heating
bismuth film of the order of 100Å thick.   They all had six
sides, containing angles of 120°, but otherwise their shapes
ranged from elongated to regular hexagons (figure 1.2.2a).

(ii) Polyhedra (Type II) particles:

These were the regular hexagonal particles, obtained
by melting and resolidifying the above platelet type particles.
Apart from the faceting, these crystallites were roughly
spherical in shape (figure 1.2.2b.).

(iii) Polyhedra (Type III) particles:

These particles were obtained by resolidifying the
liquid droplets formed by depositing the layers as liquid.
They were similar in appearance to the above polyhedra type
particles (figure 1.2.2c).   Their melting properties, however,
differed from the polyhedra (Type II) particles.

The most striking effect observed by Peppiatt in the
melting of the above types of particles, was the presence of

(a)   Platelet   (type I).

0.4 μm
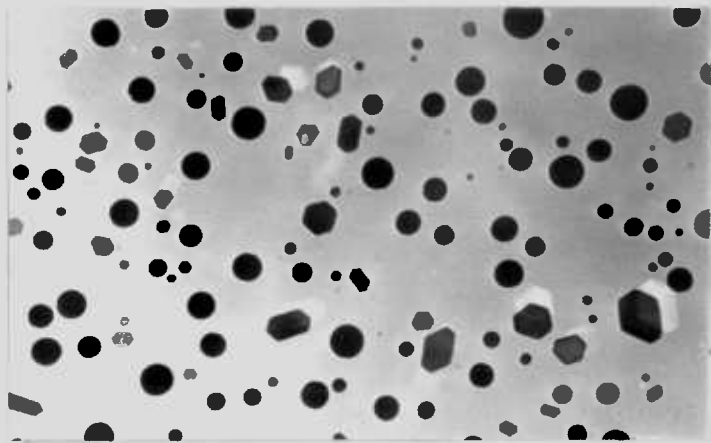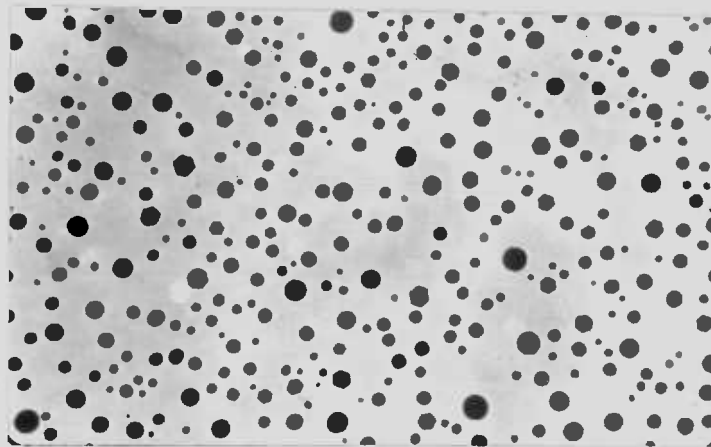
(b)   Polyhedra   (type II).
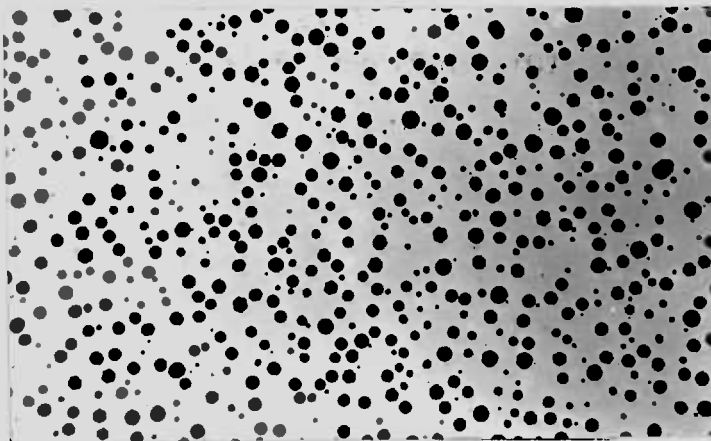
(c)   Polyhedra   (type III).

FIGURE 1.2.2.

The three types of bismuth particles, and liquid droplets on carbon substrate.   (Peppiatt, 1973).

a time delay in melting: when an aggregate of crystallites
was heated to the same temperature several times (being
cooled for observation between each period), it was observed
that a number of solid particles melted on each occasion.
If each particle had a definite melting temperature, none
would be expected to melt after the first heating. An
example of this from a typical experiment on platelet (type I)
particles, is shown in figure (1.2.3.). In this, the
fraction of particles remaining solid ($\frac{N}{N_O}$), where N_O is the
initial number of solid particles, has been plotted on a
logarithmic scale against the total time (t) that the specimen
was maintained at a given temperature. The later stages of
each experiment generally showed a good exponential decay in
the number of particles remaining solid; the initial melting
rate was often found higher than the final constant value as
seen in the curvature of the graphs (see figure 1.2.3.). The
linear portion of the graphs could be represented by the
equation

$$N = N_O \exp \left(- \frac{t}{\tau} \right)$$

where τ is the characteristic time of melting. Peppiatt
found that the characteristic time was a fairly well-defined
function of temperature within experimental error; also the
results for the three types of particles were found to be
distinctly different (figure 1.2.4.). In particular, the
platelet (type I) form had a sufficiently large time delay
even above the bulk melting point, to cause some of these
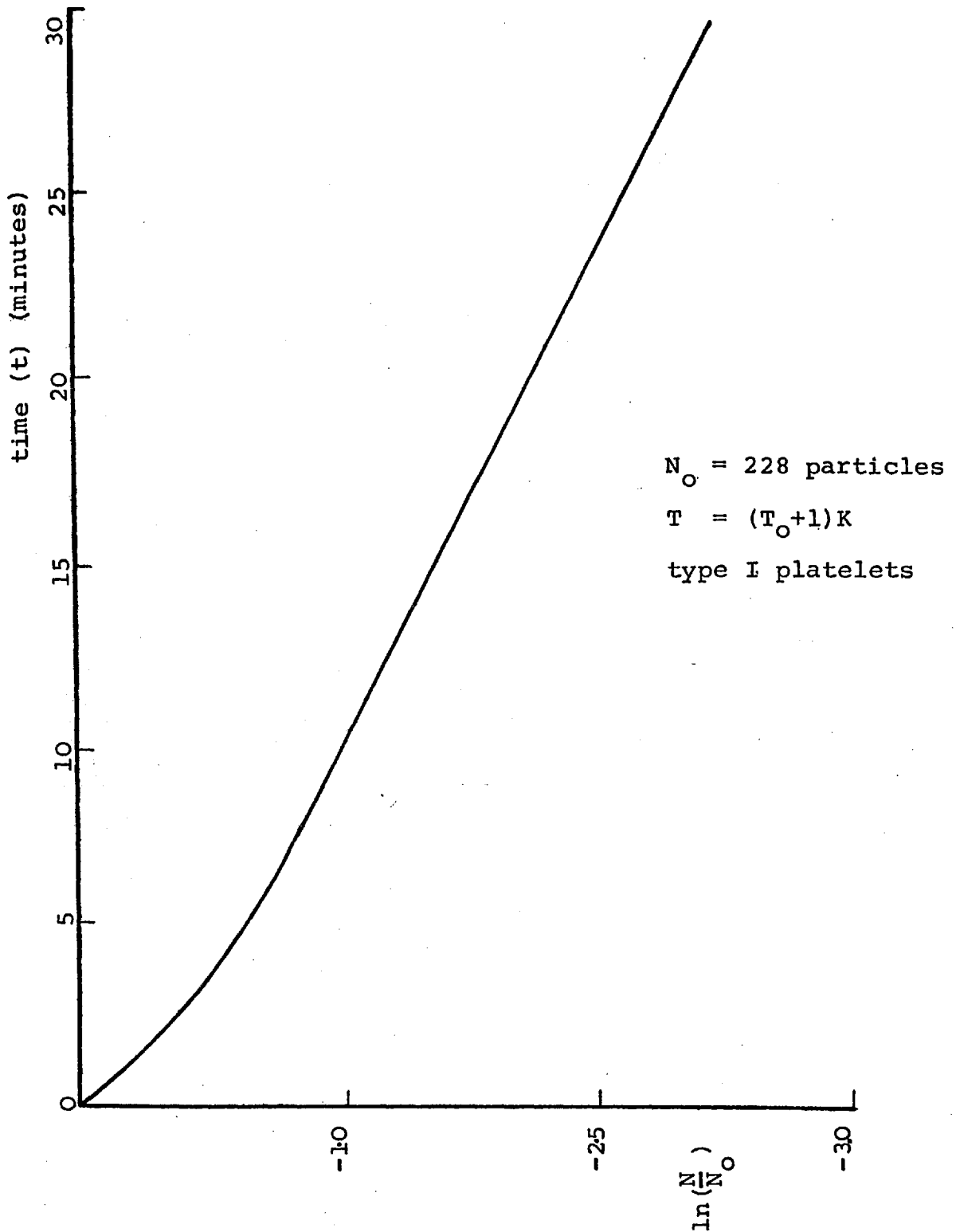
FIGURE   1.2.3.

Graph showing the variation in the number of bismuth type I
platelets remaining solid (N) with time (t), plotted on a
logarithmic scale (Peppiatt, 1973).
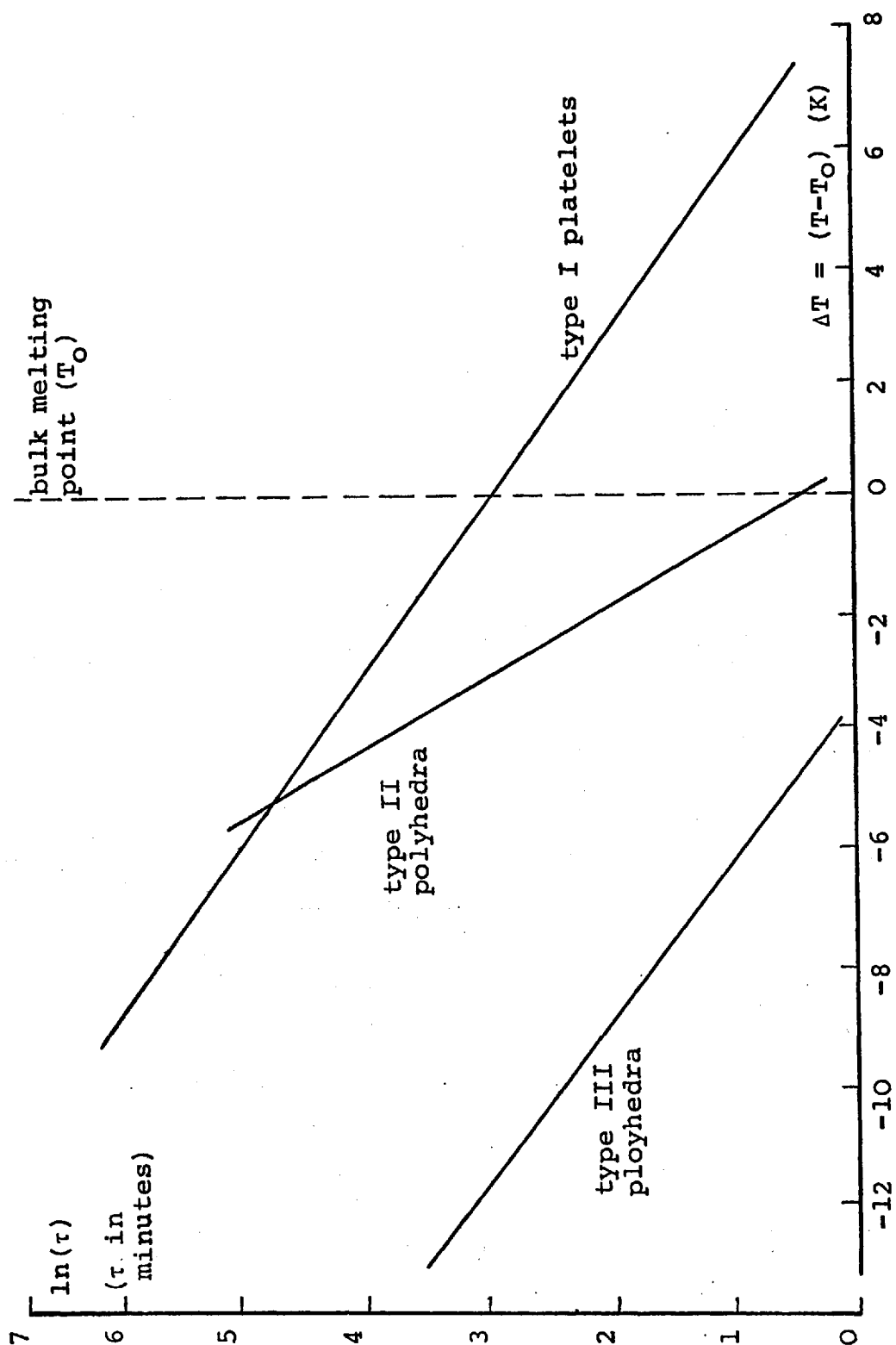
FIGURE 1.2.4.

Variation of the characteristic time (τ) with temperature
(T) for the three forms of bismuth particle, plotted on a
logarithmic scale (Peppiatt, 1975).

crystallites to be superheated by upto 7K. By performing
additional 'beam-on' experiments in which the crystallites
in a layer (held at a constant temperature) were photographed
at regular intervals, the presence of the time delay was still
observed. This indicated that the heating and cooling cycle
required for an accurate temperature measurement, did not
affect the time delay. The characteristic times for type
II and type III polyhedra were found to be independent of the
particle size involved (150Å to 600Å in diameter). For the
platelet (type I) particles, however, the characteristic
times were found to be largest for particles which upon
melting formed liquid droplets with diameters of the order
of 400Å. Both larger and smaller particles had smaller
characteristic times. Also the melting behaviour of the
platelets was seen to be independent of their shapes and
thicknesses. In an attempt to determine the time taken by
the melting process, further experiments by Peppiatt using a
cine camera have shown that bismuth particles, a fraction of
a micrometer in diameter, changed completely from the solid
to the liquid in less than 0.04 sec.

As part of the experiments described in this thesis,
the work of Peppiatt on bismuth has been extended. In
particular, the time delay in the melting of particles with
sizes greater than those studied by Peppiatt has been
investigated. In addition, the possible influence of a
crystalline base on the formation and melting behaviour of the

bismuth particles in the neighbourhood of the bulk melting

point has been studied by using single crystalline flakes of

molybdenite as substrates; see chapter 5.

1.3.   The Melting of Small Particles of Tin.

Although the transition from solid to liquid tin had

been observed by electron diffraction by Jenkins (1935),

Sayama (1941), Richter (1943) and Pines and Bublik (1954), the

first experiments on the melting of small particles of tin

were again carried out by Takagi (1954).   She used the

electron diffraction technique in reflection and crystalline

faces as substrates.   She quotes a depression from the bulk

melting point (505K) of 30K for a film of mean thickness

50$\overset{o}{A}$, with a corresponding particle radius of 43$\overset{o}{A}$ estimated

indirectly from supercooling data.

The first attempt to correlate directly the melting

point of a given tin crystallite with its size was made by

Blackman and Curzon (1959) (see also Curzon, 1960).   The

melting temperature (T_m) of a layer of crystallites was

determined by the electron diffraction method in transmission.

A histogram of the sizes of particles was plotted by measuring

the radii of the particles in the transmission electron

micrographs of the specimen after it had cooled and transferred

to an electron microscope.   From the histogram, the melting

radius (r_m) corresponding to T_m was defined such that 80% of

the crystallites in a given layer had radii equal to or less

than r_m. The accuracy of the crystallite radii measurements
was only $\pm$ 10%. By assuming the tin particles to be spherical,
their results showed that the depression in melting point of
a given tin particle varied inversely with r_m (figure 1.3.1).

Wronski (1963, 1967) later extended the work by
Blackman and Curzon, to study in detail the dependence of the
melting point of tin on crystallite size. He increased
the number of observations considerably and used a modified
method to obtain the mean radius of a given set of particles
in a layer. The melting temperature (T_m) of a given
specimen was taken to be the lowest temperature to which the
specimen had to be heated such that the photograph of the
diffraction pattern of the specimen was indistinguishable
from a similar photograph taken at 505K, the bulk melting
point of tin. To determine the melting radius (r_m),
Wronski carried out some subsidiary experiments. In these,
the diffraction pattern from a known weight of solid tin was
superimposed on the diffraction halos produced entirely by
a known weight of liquid tin (at 505K) on the same photographic
plate. By using the size distribution of the particles in
the two specimens, he considered r_m to be such that 85% of
the crystallites in a layer had radii equal to or less than
r_m. Wronski's results show that the melting point of a
given tin crystallite of radius r_m does not precisely vary
inversely with r_m, in contrast to the results obtained by
Blackman and Curzon, see figure (1.3.1.). Thin films of

bulk melting point
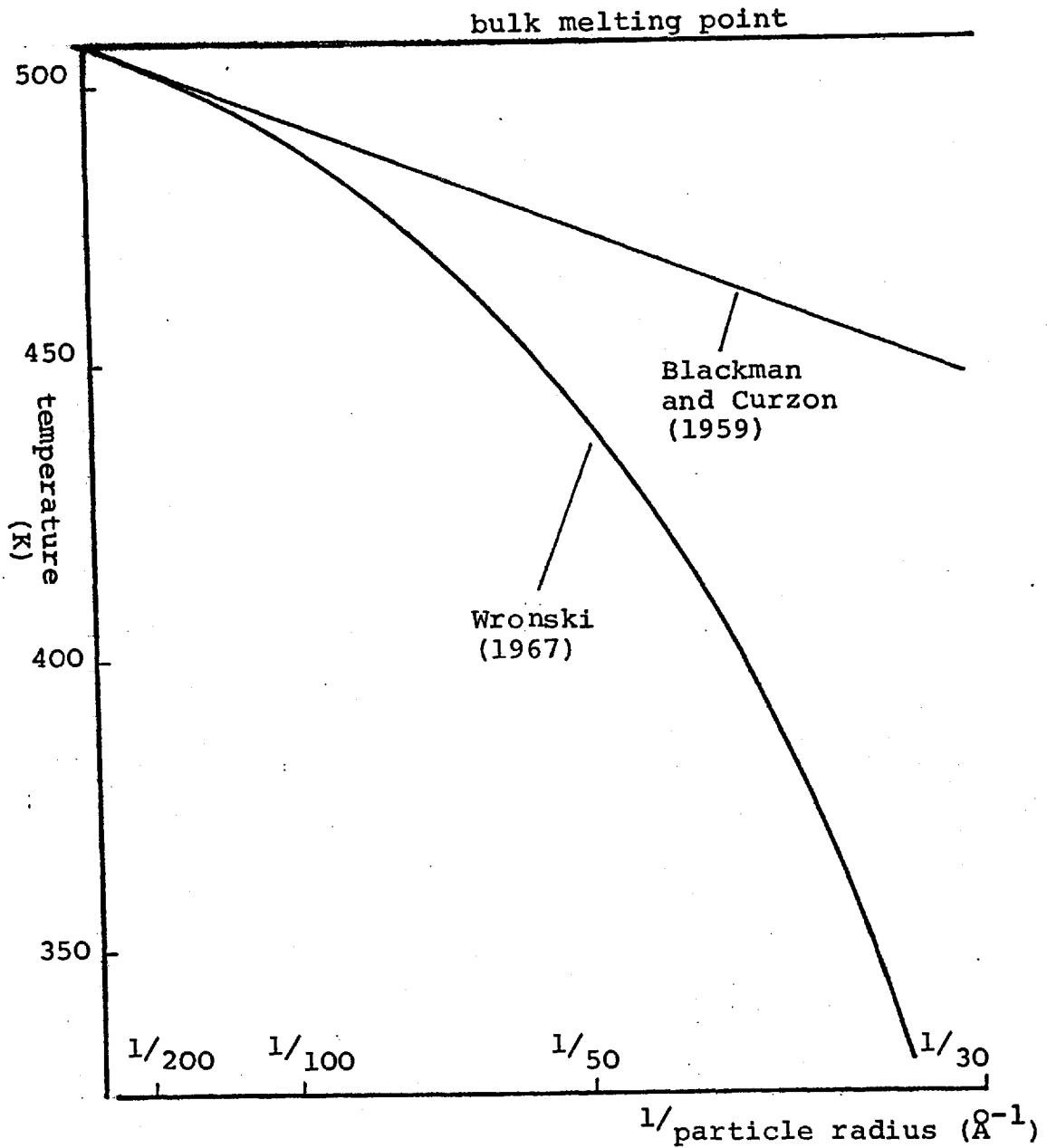
FIGURE 1.3.1.

Graph of melting temperature (T_m) against reciprocal of melting radius (r_m) for small particles of tin (assumed spherical).

amorphous carbon and siliconmonoxide (SiO) were used as substrates, although no effect of a change of substrate on the results was found (see figure 1.3.2.). The results also show that a melting temperature could be assigned to a given particle within a narrow temperature range due to the small scatter in the melting temperatures measured, see figure (1.3.2.).

Although the above authors gave results differing in the variation of the melting temperature with the sizes of the tin particles (see figure 1.3.1.), they made similar assumptions regarding the shapes of the particles in their experiments. Evidently, since the melting experiments were not performed in an electron microscope, but the particles were only observed in an electron microscope after each experiment, the actual shape and morphology of the particles as deposited, could not be known. Hence, for simplicity, they assumed the tin particles to be spherical and accordingly, made theoretical treatment of their results by taking the particles to be spherical.

In the present experiments, a study has been made of the melting of small particles of tin "in situ" in an electron microscope. Not only the melting point of individual crystallites could be determined accurately, but also morphology of the particles. Besides using thin films of amorphous carbon as substrates in a majority of experiments,
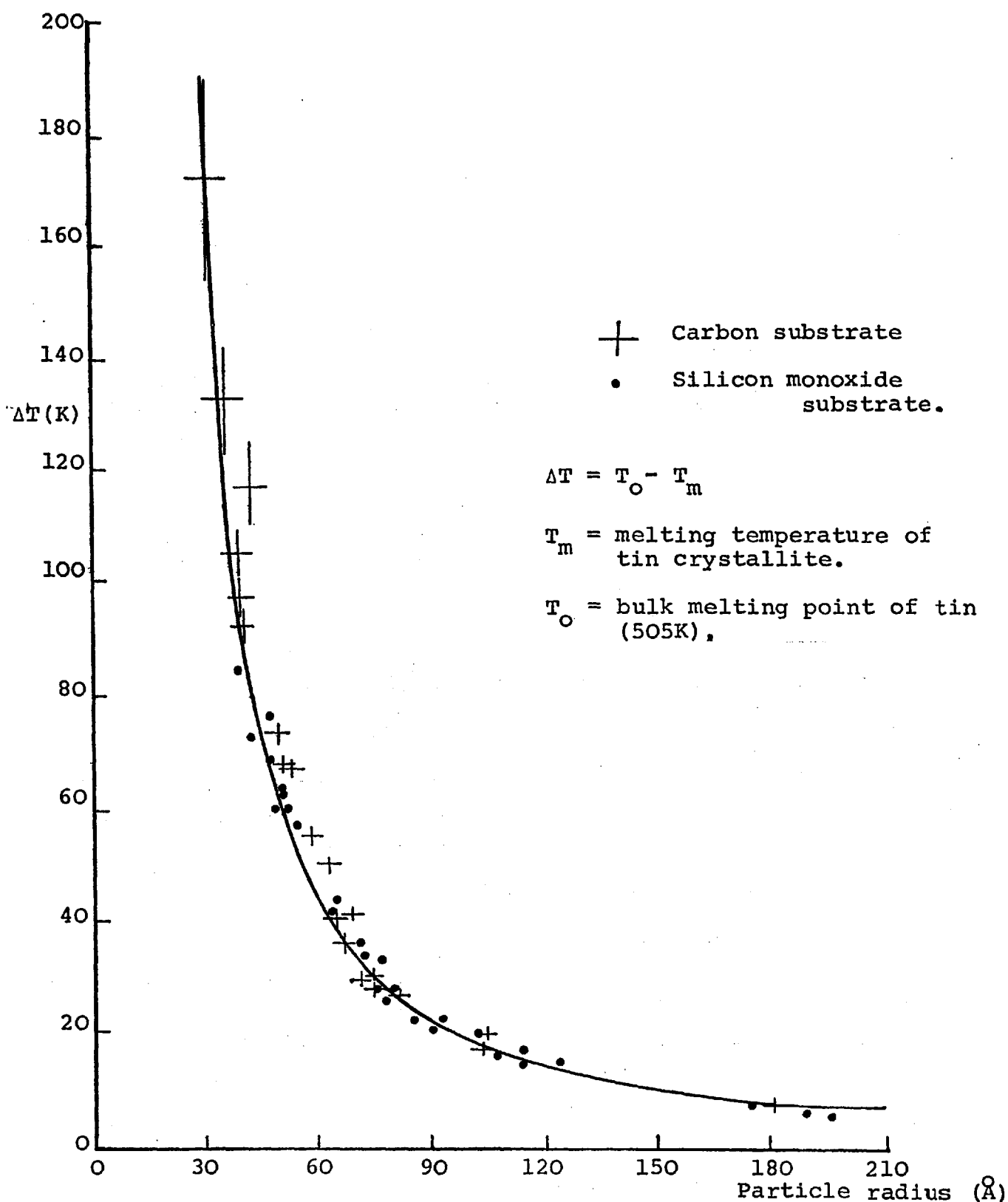
FIGURE 1.3.2.

The variation of melting temperature with size for small
particles of tin (the errors on the points of silicon monoxide
substrates are the same as for similar points with the carbon
substrates) (Wronski, 1967)

the effect of crystalline substrates on the melting of tin crystallites was also investigated in a few experiments by using thin single crystalline films of molybdenite and graphite; see Chapter 6.

CHAPTER 2

THEORY

2.1.   The Theories of the Melting of Small Particles.
2.1.1. The Size Dependence of the Melting of Small Particles.

A small particle has a very large surface area relative
to its volume. Due to the change in surface energy and density
upon melting, the free energies of the initial small solid particle
and the final liquid particle will be different from the free
energy of the bulk material, and the melting point will be altered
with respect to the bulk value.

According to the second law of thermodynamics, for any
thermodynamic process at constant volume and temperature, the
free energy will remain constant or decrease. For normal pressure,
'constant volume' can be replaced by constant pressure. It follows
that the stable state of the system has the minimum free energy.
For a bulk solid, the melting point is the temperature at which the
free energy of the solid equals that of the liquid of the same
mass. Above this temperature, the liquid is the stable phase,
while below it, the solid becomes the stable phase. Similarly, a
"thermodynamic melting point" may be calculated for a small
crystallite by equating the free energies of the initial solid and
final liquid particle. This is different from that of the bulk
material due to the increased effect of the surface energy for small
particles. For a small spherical particle of radius r_s, the
thermodynamic melting point (T_{th}) is given by

$$\ln \left(\frac{T_{th}}{T_o}\right) = - \frac{3}{L\rho_s r_s} \left[\gamma_s - \left(\frac{\rho_s}{\rho_\ell}\right)^{2/3} \gamma_\ell \right]$$

$$\simeq \frac{T_{th} - T_o}{T_o} \qquad\qquad (2.1.1.)$$

(Peppiatt, 1973)

where T_o is the bulk melting point, L is the latent heat of fusion per unit mass, γ the surface energy per unit area of the material in contact with the vapour, ρ the density of the material, and the subscripts s and ℓ refer to the solid and liquid respectively. With normal values of the physical constants involved, one finds, from equation (2.1.1.), a depression in the melting point, inversely proportional to the radius of the solid crystallite. However, the thermodynamic melting point does not take into account the actual process by which a particle will melt (see section 2.1.2.) Several possible processes have been put forward by various authors as described below.

A relation between the melting point of a small particle and its radius seems to have been first derived by Pawlow (1908-9, 1909). He considered the equilibrium of a small spherical solid particle and a liquid particle of the same mass, immersed in a common vapour. He identified as the melting point of the solid particle, the temperature at which there is an equilibrium in the solid-liquid-vapour system. His theory was later extended by Hanszen (1960). The Pawlow melting temperature (T_p) is related to the radius (r_s) of the

particle by the equation

$$\ln\left(\frac{T_P}{T_O}\right) = -\frac{2}{L\rho_s r_s}\left[\gamma_s - \left(\frac{\rho_s}{\rho_\ell}\right)^{2/3}\gamma_\ell\right] \qquad (2.1.2.)$$

$$\simeq \frac{T_P - T_O}{T_O}$$

Rie (1923) developed a theory concerning the equilibrium of a spherical solid particle within an infinite (bulk) liquid and obtained the following expression for the Rie melting temperature (T_R)

$$\ln\left(\frac{T_R}{T_O}\right) = -\frac{2}{L\rho_s r_s}\gamma_{s\ell}$$

$$\simeq \frac{T_R - T_O}{T_O} \qquad (2.1.3.)$$

where $\gamma_{s\ell}$ is the surface energy per unit area of a solid/ liquid interface.

Curzon (1960) developed the theory of the "liquid skin". This was suggested initially by Reiss and Wilson (1948) to explain the process by which a small crystallite is expected to melt. Curzon considered the solid particle to be covered by a thin skin of liquid, even at temperatures below its melting point. The liquid skin exists in equilibrium with the solid core over a range of temperature, until the 'skin melting temperature' (T_{SK}) is reached at which it becomes unstable and dissolves the solid core. The skin melting temperature (T_{SK}) for a small spherical solid

particle is given by

$$\ln\left(\frac{T_{SK}}{T_0}\right) = - \frac{2}{L\rho_s r_s} \left(\frac{\rho_\ell}{\rho_s}\right)^{1/3} \left[\gamma_\ell\left(1-\frac{\rho_s}{\rho_\ell}\right) + \gamma_{s\ell}\left\{1-\frac{\delta}{r_s}\left(\frac{\rho_s}{\rho_\ell}\right)^{1/3}\right\}^{-1}\right]$$

valid for $r_s \gg \delta$

(2.1.4.)

(Sambles, 1970)

where r_s is the radius of the solid core of the composite particle and δ the thickness of the liquid skin.

Wronski (1963) developed a similar theory to that of Curzon, considering the possibility of the formation of a liquid cap on a spherical particle, rather than a complete liquid skin. As Wronski's theory is merely a more complicated variant of Curzon's theory, it will not be further considered.

2.1.2. Discussion of the Theories of Melting.

Table (2.1.1.) shows the change in melting point from the bulk value for various sizes of tin particles (assumed spherical), calculated from each of the above expressions by taking reasonable values for the physical constants (See appendix A.4.) involved. The differences between the depressions in the melting point from the theories arise from the differences in the criterion used to define the melting point. In all cases, however, the melting temperature is below the bulk melting point.

Pawlow's method of formulating the melting point of a small

r_s (Å)	T_o-T_{th} (K)	T_o-T_p (K)	T_o-T_R (K)	$^*T_o-T_{SK}$ (K)
50	78.80	52.53	26.02	18.76
100	39.40	26.26	13.01	9,38
1,000	3,94	2.62	1.30	0.93
10,000	0.39	0.26	0.13	0.09

Table 2.1.1.

The Theoretical Melting Point of Small Tin Crystallites.

The change in melting point from the bulk value for small spherical tin crystallites as predicted by various theories. The values of the physical constants used are listed in appendix A.4.

* Neglecting the thickness (δ) of the liquid skin, compared to the radii of the particles (equation 2.1.4.).

particle is an   inadequate representation of the melting

experiments performed.   As was pointed out by Rie (1923),

(See also Reiss and Wilson, 1948), Pawlow's definition of

the melting point of a small particle corresponds to the

'triple point' for the bulk phase and does not necessarily

define the melting point of a solid sphere because when

melting occurs, the solid is not in contact with the vapour

but with liquid.   Thus, this theory fails to·consider the

actual process of melting.

Rie's theory is also inapplicable to the melting of

the small particles studied in the present experiments,

because it cannot be assumed that the particles are

surrounded by a large quantity of liquid at the melting

point.

The thermodynamic melting point, although defining the

relative stability of the solid and liquid at this temperature,

does not include the actual process of melting, as previously

mentioned.   The solid particle can only melt at the

thermodynamic melting point (T_{th}), provided there is a

suitable process by which the free energy of the solid can

be progressively lowered, or else, there is sufficent time

for a very large fluctuation to occur for lowering the free

energy.   Thus, the particle remains metastable as the

temperature is raised, until it melts either by the emergence

of a suitable melting process or by overcoming the activation

energy barrier (similar to that of supercooled liquid droplets,

see section 2.2.1.) by a small fluctuation . In the present experiments, small crystallites of bismuth and tin are found to melt at temperatures much higher than those calculated for T_{th} (equation 2.1.1.). Thus, as Peppiatt amd Sambles (1975) point out, 'the melting temperature is apparently determined by the actual process of melting, rather than the relative stability of the solid and liquid'. The thermodynamic melting point is however the lowest possible temperature at which a solid particle can melt.

By comparison with Pawlow and Rie theories, Curzon's liquid-skin theory for the melting of small particle can be considered as a better approach as it attempts to introduce a possible melting mechanism for the particles. This theory has the virtue that it assumes the liquid to be already present, covering the particle, even at temperatures below the skin melting temperature (T_{SK}) of the particle. A fuller description of this approach is given in section (2.2.4.).

****

All the above mentioned theories for the melting of small particles assume the initial solid particle to be spherical and therefore, derive the melting temperatures as a function of a single radius of curvature - equivalent to the radius (r_s) of the solid particle. However, the surfaces of the solid particle will almost certainly consist of facets, and surfaces with various radii of curvatures.

It may be expected that melting would start on the particle
at points with large curvatures rather then at those with
smaller curvatures (see section 2.3.2.).   Thus, a
derivation of thè melting point formula should also take
into account the influence of the variations of curvatures
on the melting point.

2.2. Nucleation in a Condensed System and the Application
to the Melting of Small Particles.

2.2.1. Homogeneous Nucleation in a Supercooled liquid,

In order that a supercooled liquid may transform to
the solid phase at some temperature below the equilibrium
temperature (T_o), a small number of atoms or molecules
in the liquid must come together to form a solid nucleus,
The formation of the solid nucleus in the interior of the
liquid requires an initial increase in the free energy of
the system due to the surface energy associated with the
relatively small solid nucleus.   Once the solid nucleus
reaches a critical size, gaining atoms from the liquid
(by a statistical fluctuation), further transformation
results in a continuous decrease in the free energy and so
will proceed spontaneously (Turnbull and Fisher, 1949).
It follows that crystals larger than the critical size will
almost certainly grow.   Most theories of homogeneous
nucleation are concerned with the problem of calculating
the probability of formation of nuclei having the critical
size.

Hollomon and Turnbull (1950) have studied nucleation

for the case of a supercooled liquid both theoretically and

experimentally (For a general review of the nucleation

theories, see Christian, 1965; Chapter X.).   They obtained,

for homogeneous nucleation at temperature T, the rate of

production (I) of solid nuclei per unit volume inside a

liquid as:

$$I = \frac{nkT}{h} \exp \left[- \frac{\left(\Delta F^* + \Delta F_a \right)}{kT} \right] \qquad (2.2.1.)$$

Here, n is the number of atoms of liquid per unit volume,

h is Plank's constant, k is Boltzman's constant and ΔF^* is

the height of the energy barrier which the solid nucleus

must overcome to cause solidification of the liquid.   In

their treatment, Hollomon and Turnbull consider ΔF_a as the

activation energy for self diffusion in the liquid, ΔF^*,

that is, the activation energy required for the solid

nucleus of the critical size, they calculated to be

$$\Delta F^* = \frac{16 \pi \gamma_{s\ell}^3}{3 \rho_s^2 L^2} \cdot \frac{T_o^2}{(\Delta T)^2} \qquad (2.2.2.)$$

where $\Delta T = T - T_o$ represents the amount of supercooling.   It

follows from equations (2.2.1.) and (2.2.2.), that to achieve

a significant rate of nucleation, the liquid must be super-

cooled by tens of degrees to make the activation energy

(or the height of the energy barrier), ΔF^*, smaller; for

very small supercooling, the time required to form the

critical nucleus (by statistical fluctuation) and hence, to

resolidify the liquid, would become too great to be observed
experimentally.

2.2.2. Heterogeneous Nucleation in a Supercooled Liquid

In the theory of homogeneous nucleation, it was assumed
that the critical solid nuclei have an equal probability of forming
at any point within the volume of the supercooled liquid. However,
it may be seen from equation (2.2.1.). that the nucleation rate, I,
is very sensitive to changes in ΔF^* which will drastically alter
the temperature at which the nucleation rate will be appreciable.
In heterogeneous nulceation where crystal formation is catalysed by
impurities, it is supposed that the probability of nucleus form-
ation is greater at the interface between the liquid and the foreign
surface. It is shown (see Volmer, 1925; Turnbull, 1950; and Pound
(1958) that the nucleation rate (I') per unit volume in a hetero-
geneous nucleation is given by

$$ I' = \frac{N}{V} \cdot \frac{kT}{h} \exp \frac{-(\Delta F^{*'} + \Delta F_a)}{kT} \qquad (2.2.3.) $$

where, the free energy, $\Delta F^{*'}$, for the formation of the critical
nucleus is given by

$$ \Delta F^{*'} = \frac{16\pi \gamma_{s\ell}^3}{3\rho_s^2 L^2} \cdot \frac{T_o^2}{(\Delta T)^2} \cdot \frac{(2+\cos\theta)(1-\cos\theta)^2}{4} \qquad (2.2.4.) $$

Here, θ is the equilibrium contact angle between the crystal

nucleus in the form of a spherical cap and the nucleating

surface (See figure 2.2.1.) and is determined by the equation:

$$\gamma'_\ell = \gamma'_s + \gamma_{s\ell} \cos(\theta) \qquad (2.2.5.)$$

where, γ'_ℓ is the surface energy per unit area of the surface

between the liquid and the nucleating surface, and γ'_s is

that between the solid nucleus and the surface.

When θ is equal to 180°, that is the solid does not

at all 'wet' the surface, equation (2.2.4.) reduces to

equation (2.2.2.) and the surface will have no effect upon

the nucleation.   If θ is less than 180°, $\Delta F^{*'}$ will be

lowered;   for example when θ is equal to 90°, the value of

$\Delta F^{*'}$ will be half the corresponding value for homogeneous

nucleation.

In equation (2.2.3.). the pre-exponential factor

of equation (2.2.1.) is modified, as the number of probable

nucleation sites is now limited to sites on the surface of

the liquid.   Here, V is the volume of the liquid, with N

the total number of atoms in this volume in contact with

the nucleating surface.

2.2.3. Application of Nucleation Theory to Melting of Small
Particles: Surface Melting and the Wetting Condition.

Although nucleation theory has been successfully

applied to the supercooled liquid system (and to the

condensation of vapour), its application to the process of
melting encounters serious difficulties in explaining the
sharpness of the transformation and the rarity of superheating
in solids. The reason for this is that there is an
essential asymmetry between the kinetics of the two processes:
whereas all substances will supercool, under suitable
conditions, the examples of superheating under ordinary
conditions are extremely rare (see, for example, Khaikin
and Benet , 1939; also see, Peppiatt, 1975). The theory
of homogeneous nucleation cannot explain this; it predicts
that the rate of production of liquid nuclei should not
become appreciable until the solid is superheated by an
amount comparable to the supercooling needed to resolidify
the liquid. Also a similar critical size of a spherical
liquid nucleus for homogeneous nucleation of melting would
be predicted.

An alternative explanation for the relative absence
of superheating in solids can be formulated on the basis of
the heterogeneous theory of nucleation. Under normal
conditions, melting should always begin at the surface,
which is able to act as its own heterogeneous nucleating
agent. If the liquid nucleus forms a contact angle of less
than 180° on the solid surface, the activation energy for
the formation of the nucleus would be lower on the surface
than one in the interior of the solid, even neglecting the
strain energy due to the change in density of the material

on melting. This will favour the formation of the liquid on the surface of the solid. The activation energy for the formation of a spherical liquid nucleus on the solid surface (by analogy with equation (2.2.4.) can be written as

$$\Delta F_{\ell}^{*} \ \stackrel{\cdot}{=} \ \frac{16\pi\gamma_{\ell}^{3}}{3\rho_{\ell}^{2}L^{2}} \cdot \frac{T_{o}^{2}}{(\Delta T)^{2}} \cdot \frac{(2+\cos\theta_{\ell})(1-\cos\theta_{\ell})^{2}}{4} \qquad (2.2.6.)$$

where θ_{ℓ} is the equilibrium contact angle between the spherical liquid cap and the solid surface (see figure 2.2.2.) and is given by the relation

$$\gamma_{s} = \gamma_{\ell} + \gamma_{s\ell}\cos(\theta_{\ell}) \qquad\qquad (2.2.7.)$$

From equation (2.2.7.), to produce non-zero contact angle θ_{ℓ}, we must have

$$\gamma_{s} < \gamma_{\ell} + \gamma_{s\ell} \qquad\qquad (2.2.8.)$$

This will mean that an activation energy, ΔF_{ℓ}^{*}, determined by the amount of θ_{ℓ}, will be needed for the formation of the liquid nucleus. The liquid will not completely wet the solid. The liquid nucleus below a certain critical size will be unstable with respect to the solid even at temperatures above the bulk melting point, and will therefore, recrystallize. This will result in a time delay effect, and a finite length of time is necessary for a sufficiently large statistical fluctuation to occur to form a nucleus above the

critical size which is then able to grow.

If, however, the condition of equation (2.2.8.) is not met, i.e.

$$\gamma_s \geqslant \gamma_\ell + \gamma_{s\ell} \qquad\qquad (2.2.9.)$$

there will be complete wetting of the solid surface by the liquid. The contact angle θ_ℓ will be zero and, therefore, there will be no energy barrier in forming the liquid nucleus on the solid surface. Equation (2.2.9.) is the 'wetting condition'. This means that it is energetically favourable for a liquid-skin to form on the free solid surface, since there is no activation energy barrier preventing the process occurring spontaneously. There will be no intermediate state of higher total free energy between the all solid and solid plus liquid skin stage. Indeed the inequality in equation (2.2.9.) suggests that the formation of the liquid skin is possible even at temperatures below the bulk melting point (T_o); the small gain in free energy due to the presence of the liquid skin below T_o will be more than balanced by the reduction in free energy achieved by reducing the solid of some of its free surface energy. This is the basis of the liquid-skin melting model of particles; see section (2.2.4.).

Another reason favouring the formation of the liquid nucleus on the surface of the solid is that, for a liquid nucleus to grow within the interior of a solid, it

would require a strain energy as an addition to the
activation energy of the formation of the liquid nucleus,
due to the change in density on melting.   If the initial
liquid nucleus is formed on the surface of the solid, the
change in volume will not cause a strain energy.   This is
in contrast with the formation of a solid nucleus in the
interior of a supercooled liquid.   The change in volume
of the liquid which forms the solid nucleus does not involve
any additional strain energy in the activation energy, as
the liquid is able to flow freely.   It therefore seems
that in melting, the initial liquid nucleus will form on
the free surface of the solid.

2.2.4. The Liquid-skin Melting Model.

The liquid-skin theory attempts to introduce a possible
process for the melting of small particles.   The liquid-
skin is able to form even at temperatures below the bulk
melting point, as previously mentioned.   However, if the
skin were thick enough to have bulk liquid properties, it
would inevitably resolidify below the melting point; it
must therefore be assumed to be thin (for example, in the
form of a two dimensional monolayer of liquid) without
bulk liquid properties at the initial stages of formation.
Once formed the skin will then grow in thickness with
increasing temperature, eventually becoming unstable, and
dissolving the solid at the skin melting temperature.   The
liquid-skin melting model therefore, consists essentially of

two processes: first, the formation of the two dimensional monolayer liquid skin and second, the growth of the skin leading to the eventual melting of the particle.

Two mechanisms have been suggested (Peppiatt, 1973) by which the two-dimensional liquid skin can nucleate and grow, either of which might occur depending on the material.

(a) Nucleation on the surface: In this case, the two dimensional liquid nucleus may form on the surface (figure 2.2.3a.) and subsequently grow, either by the aggregation of adatoms or by the activation of atoms directly from the solid. In the case of high adatom concentration, it is likely that the former will dominate,

(b) Nucleation in the surface: In this case, the liquid nucleus can only form and grow in the surface (figure 2.2.3b.) by the direct activation of atoms from the solid surface into a liquid like configuration.

Which of these two mechanisms dominates probably depends on the material. Nucleation on the surface seems more likely on kinetic grounds, as the aggregation of adatoms seems more likely than the sudden activation of a group of surface atoms. However, nucleation in the surface appears more favourable thermodynamically as it involves a smaller activation energy. The former process will dominate when there is high adatom concentration; while the latter seems more favourable at
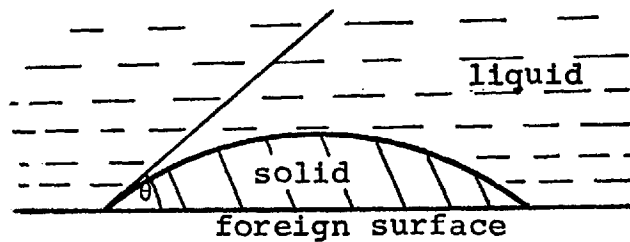
FIGURE 2.2.1.

Heteregeneous nucleation of the solid on a foreign surface (in a supercooled liquid).
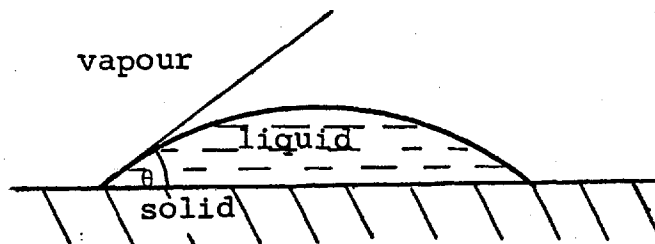
FIGURE 2.2.2.

Nucleation of the liquid on the surface of the solid

(a)

(b)
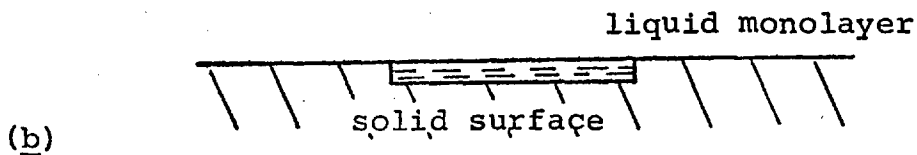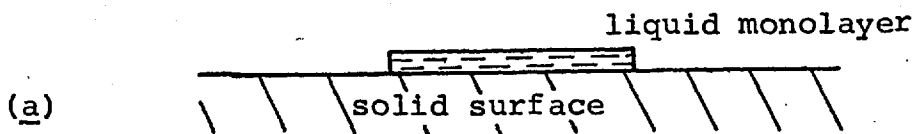
FIGURE 2.2.3.

low adatom concentration.   In both cases, suitable nucleation
sites, for example, dislocations, stacking faults or grain
boundaries would help the nucleation.

Now consider a solid particle which is being heated
from below the skin melting temperature.   Providing the
wetting condition (equation 2.2.9.) holds, as the temperature
is increased, there would be a reduction in surface energy,
together with a smaller gain in the volume energy, by the
formation of a thin liquid skin.   The variation of the
change in free energy (ΔF) of the system, on forming the
liquid skin, with the thickness (δ) of the liquid skin as
the temperature is being increased, is shown in figure
2.2.4.   When the temperature (T) is much less than the bulk
melting point (T_O), the solid is the stable phase (figure
2.2.4a.).When the temperature equals the thermodynamic
melting temperature (T_{th}) (figure 2.2.4b), the liquid
becomes the stable phase, but the solid remains unstable
and therefore will not melt within a reasonable time scale
(See section 2.1.2.).   At some temperature (T_ℓ), a thin
stable liquid skin is able to form on the particle - the
thickness (δ_{eq}) of this skin, at equilibrium with the solid,
is given by the minimum near $\delta=0$ (figure 2.2.4c.).   As the
temperature is raised further, the liquid skin grows thicker,
i.e. the minimum   moves towards the right.   Also the
maximum   in the curve, which represents the activation
energy preventing the particle from melting at T_{th}, moves
towards the left, until at the skin melting temperature
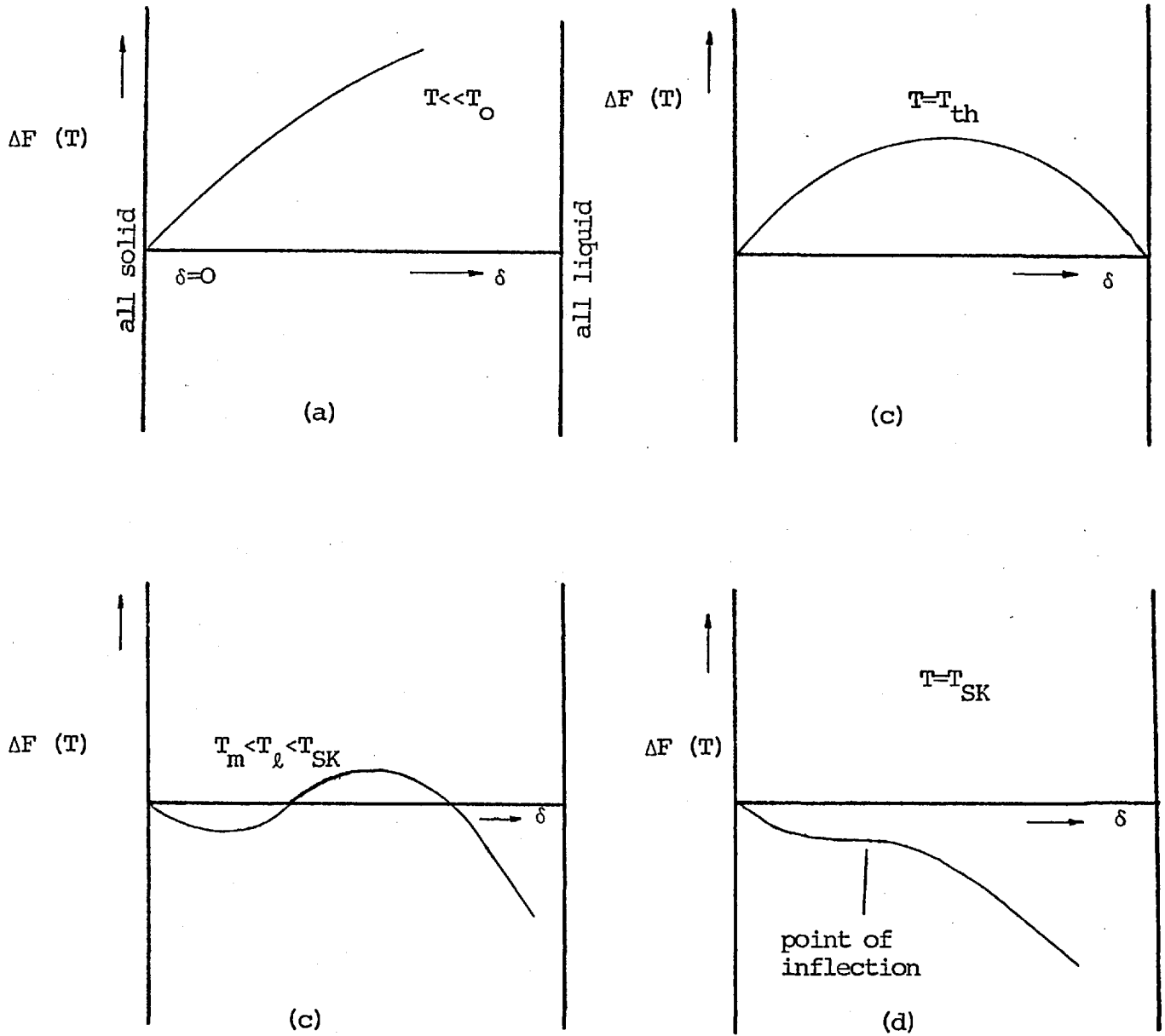
FIGURE 2,2,4,

The variation of the change in free energy (ΔF) of a solid particle, on forming the liquid skin, with the thickness (δ) of the liquid skin, on increasing the temperature.

(T_{SK}), the maximum and the minimum coincide. This results in a point of inflection (figure 2.2.4d.). At this stage, the liquid skin becomes unstable, as the particle would progressively lower its free energy by allowing the liquid skin to completely dissolve the solid. Mathematically, the skin melting temperature, T_{SK}, will be defined as the temperature, for which,

$$\left(\frac{\partial \Delta F}{\partial \delta}\right)_{\delta=\delta_1} = 0 \qquad\qquad (2.2.10.)$$

at $T = T_{SK}$.

This means that at the skin melting temperature, as soon as the liquid skin is formed, it moves into the solid without requiring an activation energy for the process and dissolves the solid completely.

A good approximation may be made for the skin melting temperature purely from thermodynamics, by making the reasonable assumption that the thickness of the liquid skin up to the point of instability is much smaller than the size of the particle. This has been done for various cases in the next section.

2.3 Calculation of the Skin Melting Temperature (T_{SK}) for Various Shapes of Crystallites.

2.3.1. A Spherical Crystallite.

Consider a spherical solid particle of radius r_s, which on melting at the surface, forms a liquid-skin of thickness δ.   Let R be the radius of the composite particle (figure 2.3.1.).   R will be different from r_s due to the change in density upon melting.

Let $f_s(T)$ and $f_\ell(T)$ be the Helmholtz's free energy per unit mass at temperature T of the solid and liquid respectively.   Now, for the composite particle,

$$\text{the volume energy, } F_{vol} = \frac{4}{3}\pi(R-\delta)^3\rho_s f_s(T)$$

$$+ \frac{4}{3}\pi\left\{R^3-(R-\delta)^3\right\}\rho_\ell f_\ell(T)$$

$$(2.3.1a.)$$

$$\text{the surface energy, } F_{surf} = 4\pi R^2\gamma_\ell + 4\pi(R-\delta)^2\gamma_{s\ell}$$

$$(2.3.1b.)$$

Therefore, the total free energy of the composite particle, which is a function of the liquid skin thickness:

$$F(\delta) = F_{vol} + F_{surf}$$

$$= \frac{4}{3}\pi(R-\delta)^3\rho_s f_s(T) + \frac{4}{3}\pi\left\{R^3-(R-\delta)^3\right\}\rho_\ell f_\ell(T)$$

$$+ 4\pi R^2\gamma_\ell + 4\pi(R-\delta)^2\gamma_{s\ell} \qquad (2.3.2.)$$
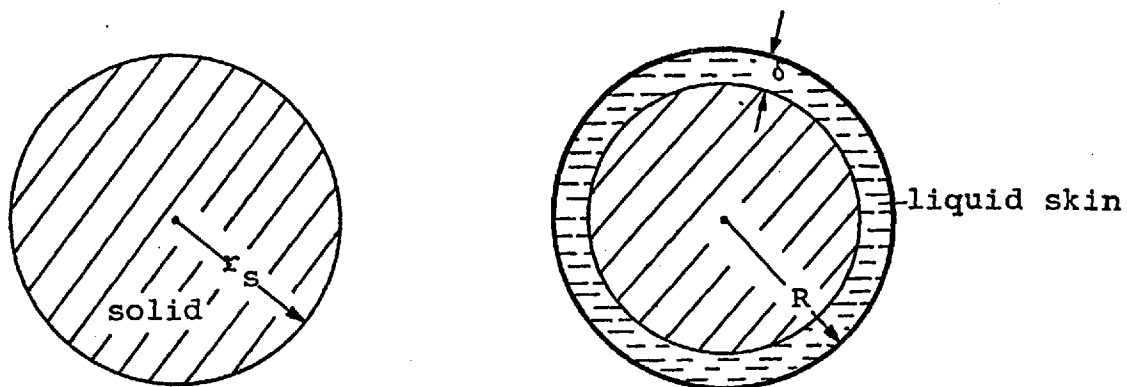
FIGURE 2.3.1.

Liquid skin formed on a spherical particle.
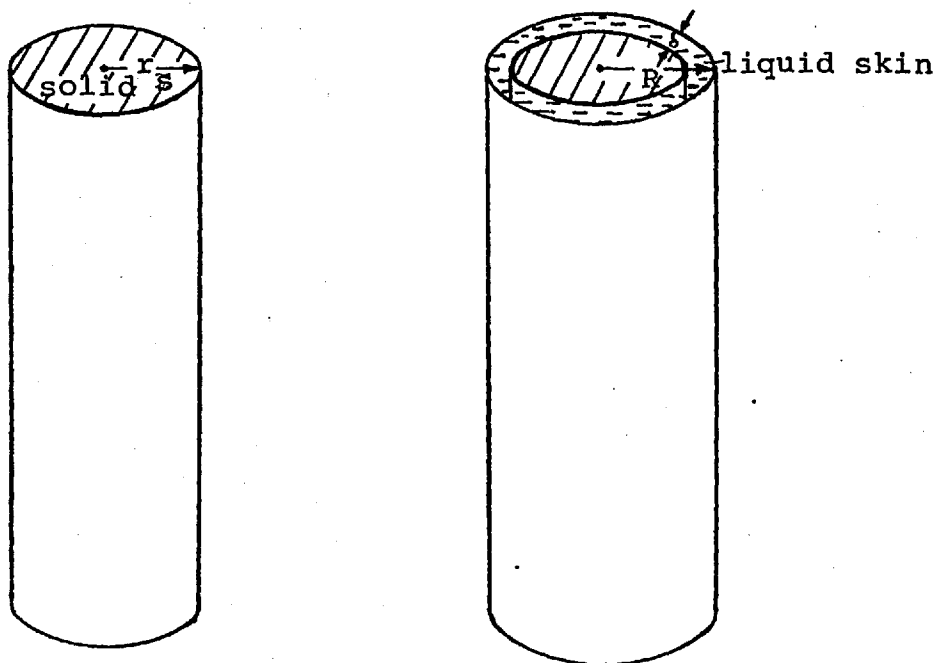
FIGURE 2.3.2.

Liquid skin formed along the length of a rod or needle-
like particle.

Also the change in the free energy from the initial state
of a very thin skin is

$$\Delta F(\delta) = F(\delta) - F(\delta=0)$$

$$= \left[\frac{4}{3}\pi \left\{ R^3 - (R-\delta)^3 \right\} \rho_\ell \left\{ f_\ell(T) - f_s(T) \right\} \right]$$

$$+ \left[4\pi(R^2 - r_s^2)\gamma_\ell + 4\pi \left\{ (R-\delta)^2 - r_s^2 \right\} \gamma_{s\ell} \right] \qquad (2.3.3.)$$

where the first bracket represents the change in volume
energy and the second that in surface energy in the formation
of the liquid skin.

The particle will melt at the skin melting temperature,
determined by the equation (2.2.10.).   Therefore,
differentiating equation (2.3.3.) with respect to δ and
substituting $\delta=0$, and also remembering that when $\delta=0$,   R
equals r_s, we get

$$\left\{ f_\ell(T) - f_s(T) \right\} \rho_\ell - 2 r_s \gamma_{s\ell} + \left(\frac{\partial R}{\partial \delta} \right)_{\delta=0} 2(\gamma_\ell + \gamma_{s\ell}) = 0 \qquad (2.3.4.)$$

Also, since the mass of the particle remains unchanged on
forming the composite particle, we must have mass of the
initial solid particle = mass of the composite particle.
Therefore,

$$\frac{4}{3}\pi r_s^3 \rho_s = \frac{4}{3}\pi(R-\delta)^3 \rho_s + \frac{4}{3}\pi \left\{ R^3 - (R-\delta)^3 \right\} \rho_\ell \qquad (2.3.5.)$$

Differentiating equation (2.3.5.) with respect to δ and
taking $\delta = 0$,

$$\left(\frac{\partial R}{\partial \delta}\right)_{\delta=0} = \frac{\rho_s - \rho_\ell}{\rho_s} \tag{2.3.6.}$$

Also, $f_s(T) - f_\ell(T) = L.\ln\left(\frac{T}{T_o}\right)$ $\tag{2.3.7.}$

(see appendix A.1.,equation(A.1.10.)

At the skin melting temperature, from equation   (2.2.10.)

$$T = T_{SK}$$

Therefore, substituting equations (2.3.6.) and (2.3.7.) in (2.3.4.), and simplifying, we have, for the skin melting temperature of the spherical particle

$$\ln\left(\frac{T_{SK}}{T_o}\right) = -\frac{2}{L\rho_s r_s}\left[\gamma_{s\ell} + \gamma_\ell\left(1 - \frac{\rho_s}{\rho_\ell}\right)\right] \tag{2.3.8a.}$$

or, to a first approximation

$$T_o - T_{SK} \simeq \frac{2T_o}{L\rho_s r_s}\left[\gamma_{s\ell} + \gamma_\ell\left(1 - \frac{\rho_s}{\rho_\ell}\right)\right] \tag{2.3.8b.}$$

(c.f. Peppiatt and Sambles (1975), equation (6)).

2.3.2. A General Expression for the Skin Melting Temperature (T_{SK}) of a Curved Surface.

Consider the formation of a thin liquid skin on a curved solid surface having two principal radii of curvature, R_1 and R_2. Providing the solid surface is completely wetted by the liquid (equation 2.2.9.), then above the skin melting temperature (T_{SK}), the liquid skin, once formed,

would melt the rest of the solid at this temperature, by

progressively moving through the crystallite without

requiring an activation energy.   The skin melting temperature

for such a curved surface is given by:

$$\ln \left(\frac{T_{SK}}{T_o}\right) = - \frac{1}{L\rho_s} \left(\frac{1}{R_1} + \frac{1}{R_2}\right) \left[\gamma_{s\ell} + \gamma_{\ell}\left(1 - \frac{\rho_s}{\rho_\ell}\right)\right] \quad (2.3.9.)$$

(see appendix A.2.)

This expression can be considered to be the general

equation of the skin melting temperature for various shapes

of crystallites.   For example, in the case of a spherical

crystallite, the two principal radii of curvature (R_1, R_2)

are equal to the radius of the spherical crystallite (r_s).

Therefore, substituting r_s for both R_1 and R_2 in equation

(2.3.9.), the relevant expression (equation 2.3.8.) for

the skin melting temperature of a spherical particle is

obtained.

In the following two sections, approximate expressions

for the skin melting temperaturers of a rod or needle-like

crystallite and a disc-type crystallite will be derived, by

applying equation (2.3.9.), for the skin melting temperature

of a curved surface.

2.3.3.   A Rod or Needle-like Crystallite.

A rod or needle-like crystallite may melt in either

of the two ways, (i) the liquid skin may form along the

length of the crystallite, so that the composite particle has
a cylindrical solid core surrounded by a cylindrical shell
of the liquid skin, or (ii) the skin may form at one end of
the crystallite and progress through it at the skin melting
temperature and eventually dissolve it.

(i) Liquid skin formed along the length of the
crystallite.

Consider a rod or needle-like crystallite of radius
r_s and length l, along which a liquid skin of thickness δ
is formed (figure 2.3.2.). For this composite particle,
the two principal radii of curvature will be:

$$R_1 = r_s$$

$$R_2 = \infty$$

(2.3.10.)

(along the length of the crystallite)

Therefore substituting equation (2.3.10.) in (2.3.9.), the
skin melting temperature for the crystallite in this case
will be

$$\ln \left(\frac{T_{SK}}{T_o}\right) = - \frac{1}{L\rho_s r_s} \left[\gamma_{s\ell} + \gamma_\ell (1- \frac{\rho_s}{\rho_\ell})\right] \qquad (2.3.11.)$$

Thus, in this case the depression of the skin melting
temperature from the bulk value is half that of a spherical
particle (equation 2.3.8.).

(ii) Liquid skin formed at one end of the crystallite.

Let a liquid skin of thickness δ be formed at one
end of the crystallite (radius r_s) in the form of a spherical

(sectional view)
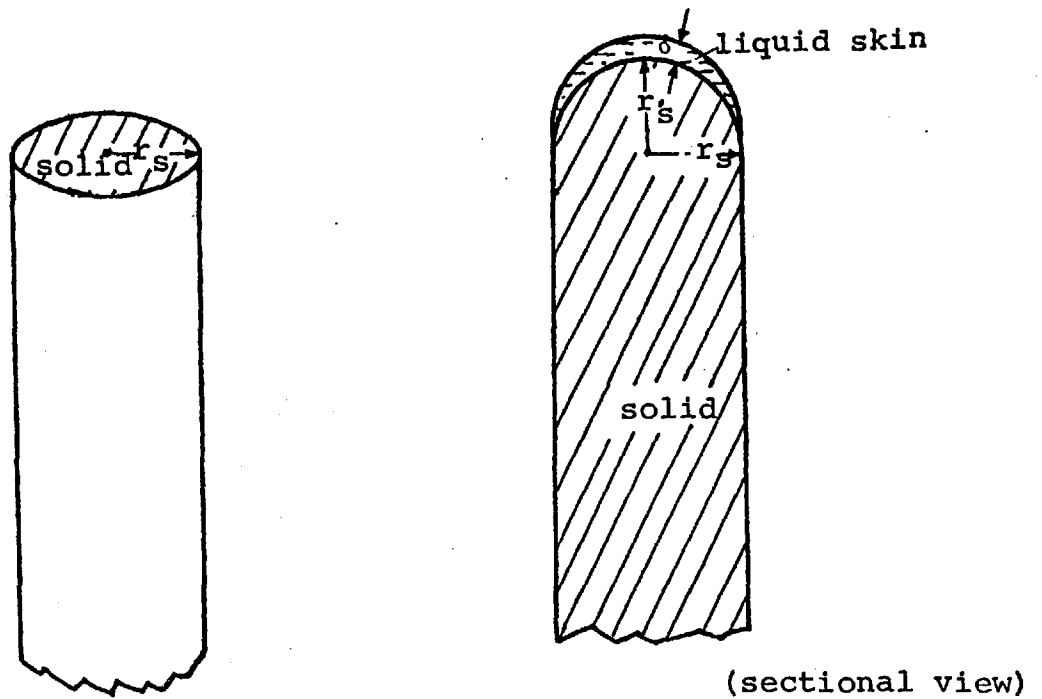
FIGURE 2.3.3.

Liquid skin formed at one end of a rod or needle-like particle.

(a)   (b)
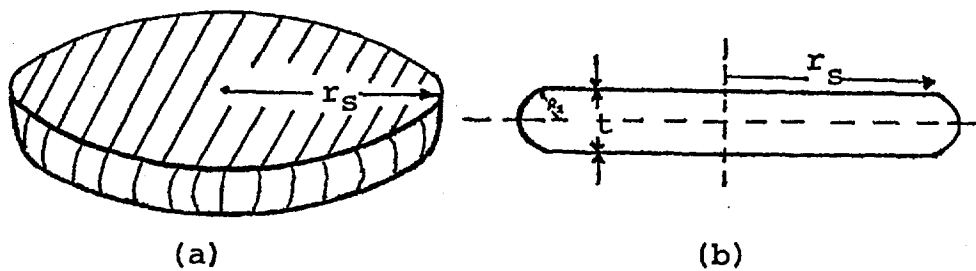
FIGURE 2.3.4.

A disc-type particle.

cap, as shown (figure 2.3.3.). By assuming that the cap-like liquid skin has approximately the same radius of curvature as the crystallite, the two principal radii of curvature will be

$$R_1 \approx R_2 \approx r_s \qquad\qquad (2.3.12.).$$

By substituting equation (2.3.12.) in (2.3.9.), the skin melting temperature for the rod or needle-like crystallite can be obtained as

$$\ln \left(\frac{T_{SK}}{T_o}\right) = -\frac{2}{L\rho_s r_s} \left[\gamma_{s\ell} + \gamma_\ell (1-\frac{\rho_s}{\rho_\ell})\right] \qquad (2.3.13.)$$

Here the skin melting temperature is the same as that of a spherical particle of radius r_s (equation 2.3.8.).

2.3.4. A Disc-Type Crystallite.

Consider a spherical solid disc of radius r_s and thickness t, and having a flat top surface and a curved edge (figure 2.3.4.a). It is unlikely that the melting will be initiated from the top flat surface, as this surface has an infinite radius of curvature. Consequently the liquid skin would probably form around the curved edge, and at the skin melting temperature, would melt the crystallite.

Now, from figure (2.3.4b.), we have for the two principal radii of curvatures of the curved edge:

$$R_1 \equiv r_s$$

and   (2.3.14.)

$$2R_2 \simeq t$$

or, $R_2 \simeq \dfrac{t}{2}$

Therefore, substituting equation (2.3.14.) in equation

(2.3.9.), the approximate expression for the skin melting

temperature of the disc will be

$$\ln \left(\frac{T_{SK}}{T_o}\right) \simeq -\frac{1}{L\rho_s} \left(\frac{1}{r_s} + \frac{2}{t}\right) \left[\gamma_{s\ell} + \gamma_\ell (1 - \frac{\rho_s}{\rho_\ell})\right] \quad (2.3.15a.)$$

or, to a first approximation

$$T_o - T_{SK} \simeq \frac{T_o}{L\rho_s} \left(\frac{1}{r_s} + \frac{2}{t}\right) \left[\gamma_{s\ell} + \gamma_\ell (1 - \frac{\rho_s}{\rho_\ell})\right] \quad (2.3.15b.)$$

2.4.   The Change in Skin Melting Temperature due

to Other Effects.

As stated previously, a solid particle will melt

at the skin melting temperature (T_{SK}) determined by

$$\left(\frac{\partial \Delta F}{\partial \delta}\right)_{\delta = \delta_1} = 0 \qquad \text{equation (2.2.10)}$$

Here, $\Delta F(T)$ is the change in the total free energy of a

solid particle which on melting at the surface forms a liquid

skin of thickness δ.   However, if there is an additional

effect, for example, a strain or dislocation, which alters the

free energy of the solid particle or the liquid skin, the skin

melting temperature will occur at a different temperature,
T'_{SK}: This temperature can be derived in a similar manner
to that used for the normal skin melting temperature (T_{SK}).
For example, consider the effect of a uniform strain energy
in the solid of E per unit volume on a curved surface of
principal radii of curvature R_1 and R_2. If the surface
melts to a thickness δ, then the strain energy released
per unit area would be $E\delta$.

Therefore, in the presence of a strain in the curved
surface, the change in free energy on melting is

$$\Delta F' = \Delta F - E\delta \qquad (2.4.1.)$$

Melting will begin at the surface at the skin melting
temperature, T_{SK}', given by

$$\left(\frac{\partial \Delta F'}{\partial \delta}\right)_{\delta=\delta_1} = 0 \qquad (2.4.2.)$$

Hence, from equation (2.4.1.)

$$\left(\frac{\partial \Delta F}{\partial \delta}\right)_{\delta=\delta_1} - E = 0 \qquad (2.4.3.)$$

Following the derivation of the normal skin melting temperature
(T_{SK}) for a curved surface (see appendix A.2.) with the
inclusion of an additional term due to the strain energy,
we obtain for small changes of melting point

$$\frac{T_{SK}' - T_o}{T_o} \simeq \frac{-1}{L\rho_s} \left[\left(\frac{1}{R_1} + \frac{1}{R_2}\right) \left\{ \gamma_{s\ell} + \gamma_\ell \left(1 - \frac{\rho_s}{\rho_\ell}\right) \right\} + E \right] \qquad (2.4.4.)$$

For a discussion of the effect of strain due to the
bending of the tin platelets observed in the present
experiments, on the melting temperature of such particles,
see section 8.1.3.

CHAPTER 3.

APPARATUS

3.1 General.

The experiments were carried out in a J.E.M.6A
electron microscope, using a 80kV electron beam. The
resolution of the microscope with the specimen heater-
stage in position, was approximately 20Å.

The specimens were prepared by "in-situ" evaporation
of the material under investigation, onto thin substrates
mounted on a molybdenum grid in the heater cartridge. In
order to improve the vacuum in the vicinity of the specimen,
and therefore reduce the contaminating effects of the
residual gases, a liquid nitrogen cold trap was incorporated
between the evaporator unit and the heating stage (see section
3.2. and figure 3.1.).

The observations were recorded on "Ilford, Special
Lantern Contrasty" photographic plates, by using the
normal plate camera of the microscope. The plates were
outgassed for several hours, in a special chamber, using a
diffusion pump separate from the main pumping unit, before
inserting them into the microscope.

Magnifications in the microscope of up to 50,000
diameters were used. For analysis, the micrographs were
printed on bromide photographic paper, with a further
magnification of the micrographs.

3.2   The Cold Trap and Evaporator Unit.

A vacuum of the order of 4×10^{-7} torr was obtained in the microscope column without any extensive alterations being made to the specimen chamber arrangement (as for instance, Poppa, 1965). This was achieved by the incorporation of a liquid nitrogen trap, as previously mentioned.   The cold trap was placed as close to the specimen as possible.   The arrangement of the cold trap and the relative positions of the evaporator unit and the heating stage is shown in fugure 3.1.

The cold trap consisted of two sections, a large reservoir (capacity 0.5 litres) and a smaller one of about 0.1 litres.   The smaller reservoir was placed immediately above the specimen heating stage, and had a central cylindrical aperture allowing the passage of the electron beam and the evaporant.   (A detail description of the cold trap has already been published, see Peppiat & Sambles 1975). By placing the larger reservoir at a slightly higher level than the smaller one, the latter was constantly full of liquid nitrogen passing from the larger reservoir.   To increase the cold surface, and hence improve the pumping speed, fins were added to the smaller reservoir.

The specimen was evaporated "in-situ" from a spiral filament, by resistance heating.   The filament was mounted, off centre, on a rotating vacuum seal, so that it could be moved into the line of the specimen for the deposition, and
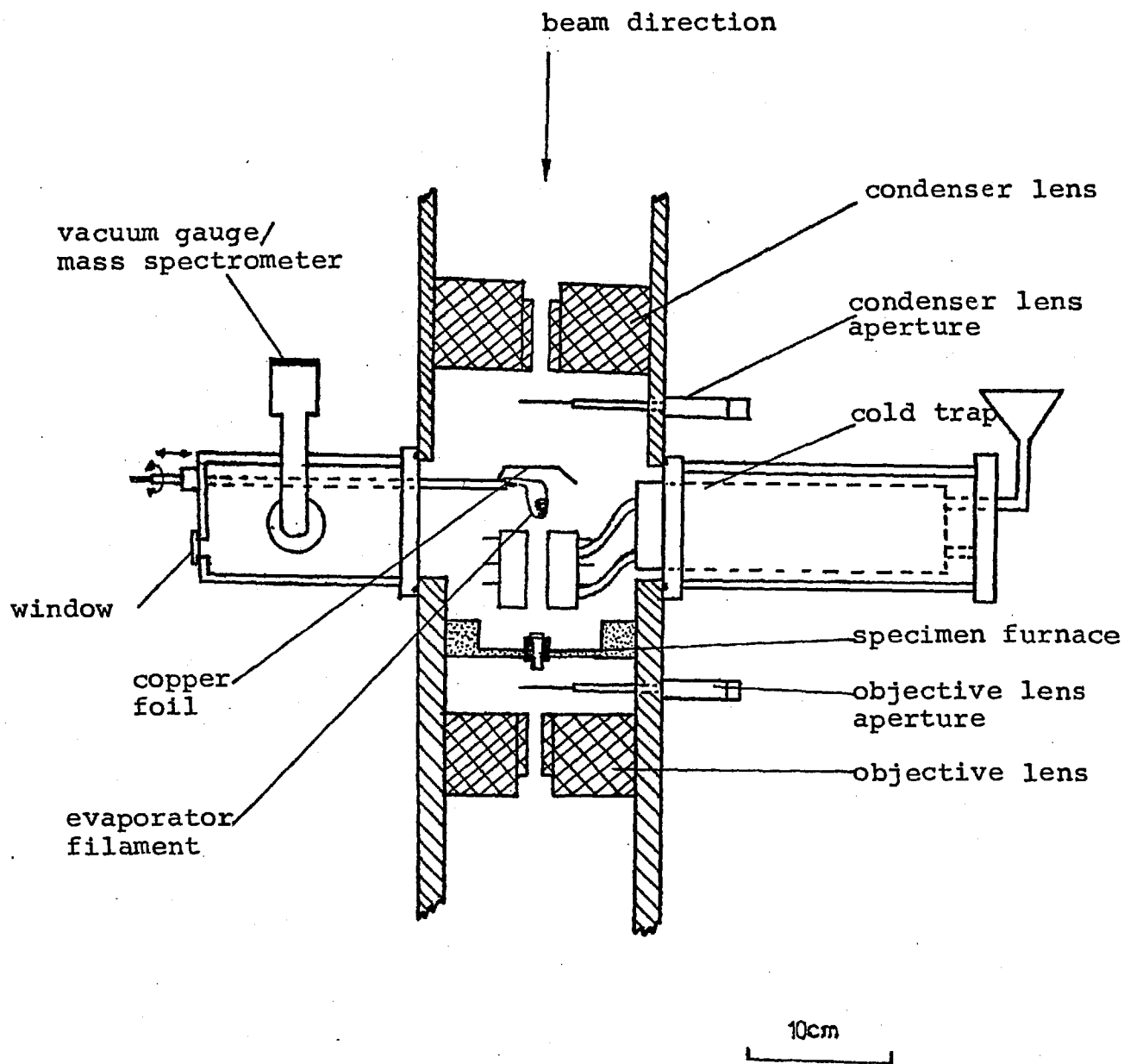
FIGURE 3.1.

Arrangement of the cold trap and evaporator unit in the electron microscope.

out of line of the electron beam for observation. A viewing window was attached to the evaporator unit, (see figure 3.1.), to facilitate the alignment of the evaporator filament with the substrate in the heater cartridge. The residual gas pressure was measured by a hot ion gauge mounted on one side of the evaporator unit.

By wrapping the external surfaces of the cold trap and evaporator unit with "Heat by the Yard" tape and baking them overnight at a temperature of 60 to $70^{\circ}C$, a vacuum of the order of $4x10^{-7}$ torr was generally obtained during an experiment.

The substrate provides some protection to the specimen (resting on top of the substrate) from being contaminated by the oil vapours streaming up the microscope column from the plate chamber. The major source of contamination of the specimen (even when the cold trap is being used) is probably the residual gases streaming downwards, from the electron gun chamber, along the path of the electron beam. In order to reduce the amount of these gases streaming downwards to the specimen, the condenser lens aperture was coated with a thin film of carbon. To avoid the deposition of the evaporant on this film, a copper foil was attached above the evaporator filament (see figure 3.1.). Although this produced a lower intensity image by slightly scattering the electron beam, no noticeable change was found in the resolution of the microscope.

3.3   The Mass-Spectrometer.

The ion-gauge in the evaporator unit (figure 3.1.),
could be replaced by a mass-spectrometer head to examine
the residual gases within the microscope vacuum.   The
spectrometer, a CENTRONIC AIG 50,   could also be employed
to measure   the total pressure in the microscope column.
The readings from the mass-spectrometer were recorded
directly on a chart recorder and are described in section
7.4.

3.4   Specimen Heating Furnace.

The specimens were heated in the microscope using
JEOL transmission furnaces.   The standard furnaces were
adapted to measure the specimen temperature as accurately
as possible, following the original design of Sambles (1973).
In this, a copper-constantan thermocouple was sandwiched
between two halves of a double tantalum washer and was
mounted above the specimen in the heater cartridge (figures
3.2. and 3.3.).   A second tantalum washer was placed below
the specimen.   The specimen grid was then tightly sandwiched
between the two washers using a tantalum screw.   The
apertures in the washers and the screw were made as small as
possible (∿0.5 mm), to minimise the heat loss by radiation,
and therefore achieve a uniform temperature across the
specimen.

The thermocouple wires were led through the centre
of the furnace, to terminals constructed on the top of the
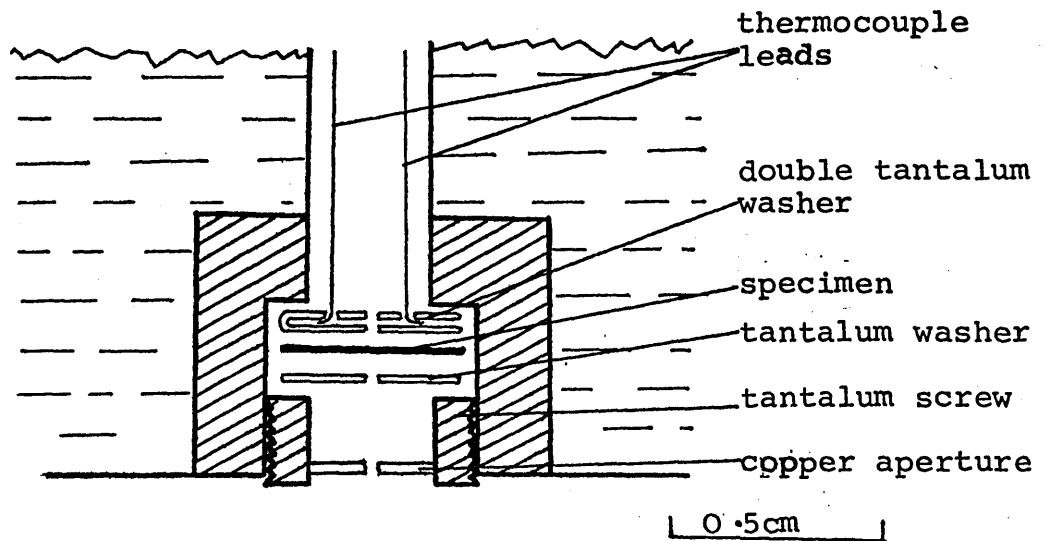
FIGURE   3.2.

Arrangement of thermocouple in specimen furnace.
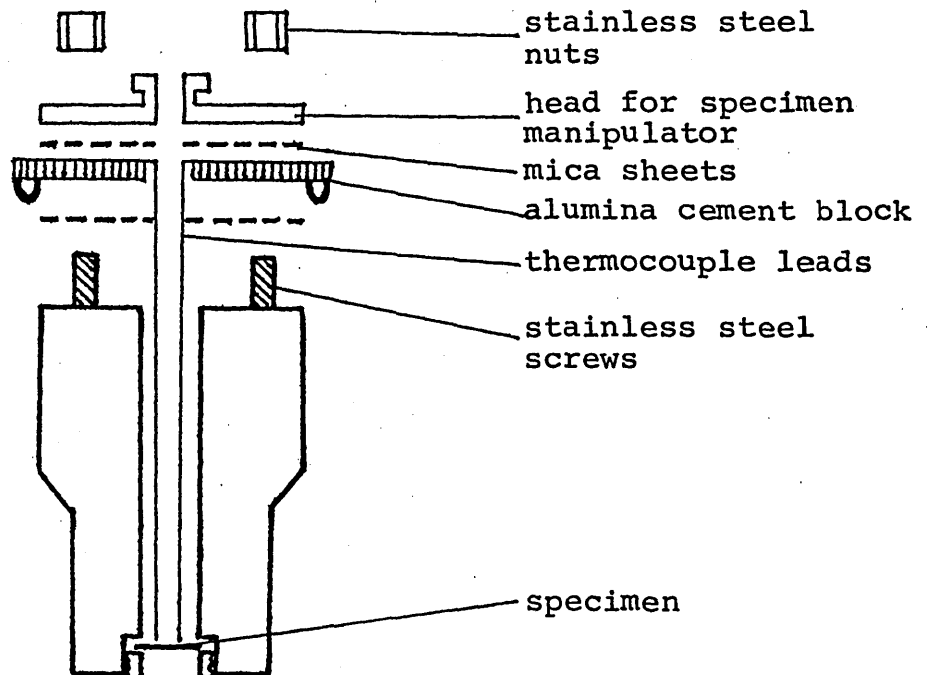
FIGURE 3.3.

Construction of thermocouple terminals on specimen furnace

furnace (see figure 3.3.).   The terminals were made of copper and were insulated from each other and the furnace using thin mica sheets and alumina cement - shaped to fit the top of the cartridge.   To help ensure that the specimen was at the same temperature as the thermocouple, very thin thermocouple wires (∿0.0610mm dia) were used to prevent the heat loss by conduction.

The furnaces were supported by a JEOL ceramic heating-stage.   The thermocouple terminals located into contacts built onto the heating-stage.   The respective copper and constantan wires were led away from these contacts, out of the microscope column using copper and constantan lead-throughs.   The external junction was maintained at the temperature of melting ice, and a digital voltmeter was used for the measurement of the resultant thermal e.m.f.

The heating current was supplied by a stabilized power unit (SOLARTRON AS 1218).   The current was measured using a milliammeter, to an accuracy of $\pm$3mA, a maximum of 0.8A being used.

In order to avoid specimen contamination , two separate heater furnaces were used for the experiments on bismuth and tin respectively.

CHAPTER 4.

EXPERIMENTAL METHOD.

4.1.   The Melting Experiments.

4.1.1. Determination of the Melting Temperature.

The main problem in the accurate determination of the melting temperatures of the specimens in an electron microscope is the effect of the localized heating by the intense electron beam.   The amount of beam heating will depend principally on the intensity and energy of the beam and the type and thickness of the substrates used.   By using thin ($\sim 100\overset{\circ}{A}$) carbon films as substrates, it was observed that the temperatures of the specimen regions under the 80kV electron beam (in the present experiments) were raised by 20 to 40K.   For accurate temperature measurements of the specimens, therefore, the effect of electron beam heating in the microscope has to be avoided.

A method in which all the relevant temperature measurements were made while the electron beam was not in operation and using the fact that liquid droplets can be supercooled by tens of degrees below the melting point, was devised by Dr.J.R. Sambles in this laboratory (Peppiatt and Sambles, 1975).   This method was successfully applied by Peppiatt (1973, 1975.) in the investigation of the melting of the small particles of bismuth and lead and is also followed in the present work, as described below.

The specimen film was deposited (see section 4.2.2.) and heated immediately (at a heating rate of 20K min^{-1}) to

within 5OK of the bulk melting point, see figure 4.1.   By
adjusting the heater current, the deposit was stabilized at
this temperature for about two minutes.   This temperature
was below the annealing temperatures to be used in the rest
of the experiment.   During the heating and the stabilization
of the temperature, the electron beam was switched off.
The specimen was next cooled by about 5OK, and again
stabilized, and at this stage, the beam was switched on for
observation.   As the beam heating is no more than 4OK under
these conditions, the deposit will still be below the first
annealing temperature.   The measurement of this temperature,
hence, will not be invalidated by the beam heating and this
temperature could be determined by the   thermocouples
within the accuracy of their calibration.

        A suitable region of the specimen close to a grid bar
(see section 4.3.1.) was chosen and a number of micrographs
were taken around this area.   These micrographs were taken
around an easily distinguishable mark in the substrate (for
example, a crack or a dust particle on the substrate) so that
the same area could be photographed repeatedly on the
subsequent heating and cooling of the specimen.   The beam
was next switched off and the deposit heated to a temperature
at which some of the particles were expected to melt.   The
temperature was stabilized for about two minutes, and the
specimen was again cooled by 5OK for the observation.   The
particles which melted would remain as supercooled liquid
droplets and the solid particles still present would not be
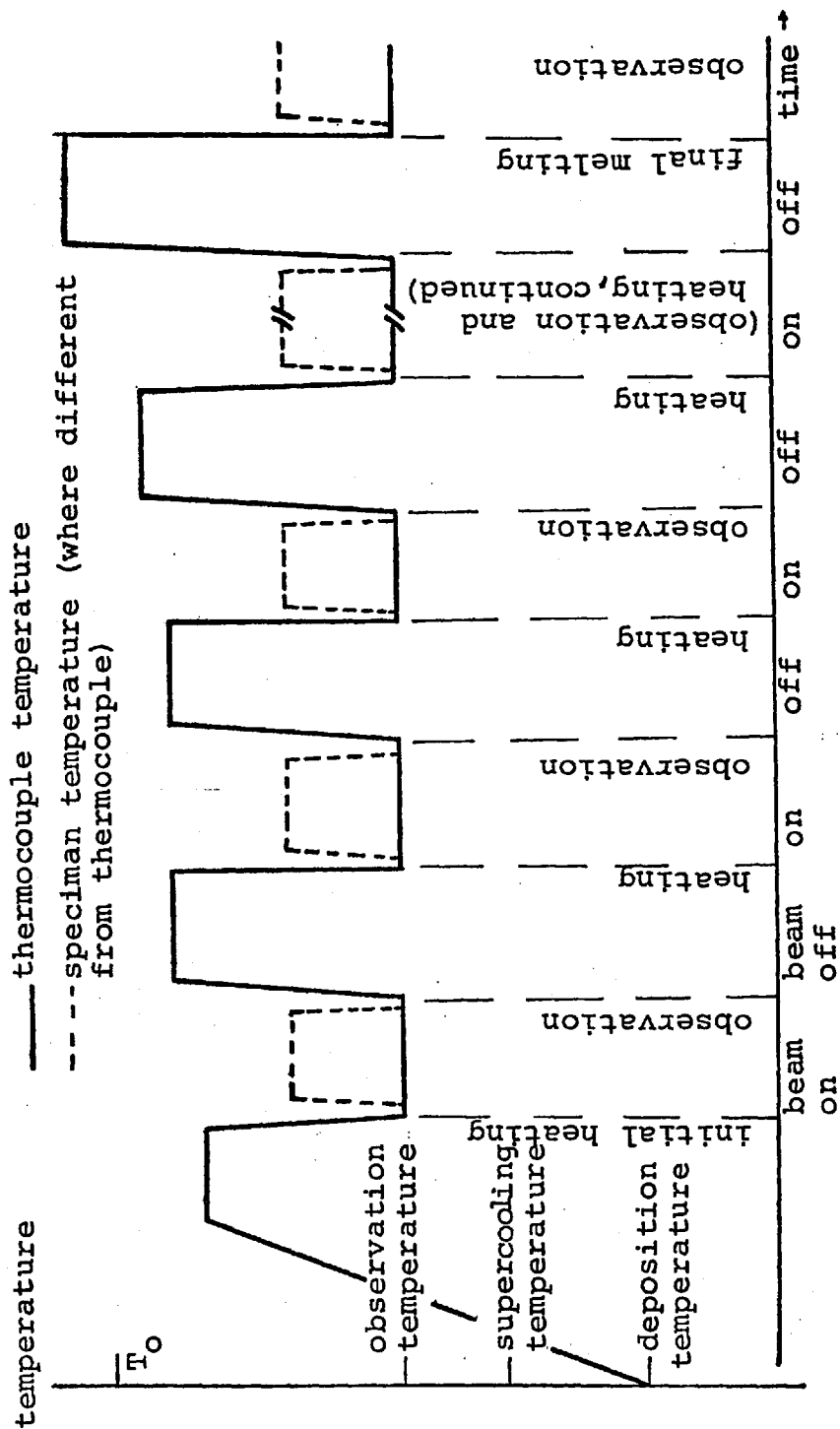
FIGURE 4.1.

Graph showing experimental method used in the melting of small particles.

melted by beam heating.   The specimen region previously
observed was re-photographed, so that any particle which
had melted, could subsequently be identified.   The
experiment was continued either by heating the deposit to
one particular temperature for various lengths of time, or
by gradually increasing the temperature used. The deposit
was finally completely melted by heating to above the
bulk melting point.   The volume of the particles could be
determined by measuring   the diameters of the resultant
liquid droplets.

4.1.2. Analysis of the Micrographs;

For analysis, the best set of micrographs from each
experiment was printed on photographic paper.   The micrographs
from the experiments on bismuth particles were enlarged by
a factor of four; for the experiments on tin, an enlargement
of about twenty was used, in order to increase the accuracy
of the measurement of the areas of the tin platelets.
Typical series of micrographs from an experiment on the
melting of tin platelets is shown in figure 4.2.

To determine on which subsequent micrograph each
individual solid particle had become molten , a method
identical to that employed by Peppiatt (1973), was used. A
grid, consisting of a few vertical and horizontal lines, was
drawn in identical positions on all the prints.   By using
the grid to identify each solid particle in each of the
micrographs - corresponding to each stage of an experiment -
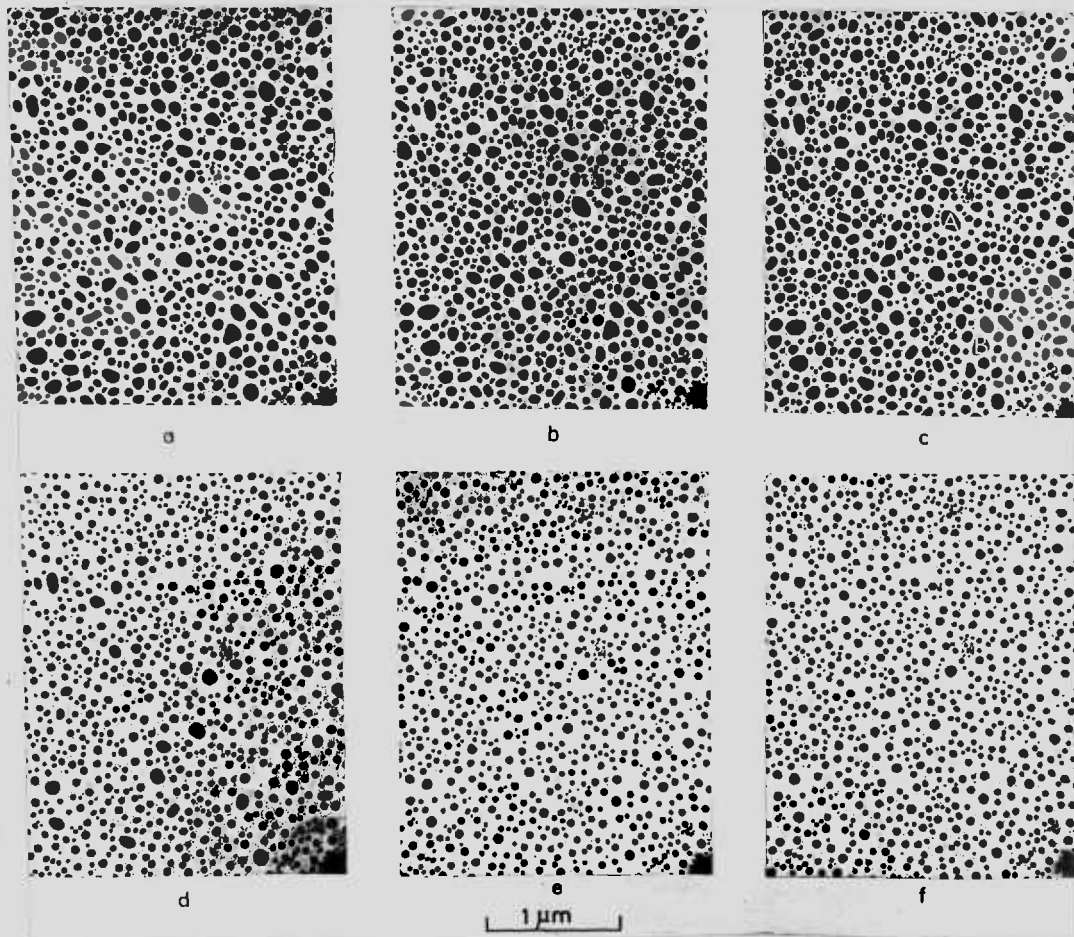
(<u>a</u>) T_O - 1OK for two minutes   (<u>d</u>) T_O - 4K for two minutes

(<u>b</u>) T_O - 8K for two minutes   (<u>e</u>) T_O - 2K for two minutes

(<u>c</u>) T_O - 6K for two minutes   (<u>f</u>) Particles melted

FIGURE 4.2

Typical series of micrographs from an experiment on the melting of tin particles.

the point at which the particles melted was noted on the
last micrograph containing the liquid droplets only.   This
was continued until all the solid particles were marked on
the last micrograph.   The number of particles melting at
each stage of an experiment could then be found from this
micrograph.   The diameters of the marked droplets were
measured   to the nearest half - or quarter millimeter using
a transparent ruler.   It was then possible to plot a histogram
of the sizes of the particles melting at each stage of the
experiment.

In order to find the thicknesses of the tin platelets,
it was necessary to measure their visible areas.   The areas
of the elliptical tin platelets (for example, particle A,
figure, 4.2(c)) were determined using the expression πab
for the area of an ellipse (where 'a' and 'b' are the major
and minor axes), while a planimeter was used to measure
the areas of the irregularly shaped platelets (for example,
particle B, figure 4.2(c)).   By neglecting the change of
density upon melting, the thicknesses of the platelets could
be determined by dividing the volumes of the liquid droplets
by the above areas of the platelets.   In determining the
volumes of the liquid droplets, a correction was made
allowing for the fact that the liquid droplet, resting on
a substrate, is not a complete sphere but forms a hemisphere.
For this reason, 80% of the volume of a complete sphere, as
found from the diameter of a liquid droplet, was taken while
determining the thicknesses of the tin platelets.

4.2.   Preparation of the Specimen Films.

4.2.1. Preparation of the Substrate Films.

In a majority of the melting experiments in the present work, amorphous carbon films of about 100Å thickness were used as substrates.   The carbon films were prepared, in a vacuum of 10^{-5} torr in a vacuum evaporation plant, by carbon-arc evaporation onto air cleaved mica substrates. The films were subsequently floated off in distilled water and were mounted on molybdenum microscope grids.   Molybdenum grids were chosen because this high melting point metal diffuses little at the temperatures of the present experiments and would therefore, not contaminate the specimens.

In addition to the amorphous carbon films, thin single crystalline films of molybdenite (MoS_2) and of graphite were occasionally used as substrates.   These substrates were obtained as thin cleavage flakes, using the technique of Pashley et al.(1964),   In this, they were repeatedly cleaved between two strips of "Sellotape" and were subsequently removed from the sellotape by dissolving the adhesive in chloroform.   The flakes were washed in several charges of chloroform, followed by washing in ethyl alcohol, and finally in warm distilled water.   Suitable flakes were collected onto a cleaved mica substrate which was then coated with a thin film of carbon in an evaporation plant.   The composite film was floated off in distilled water and the individual areas containing the flakes were collected on molybdenum

grids.   In this way, the crystalline flake was sandwiched
between the grid and the amorphous carbon film, ensuring
better adhesion to the grids and hence, improving the thermal
contact with the furnace.

4.2.2. Preparation of the Specimen Films.

Thin films ($\sim$ 100Å - $\sim$ 200Å) of bismuth and tin were
prepared by 'in-situ' condensation of the material onto thin
substrates mounted in the heater cartridge of the JEM-6A
electron microscope.   The condensation was carried out by
using a helical evaporator which had been previously outgassed;
a tungsten filament was used for making bismuth, and a
tantalum filament for making tin specimens. (Holland,1956).
Before each deposition, the furnace was heated to about
700K to remove any volatile contaminants from the substrate.
To reduce the contaminating effect of the residual gas vapours
on the specimen films, the deposition was generally carried
out with the substrates held at temperatures above room
temperature, following the suggestions of Ennos (1954) and
Pashley et al (1966).   By avoiding examination of the
specimen films with the electron beam immediately after
their depositon, and heating them rapidly to the first
annealing temperature (usually 50K below the bulk melting
point), a further reduction in the contamination rate was
effected.

In all of the experiments, "Spec-pure" materials
were used for deposition.

4.3. The Calibration Methods.

4.3.1. Calibration of the Thermocouples.

The thermocouples were calibrated for temperature measurements, 'in-situ', in the heater furnaces in conditions identical to the melting experiments. In this method, a very thick deposit was melted, using the normal heating and cooling cycle of a melting experiment. The deposit, approximately 0.1μm thick, was obtained by evaporating a full evaporator filament, which was normally sufficient for several experiments. Such a film could be assumed to melt very close to the bulk melting point. Starting from an annealing temperature of about 20K below the bulk melting point of the material, the deposit was heated in successive stages, with the temperature being increased by 1K at each stage of heating. The temperature at which general melting of the deposit occured was taken to be the bulk melting point, within a degree.

The thermocouples were calibrated in both the bismuth and the tin furnaces, and also, the three substrates - amorphous carbon, crystalline molybdenite and graphite - were used separately in the calibrations.

The method of melting a very thick specimen film also provided information about the presence of a thermal gradient across the substrates. It was observed that parts of the deposit farthest from the grid bars melted about 2K higher than those close to the grid bars. This indicates that the

parts of the substrate away from the grid bars were lower
in temperature by two degrees.than those close to them.
For this reason, melting experiments were performed by
selecting specimen regions close to the grid bars.

4.3.2. Calibration of the Microscope Magnification.

The calibration of the microscope magnification was
done by the method devised by Skinner (1969).   This method
required the use of a copper mesh with known spacing, which
when photographed in the microscope, gave a direct
magnification calibration.   The copper mesh employed had
previously been found by spectroscopic methods to have a
mean spacing of 8.45μm.   With the mesh placed in the
specimen position in the microscope, the lowest magnification
(about 1,800 diameters) was determined by photographing the
mesh and measuring the mesh image with a travelling microscope.
Seven other standard magnifications were then calibrated
with respect to this magnification by measuring the relative
sizes of bismuth and tin particles (remaining after a given
experiment) on the micrographs.   Magnifications of 1,800;
9,000; 11,000; 18,000;   30,000; 39,000 and 50,000 diameters
were used as the standard magnifications.

The accuracy of the calibration was of the order of
4% as determined by the comparison of micrographs of nominally
the same magnification.

CHAPTER 5

RESULTS OF THE MELTING OF SMALL PARTICLES

OF BISMUTH.

5.1.   Introduction.

The time delay in the melting of small particles

of bismuth has been found by Peppiatt (1973, 1975) to

depend upon the method of formation and the morphology of

the crystallites (see section 1.2.).   In particular, he

found that a platelet form had a characteristic time

sufficiently large at temperatures above the bulk melting

point (544K) to allow several crystallites to be superheated

by about seven degrees.   He also found that the compact

polyhedral particles formed by melting and resolidifying

the platelets exibited the time delay phenomenon but at

temperatures below the bulk melting point.

In the present experiments, a study has been made

of the existence of a possible time delay in the bismuth

crystallites larger than those investigated by Peppiatt

who generally carried out experiments with particle sizes

ranging from 400Å to 1,000Å in diameter.   It was found

that the particles above 1400Å in diameter melted 'sharply'

at the bulk melting point, and therefore the characteristic

time of melting for these particles could not be determined

within the time scale of the present experiments (section

5.4.1.).   In these experiments, it was also found that the

polyhedral particles present in an initial solid layer have

similar characteristic times to those of the resolidified polyhedra.   The characteristic time of the resolidified polyhedral particles was found, at some temperatures,   to vary inversely with the surface area (section 5.4.3.).

Although the majority of the melting experiments were carried out with carbon substrates, experiments were also performed to investigate the effect of a crystalline substrate on the melting of bismuth particles.   The crystallites obtained on the   001   cleavage flakes of molybdenite again showed the time delay.   The crystallites on this substrate however, could only be superheated by about two degrees (section 5.4.4.).   For each form of crystallite on carbon and molybdenite substrates, the characteristic time was found to be a well-defined function of temperature (section 5.4.5.)

5.2.   General Observations On the Bismuth Melting
Experiments.

5.2.1.   Bismuth on Carbon Substrates.

For most experiments, bismuth films of thicknesses from about 100Å to 200Å were deposited on carbon substrates at room temperature.   The deposited layers usually consisted of a continuous, mottled film (figure 5.2.1a). producing highly textured diffraction patterns (figure 5.2.1b), consistent with the basal   (000.1) plane (in the hexagonal description) of a large proportion of the deposit lying parallel to the substrate.   The texturing was found to

(a)   (b)
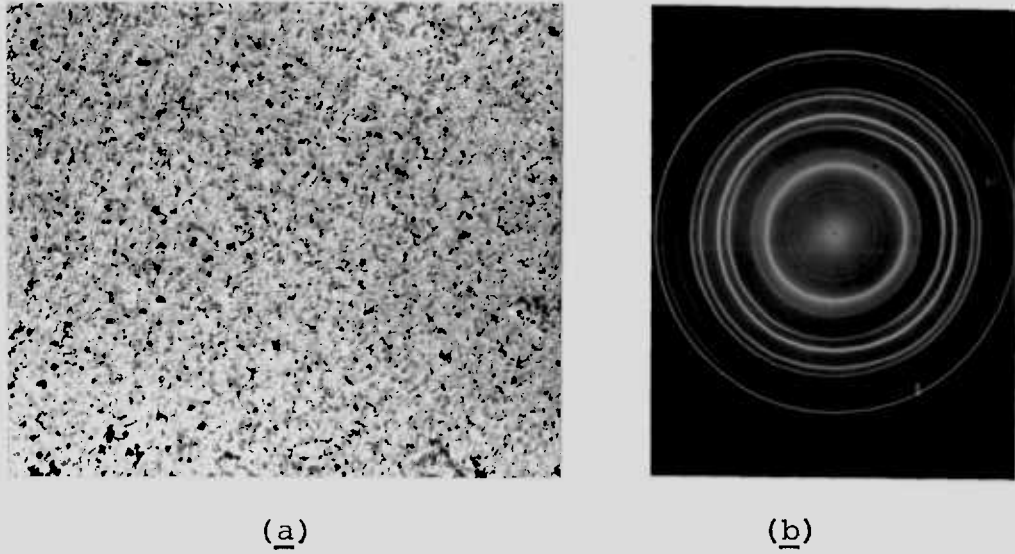
FIGURE 5.2.1.

A bismuth deposit (~ 100Å thick), at room temperature, and
the corresponding diffraction pattern.

(a)   (b)

O'4μm
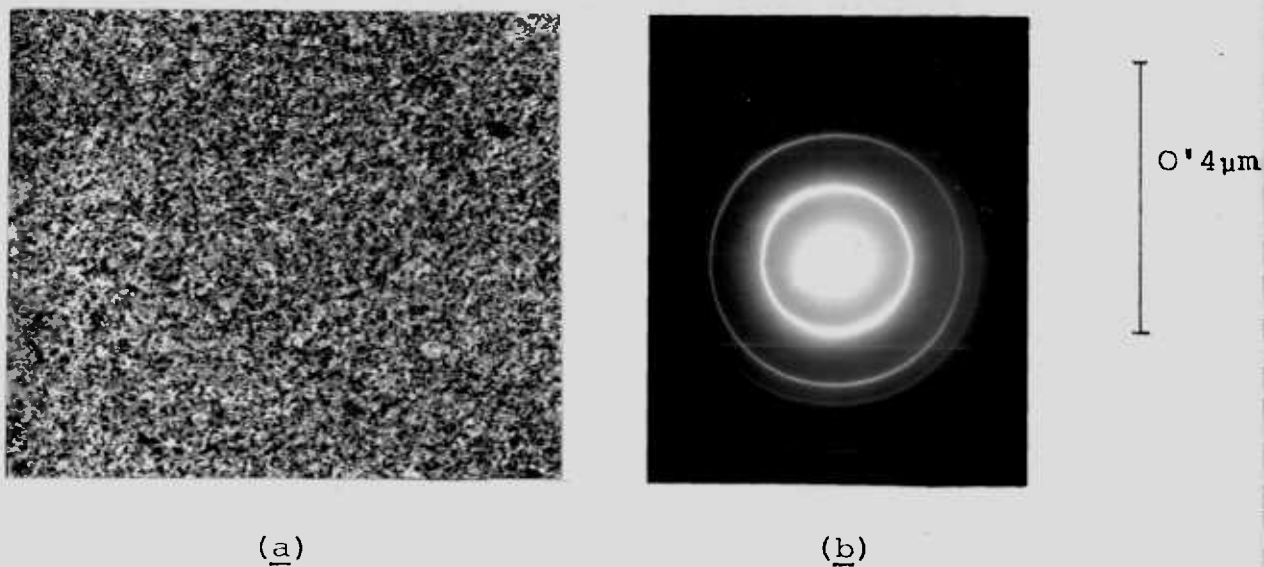
FIGURE 5.2.2.

A bismuth deposit (~ 200Å thick), at room temperature, and
the corresponding diffraction pattern.

increase with increasing thicknesses of the deposit; figures 5.2.2a and 5.2.2b show such a deposit of 200Å thick and the corresponding diffraction pattern which is almost completely fibrous.

When the layers were heated to within 50K of the bulk melting point, pronounced diffusion occurred (see figure 5.2.3.), causing the deposit to break up into islands. At this stage, sharp edges have formed together with many 120° angles characteristic of a basically hexagonal structure viewed along the (000.1) direction. Upon further heating, the misshapen crystallites tended to either split into separate crystallites, or to grow into a more perfect crystal, causing the particles to become thicker.

The crystallites, after melting and resolidification, formed as compact polyhedra (figure 5.2.4a). The diffraction pattern from such a layer is what would be expected from a completely random layer (figure 5.2.4b).

The crystallites obtained in a layer are classified according to their origin and morphology as follows:

(i) PLATELET (TYPE I) PARTICLE.

These are in the form of thin platelets, transparent to the 80KV electron beam and having shapes ranging from elongated to regular hexagons (for example, particle marked A, figure 5.2.5a). These crystallites all have six sides, containing angles of 120°. Their heights are small relative
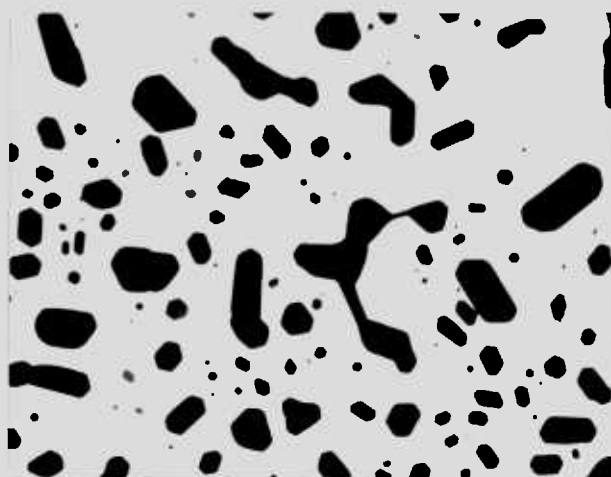
FIGURE 5.2.3

The break-up of a layer of bismuth
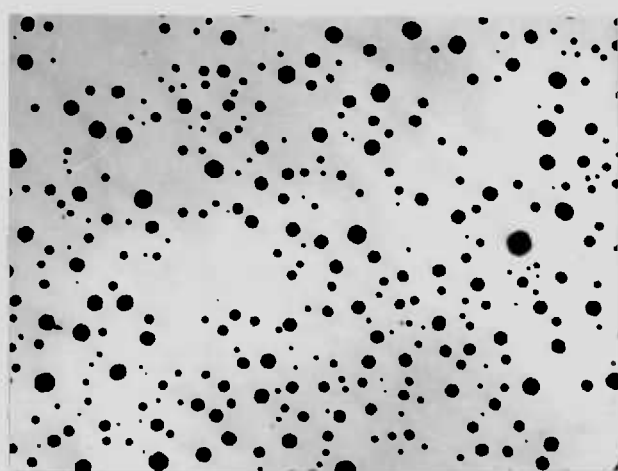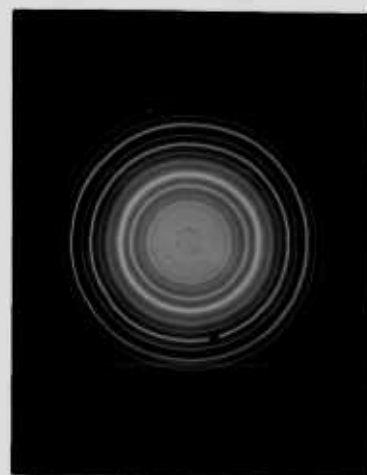
0,4 μm   (a)   (b)

FIGURE 5.2.4.

The bismuth crystallites in a layer which had been melted
and resolidified, and the corresponding diffraction pattern
from the layer.

to their basal dimensions, as may be inferred from the size of the spherical liquid droplets formed upon melting (figure 5.2.5b). The shapes of these crystallites remained unchanged on heating, till finally melting into spherical liquid droplets. These particles are identical to those termed platelet (type I) particles by Peppiatt (1973, 1975), and in the present work the same nomenclature is retained. The characteristic time of melting of these particles has been determined by the author in conjunction with the polyhedral particles obtained in a single layer, (see sections 5.4.1. and 5.4.2.)

(ii) POLYHEDRA (TYPE I) PARTICLE.

Particles obtained by heating layers of 200$\overset{o}{A}$ or more thickness, were initially irregular in shape, having several re-entrant angles, many of which vanished on further heating near the bulk melting temperature (figure 5.2.6; see also figure 5.4.1a). These are thick crystallites, with a height-to-radii of the liquid droplets ratio in the range 0.6 to 0.8. The maximum liquid droplet diameter from such particles was about 6500$\overset{o}{A}$, while the minimum was of the order of 1400$\overset{o}{A}$.

(iii) POLYHEDRA (TYPE II) PARTICLE.

Particles obtained by melting and resolidifying the above platelet (type I) and polyhedra (type I)

particles, are nearly spherical in shape. These

particles, however, could only be distinguished

from their liquid droplets from the faceting on

the side faces. The sizes of such particles

ranged from a few hundred angstroms to a few thousand

angstroms in diameter of the liquid droplets.

These particles, obtained similarly and referred to as

polyhedra (type II) particles by Peppiatt (1973,1975), will

also be termed polyhedra (type II) particles .

(iv) POLYHEDRA (TYPE II[*]) PARTICLE.

These are similar in morphology to the above

polyhedral particles, except that they occurred in

an initial solid layer (for example, particle marked

B, figure 5.2.5a). They were found   in layers

with thicknesses intermediate between $100\overset{o}{A}$ and

about $200\overset{o}{A}$, occurring together with the platelet

(type I) particles, and had sizes upto a few hundred

$\overset{o}{A}$ngstroms in diameter.

5.2.2. Bismuth on Molybdenite Substrates.

For the experiments on the molybdenite substrates,

the films were always deposited on the substrates at temperatures

a few degrees below the supercooling temperature.   In most

of the experiments, the deposits were not examined after the

evaporation, but immediately heated to the experimental

temperature in the absence of the electron beam.   Figure

5.2.7a shows a layer of about $100\overset{o}{A}$ thickness, which however
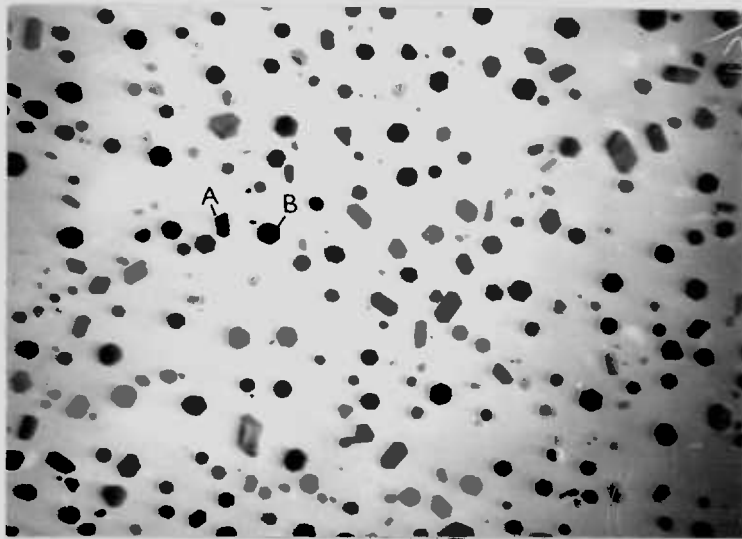
(<u>a</u>)   ⌊_ O'4µm _⌋
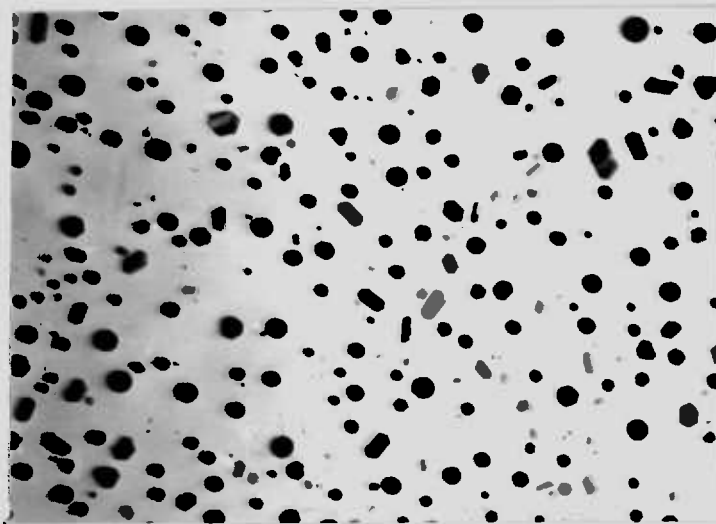
(<u>b</u>)
                        <u>FIGURE   5.2.5.</u>

A layer of bismuth (∿150Å thick) containing platelet (type I)
and polyhedra (type II*)particles (b) after heating the
layer (a) as above for 2 minutes at T_O- 4K.
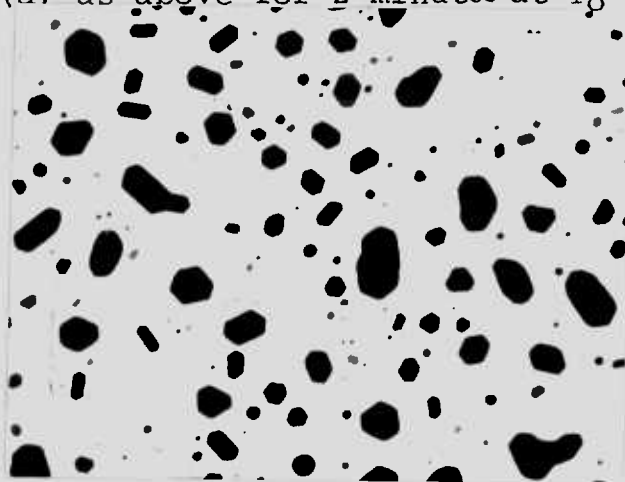
                                                        ⌊_ O'8µm _⌋

                        <u>FIGURE   5.2.6</u>

A bismuth layer (∿200Å) containing polyhedra (type I) and
platelet (type I) particles.

was observed after being deposited.   The layer consisted of a large number of elongated ("needle-like") oriented crystallites, joined with each other at an angle of $\sim 60^{\circ}$ into a 'mesh-like' pattern.   The diffraction pattern from the layer indicated a large proportion of these crystallites to be oriented with their (000.1) plane parallel to the substrate.

When the above layer was heated to within 30K of the bulk melting point, the mesh-like pattern broke up into individual crystallites (figure 5.2.7b).   Many of these still retained their needle-like shape, while some were found to be irregular in shape.   In general, these particles had the ratio of their heights to the radii of the liquid droplet in the range 0.4 to 0.6;   the ratio of the length to the diameter of the liquid droplet of the needle-like particles varied between 2 and 5.   Upon melting   the crystallites, the liquid droplets were always located at one end of the crystallites.   By resolidifying the liquid droplets, nearly spherical particles were obtained.   Due to the lack of any distinguishable faceting in almost all of these particles, no melting experiments on such particles were carried out.

Films thicker than those above were found, for the most part, to be almost continuous, containing a few irregular holes.   These layers did not break up into individual crystallalites when heated to temperatures close to the bulk melting temperature;   instead oriented hexagonal holes developed.   These layers melted at the bulk melting point.

(a)

L O.2μm   l

(b)

FIGURE 5.2.7

(a)   A layer of bismuth ($\sim100\mathring{A}$ thick), on molybdenite
      substrate (substrate temperature, 425K);
(b)   The same layer after heating for two minutes at 30K
      below the bulk melting point (544K).   (The arrow
      indicates a 'decorative' step on the substrate).

5.3.   The Experiments on Time Delay.

By heating the crystallites in a layer of bismuth to the same temperature several times, the variation in the number of crystallites remaining solid was determined as a function of time.   Decay curves were then plotted in which either $\frac{N}{N_O}$ or $-\ln \frac{N}{N_O}$ was plotted against the total time, t, for which the layer was heated.   From these curves, a value of the characteristic time (τ) of melting at the given temperature was determined using the equation

$$N = N_O \exp \left(- \frac{t}{\tau} \right)$$

where N_O is the initial number of solid particles, $N(t)$ is the number remaining solid when heated at a given temperature for the total time t.   For those experiments with very large or very small characteristic time, however, a value of τ was estimated from the small portion of the decay curve obtained.

It was often found possible with layers having large particle density, to repeat the heating process by increasing the temperature in steps of 1K, provided a sufficient number of particles still remained solid at the end of one experiment. By this, values of τ could be determined at several temperatures by using the same specimen.   This was continued until the number became too low (less than 50).

5.4. The Characteristic Time of Melting for the Various Types of Particles.

5.4.1. Absence of Time Delay in the Polyhedra (Type I) particles.

When the polyhedra (type I) particles were heated to different temperatures below the bulk melting point, for various periods of time, it was observed that none of these particles melted at these temperatures.   All these particles, however, melted at the bulk melting temperature when heated to this temperature for about two minutes which was the maximum time required to stabilize the temperature over the entire specimen.

Figure 5.4.1a shows a series of micrographs from a typical experiment in which the layer also contained the platelet (type I) particles.   A histogram of the size distribution (given as the diameter of the liquid droplets) is shown in figure 5.4.1b.   The minimum size of the polyhedral particles in the layer is $\sim$ 1,400Å in diameter. The layer was heated to temperaturers of 4K, 2K and 1K below the bulk melting point for total time of 20, 10 and 10 minutes at each temperature respectively.   The layer was finally heated at the bulk melting temperature for 2 minutes.   At temperatures below the bulk melting point, the number of platelet type particles only decreased steadily each time the layer was heated.   The polyhedral particles gradually became thicker and grew into regular hexagons but otherwise remained
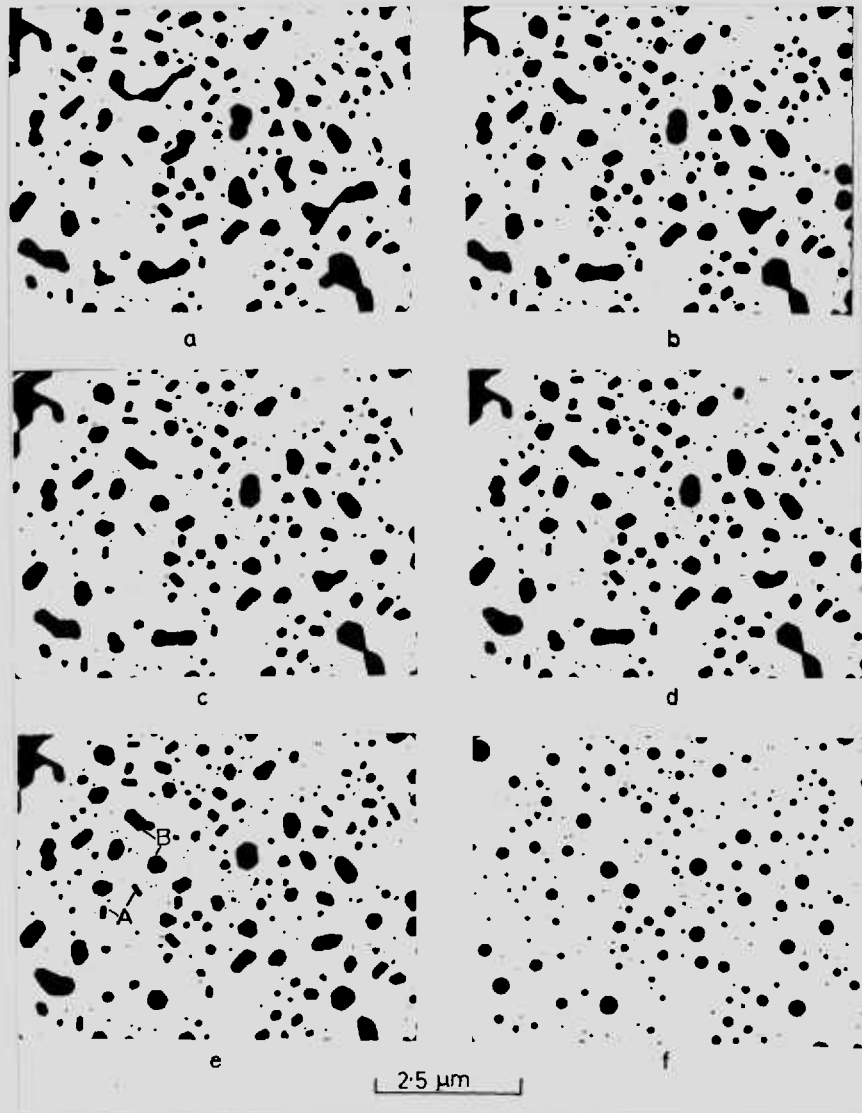
(a) T_O – 4K for 10 minutes

(b) T_O – 4K for a further 10 minutes

(c) T_O – 2K for 5 minutes

(d) T_O – 2K for a further 5 minutes

(e) T_O – 1K for 5 minutes.

(f) After 2 minutes at T_O

FIGURE 5.4.1.a

A typical series of micrographs from a time delay experiment on a bismuth layer containing polyhedra (type I) and platelet (type I) particles.

solid during this period. The polyhedral particles melted
at the bulk temperature, while a few platelets still remained
solid at this temperature. The situation is shown
graphically in figure 5.4.2. in which $\frac{N}{N_o}$, the fraction of
particles remaining solid is plotted against the total time
(t) for the two types of particles. The temperatures are
also shown along the abscissa. Since none of the poly-
hedral particles melted at the temperatures below the bulk
melting point, the graph for these particles remains parallel
to the abscissa. The slope of the graph, however, changes
abruptly at the bulk melting point when all of these particles
melted. In view of the 'sharp' melting of these particles
at the bulk melting temperature, τ for these could not be
determined; also at temperatures below the bulk melting
point, τ is too large to be determined in the present
experimental time. Values of τ for the platelet type
particles could be determined at each of the experimental
temperatures.

Thus, even if a time delay in the melting of the
polyhedra (type I) particles does exist, the τ of such
particles is so high (at temperatures below the bulk melting
point) and so low (at the bulk melting point) that it could
not be determined in the time scale of the present experiment.
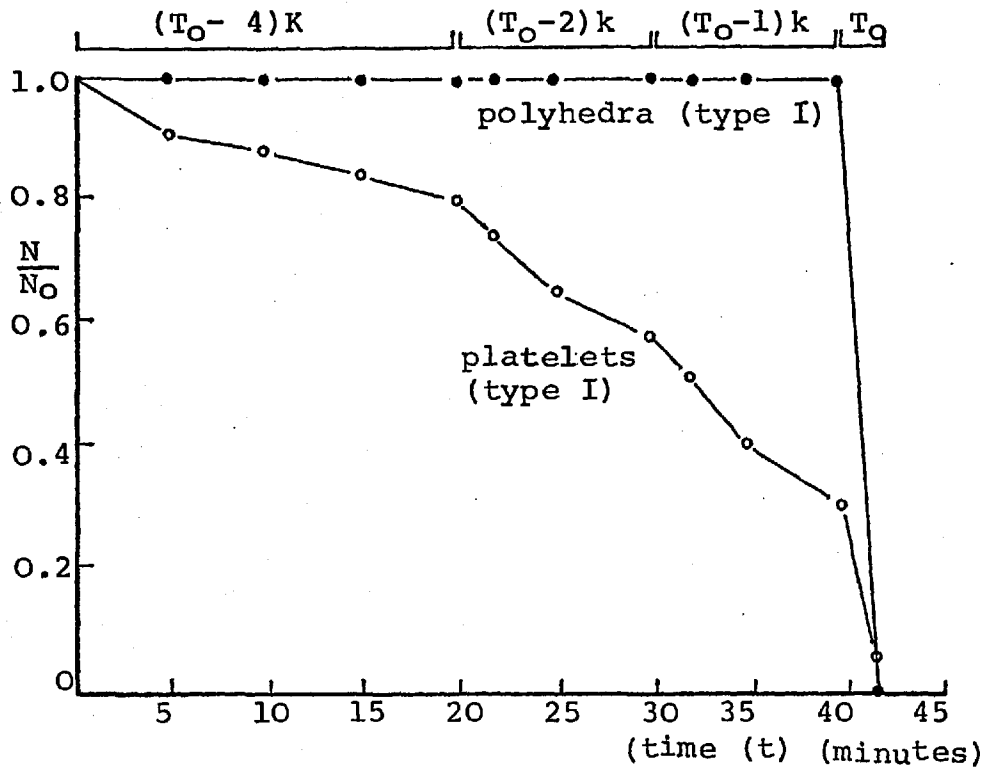
FIGURE 5.4.2.

Graph showing the variation in the number of bismuth
type I polyhedra and type I platelets remaining solid (N)
with time (t).
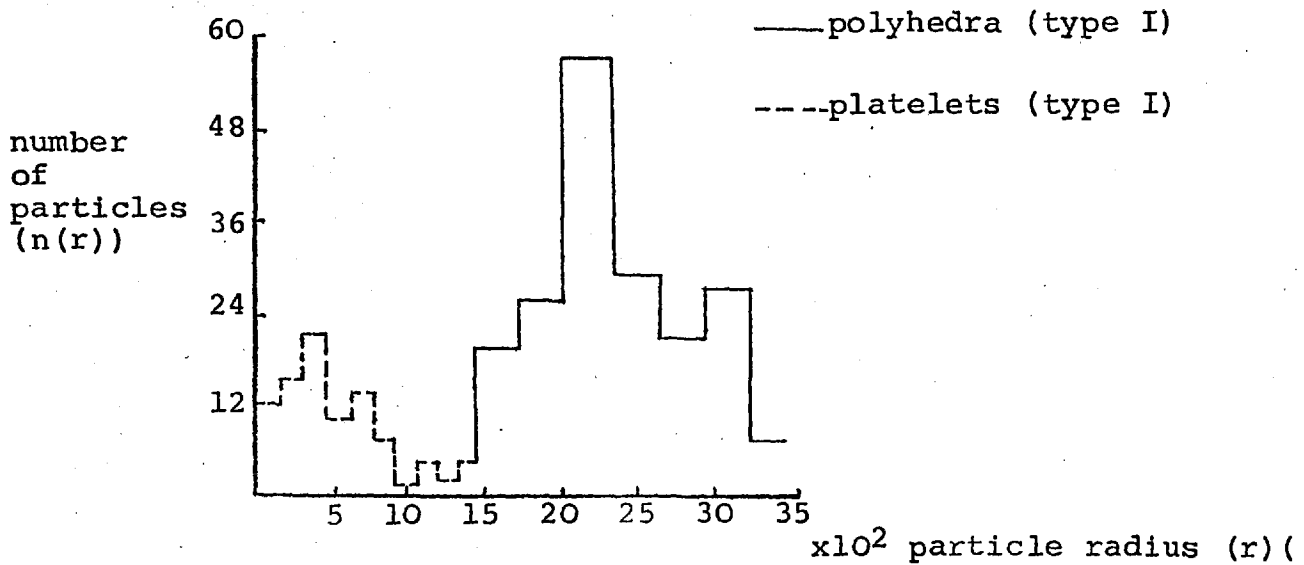
FIGURE 5.4.1b.

Size distribution of the bismuth type I polyhedra and
type I platelets, shown in figure (5.4.1a).

5.4.2.   The Characteristic Times of Platelet (Type I)

Plus Polyhedra (type II*) Particles in a Single Layer.

Figure 5.4.3. shows the decay curve from a time delay experiment on a layer containing the platelet (type I) and polyhedra (type II*) particles.   In this, $-\ln \frac{N}{N_O}$ is plotted against time, t.   The graph is curved in the initial stages of heating, before approximating to a straight line. A value of τ was determined from the straight line portion of the curve.   A lower value of τ is, however, represented by the initial curved portion of the decay curve, indicating a higher melting rate (which is $\frac{1}{\tau}$) at this stage.

It was observed that a large number of the polyhedra (type II*) particles melted during the initial heating period, compared to the platelet (type I) particles (for example, see figure 5.2.5.).   In figures 5.4.4a. and 5.4.4b. decay curves have been drawn separately for the polyhedra and the platelet type particles.   The curves approximate to straight lines in each case and therefore, values of τ for both types of particles could be determined.   It is found that these curves jointly give the decay curve of figure 5.4.3.

5.4.3.   The Characteristic Time of Polyhedra (Type II)

Particles as a Function of Surface Area.

The polyhedra (type II) particles in a layer were divided into suitable size ranges (usually in intervals of 50Å), so that a large number of particles (at least 150) was
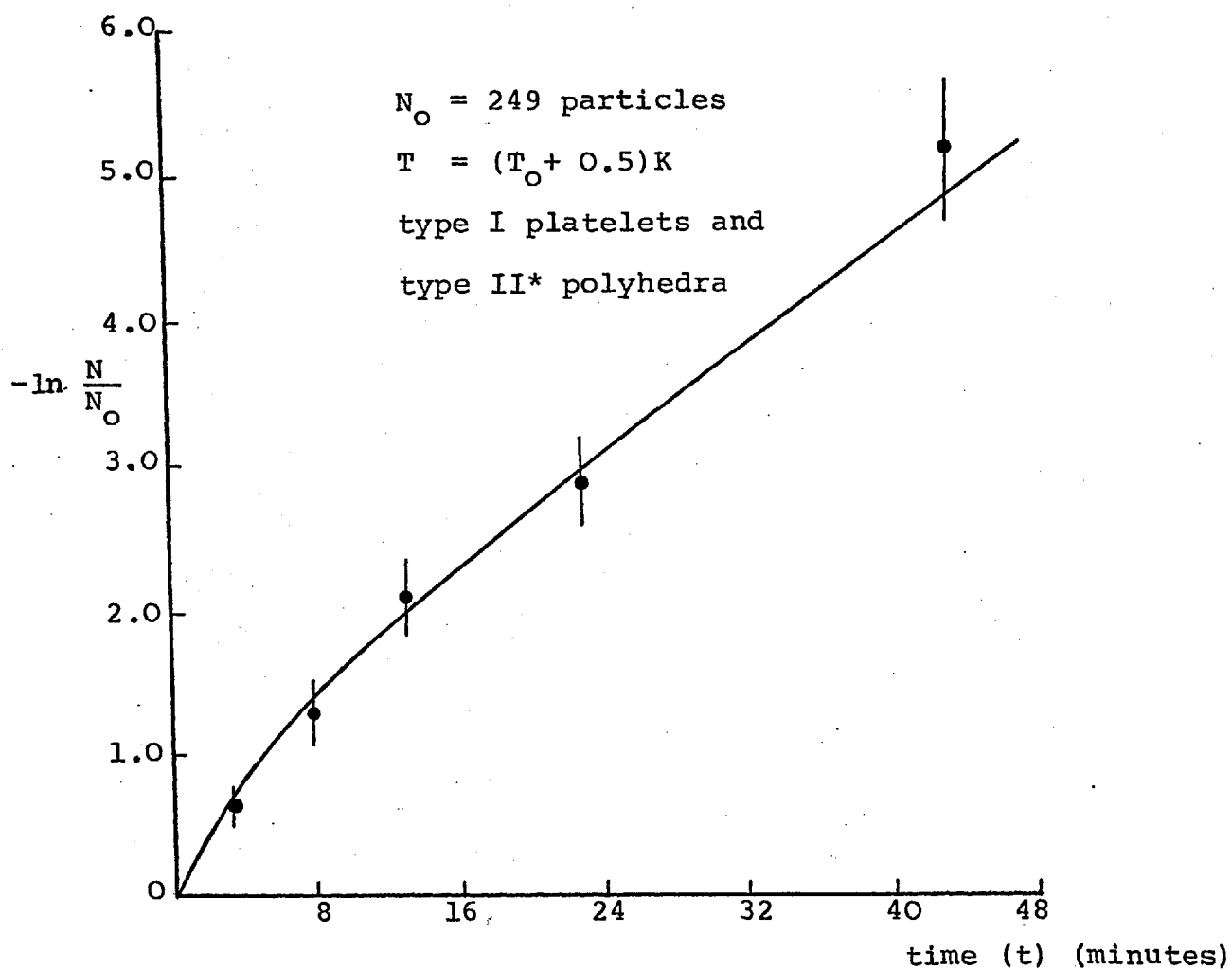
FIGURE 5.4.3.

Variation in the number of bismuth type I platelets and type II* polyhedra remaining solid (N) with time (t), plotted on a logarithmic scale.

FIGURE 5.4.4.

(a)

Variation in the number of bismuth type II* polyhedra
remaining solid (N) with time (t).
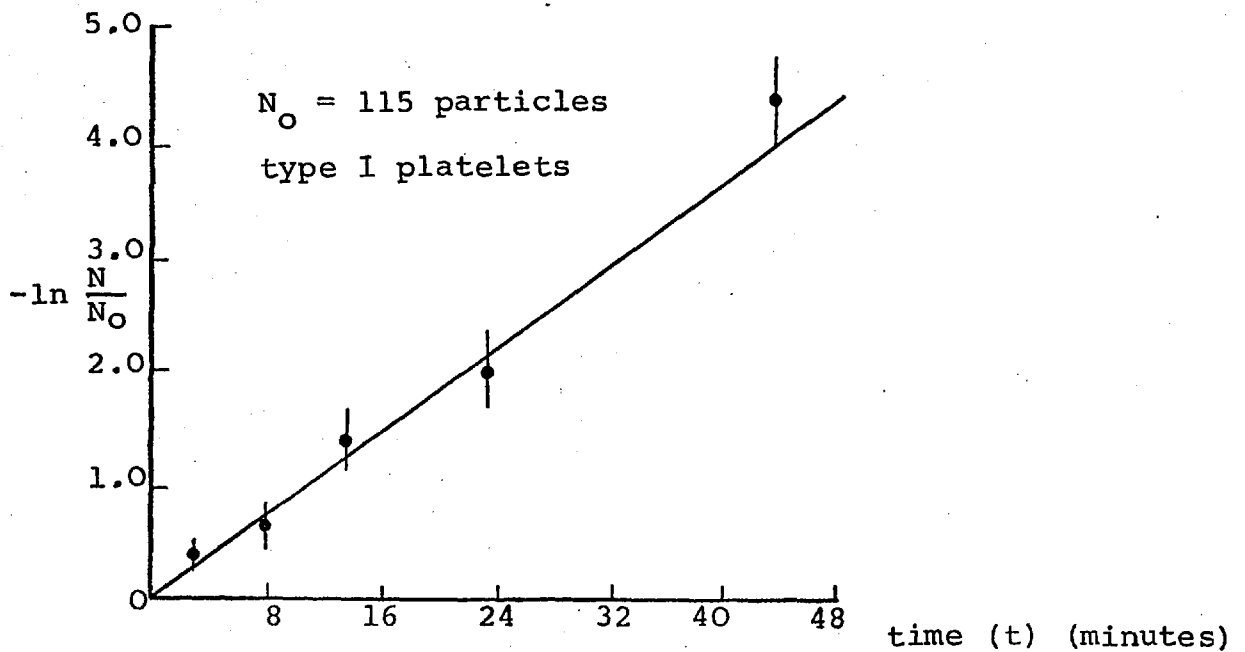
(b)

FIGURE 5.4.4.

Variation in the number of bismuth type I platelets
remaining solid (N) with time (t).

included in each size range,   The characteristic times of

melting of the particles in each size range was determined

at different temperatures...   This was done using either

the particles in different specimens at different temperatures

or using specimens with large particle density, by heating

the particles at a higher temperature from the previous one,

provided a large number of particles in each size range

still remained solid at the end of the first experimental

temperature.

It is found that at temperatures within a few degrees

of the bulk melting point, the characteristic time of the

particles depended inversely on their surface area.   The

surface area was taken as being proportional to r^2, where r

is the radius of the liquid droplet.   Figure 5.4.5. is a

plot of τ versus $\dfrac{1}{r^2}$ at a temperature of 3K below the bulk

melting point.   At temperatures much lower than the above,

very few of the larger particles melted, and consequently

τ is very high for these particles at such temperatures

At these temperatures, there was a departure from linearity

of the characteristic time with the surface area, and the

graph curved upwards at the larger particle end of the graph

(figure 5.4.6, curve (a)),   Upon heating the same particles

at a higher temperature, the linearity of the characteristic

time with the surface area of the polyhedral particles was

observed once again (figure 5.4.6, curve (b)).
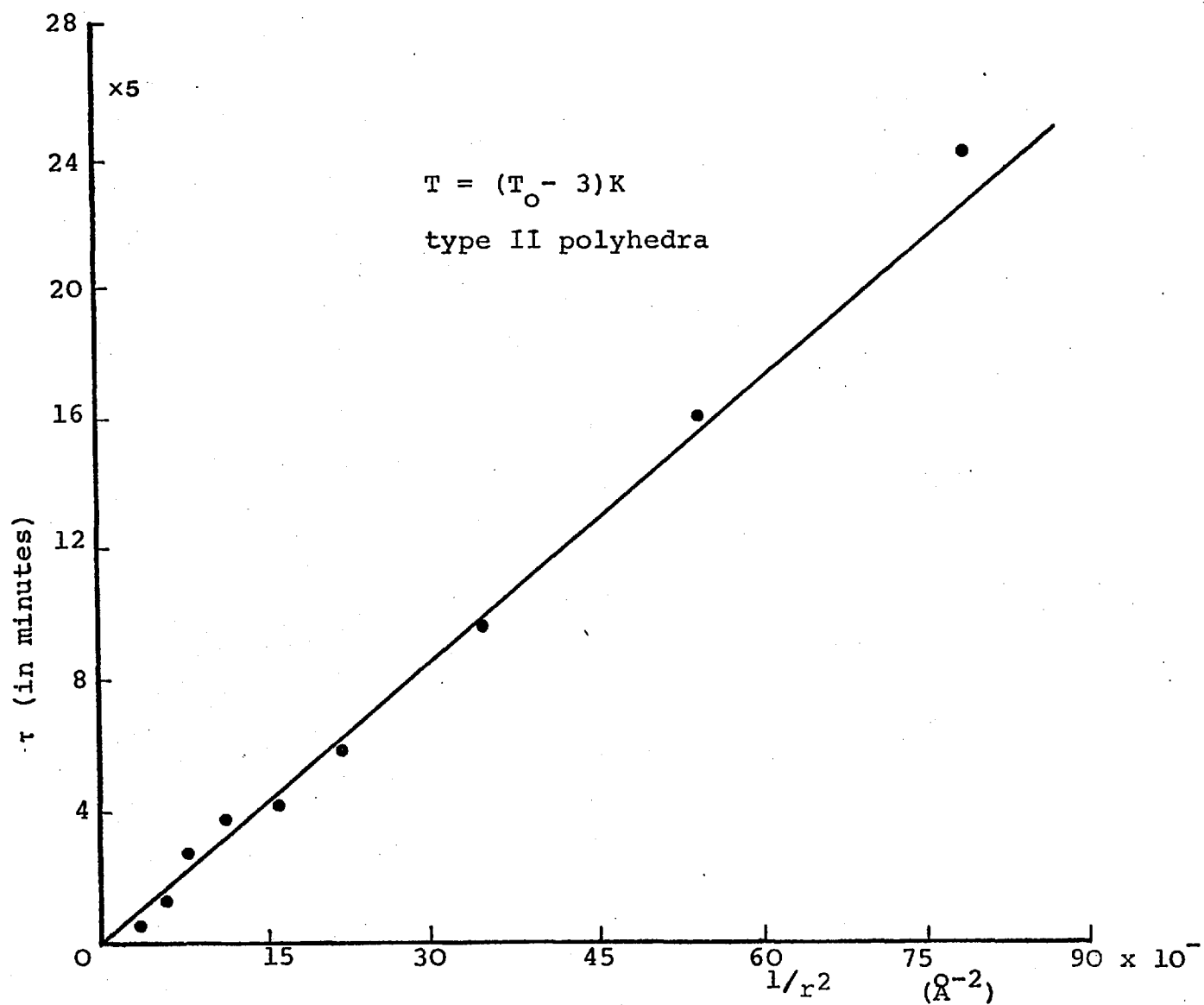
FIGURE 5.4.5.

Variation of the characteristic time (τ) with the surface area (r^2) of the polyhedra type II particles (r is the particle radius).
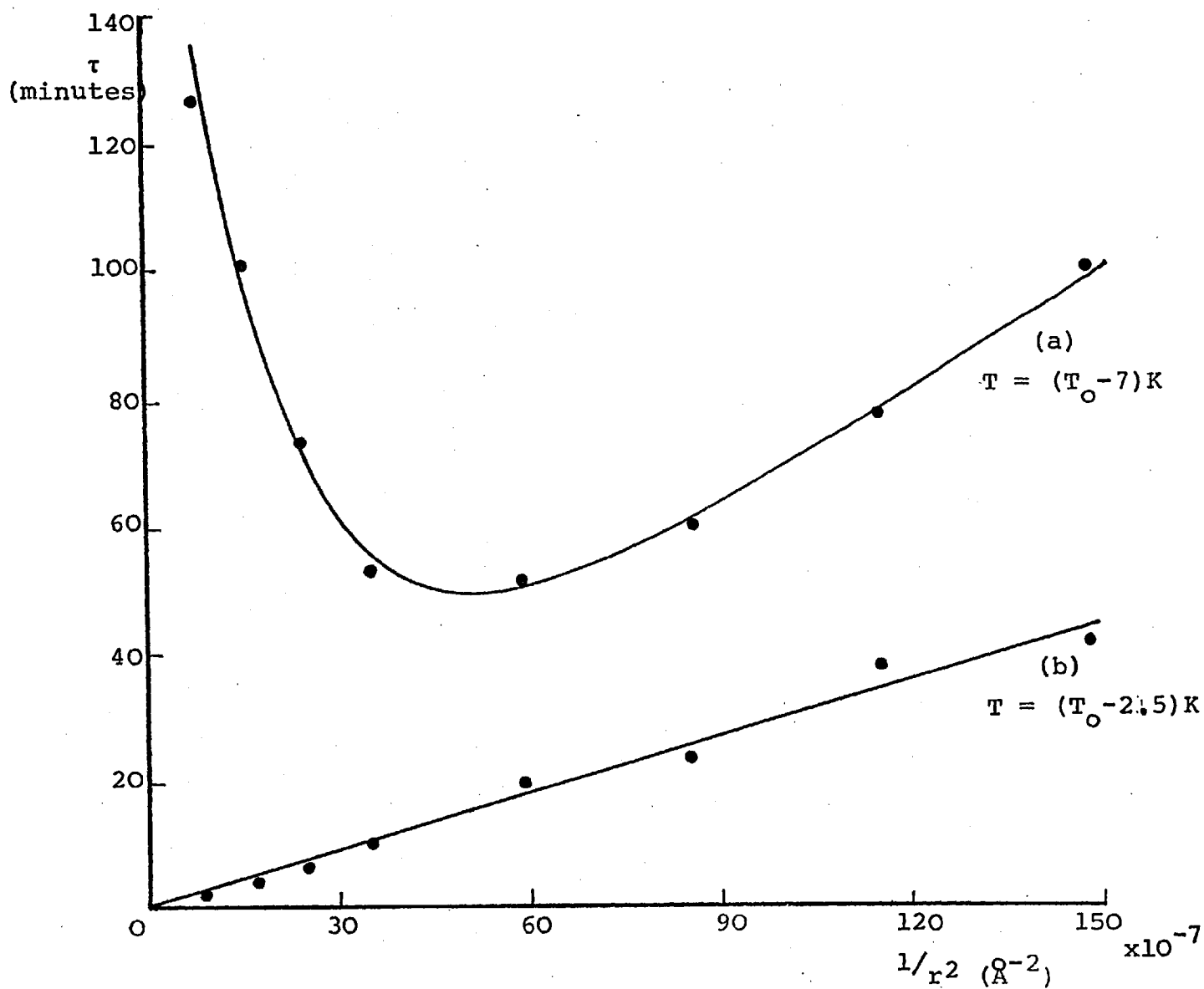
FIGURE 5.4.6.

Variation of the characteristic time (τ) with the surface area (r^2) of polyhedra type II particles at two different temperatures.
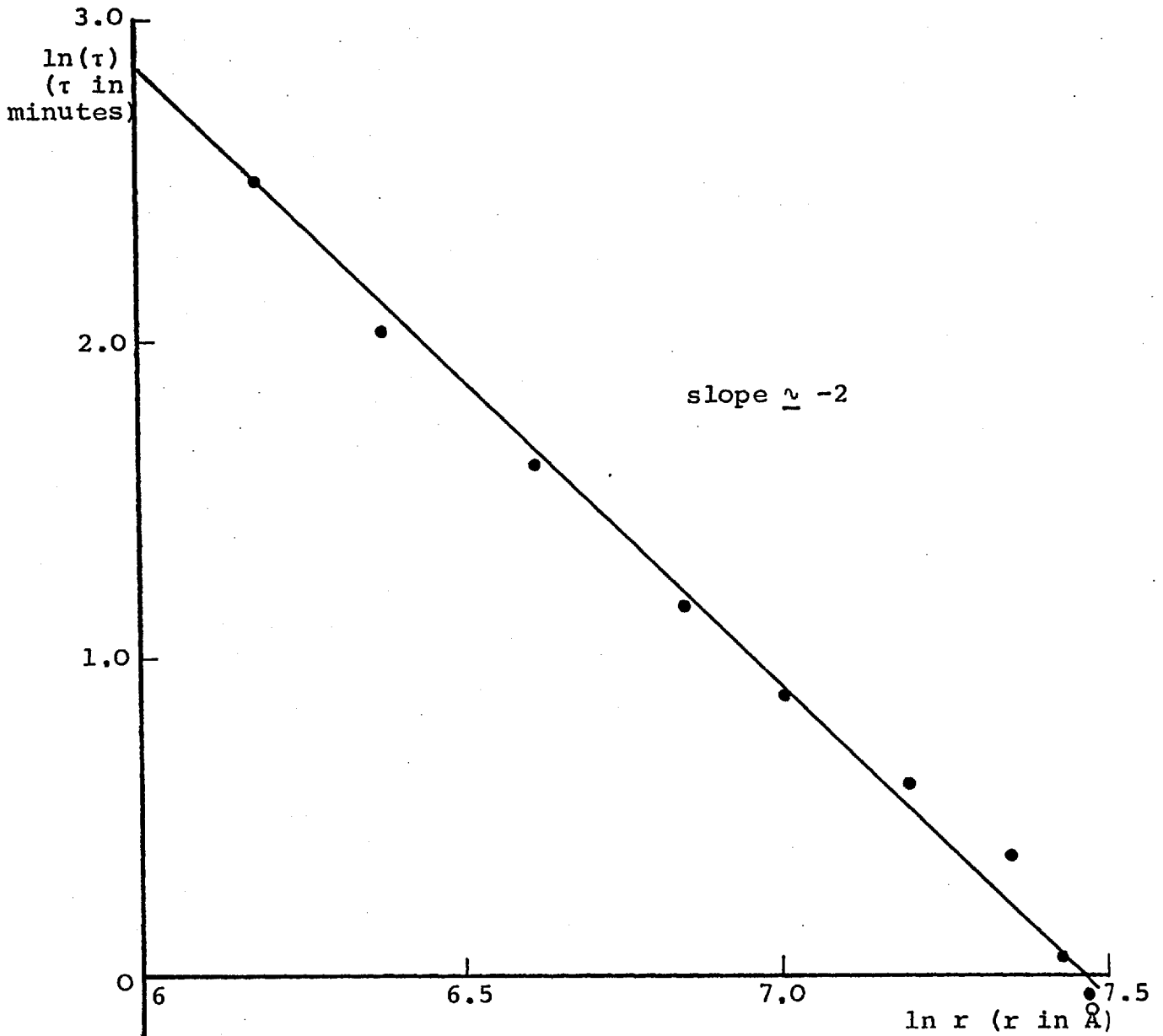
FIGURE 5.4.7.

Variation of the characteristic time (τ) with the particle
radius (r) of type II polyhedra, plotted on a logarithmic scale.

A more quantitative idea of the dependence of the

characteristic time of the polyhedra (type II) particles on

their surface area can be obtained from the graph of figure

5.4.7. in which τ is plotted against r on a logarithmic

scale.   The slope of the straight line is approximately 2,

suggesting surface area dependence of the characteristic

time of melting for such particles.

5.4.4.   The Characteristic Time of Melting of The Particles on Molybdenite.

The time delay in melting is found to be present

in bismuth particles on molybdenite substrates.   In figure

5.4.8, the fraction of particles remaining solid $\frac{N}{N_O}$ with

time at a given temperature is plotted on a logarithmic

scale against the total time (t) for which the particles

were heated.   The layer consisted of both the needle-like

and the irregularly shaped crystallites.   It can be seen

that the later stages of the decay curve generally show a

good exponential decay in the number of particles remaining

solid; the initial rate of melting, however, is higher

than the final constant value, as demonstrated by the curvature

of the graph.   A value of τ was deduced from the linear

portion of the graph.

The higher melting rate at the initial stages of

heating was found to occur with both the needle-like and

irregularly shaped crystallites.   Figure 5.4.9. shows the
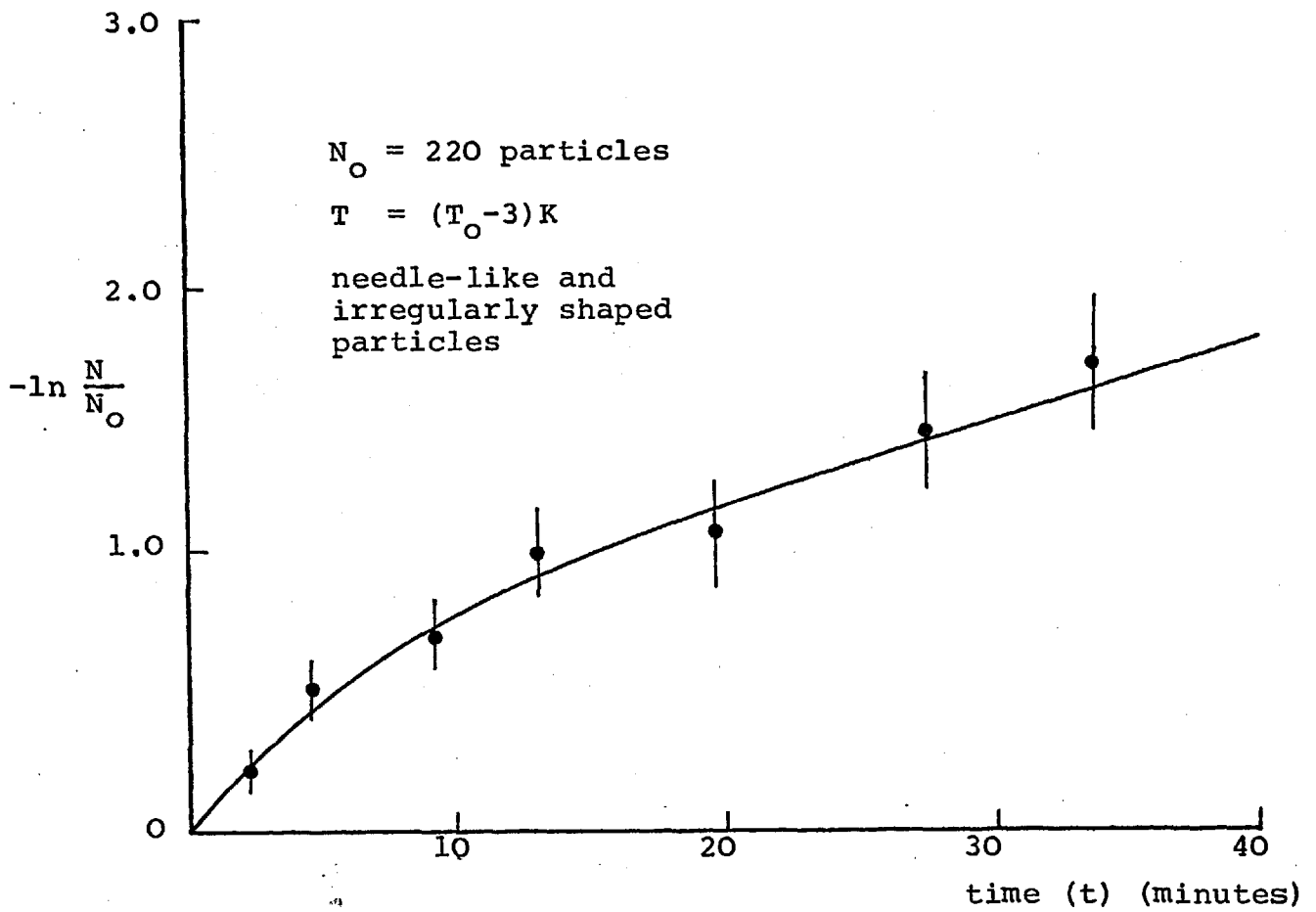
FIGURE 5.4.8.

Variation in the number of particles remaining solid (N) with time (t), plotted on a logarithmic scale.
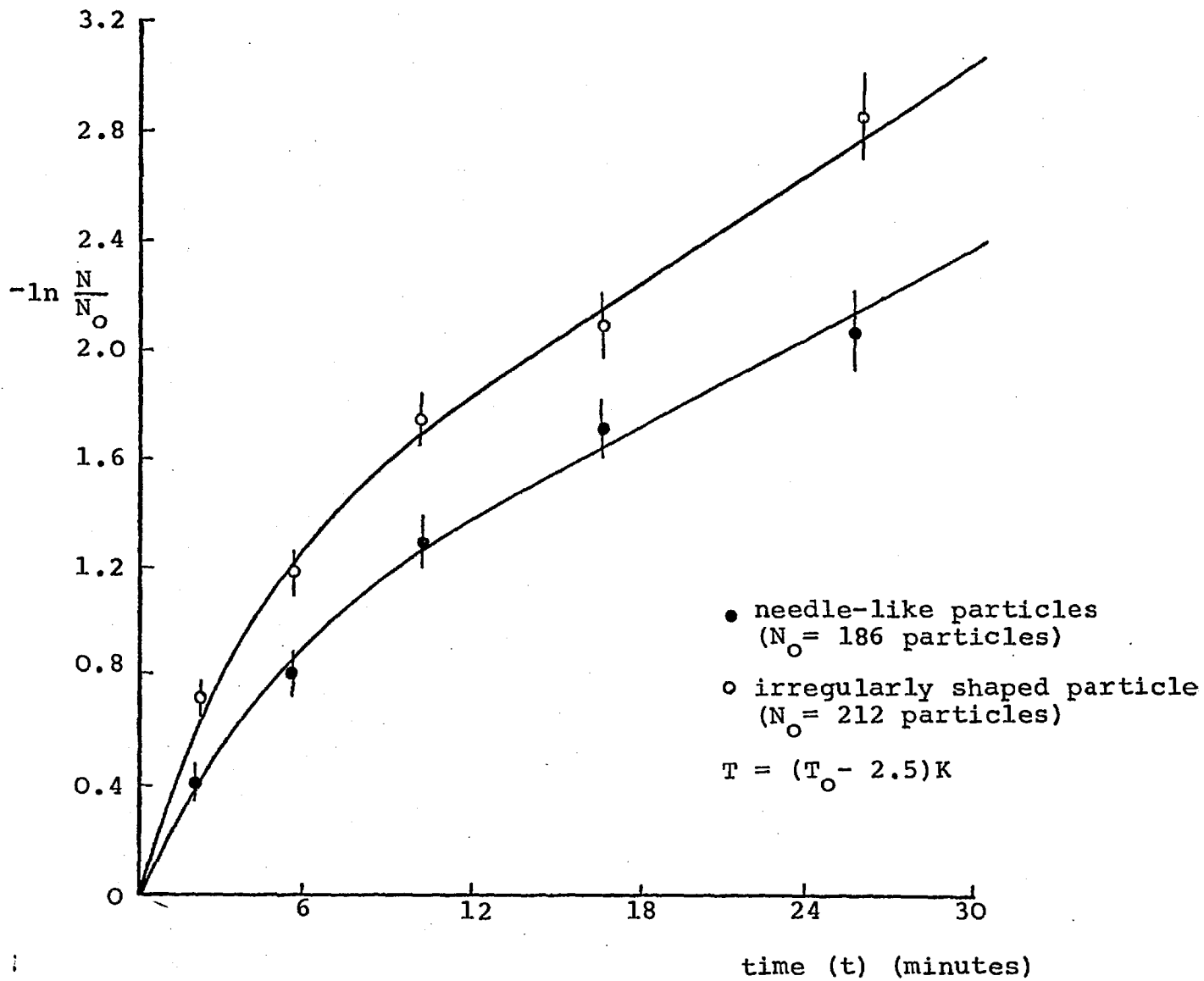
FIGURE 5.4.9.

Variation in the number of needle-like and irregularly
shaped particles remaining solid (N) with time (t) plotted
on a logarithmic scale.

two decay curves drawn separately for the two type of particles present in the same layer.   Although the initial melting rate for both types of particles were greater than their respective final constant values, the final melting rates for both the particles, however, were often themselves generally found to approximate a single constant value.

The maximum temperature at which some particles still remained solid was about 2K <u>above</u> the bulk melting temperature, so that a value of the characteristic time of melting (τ) could be determined at this temperature.   Almost all the particles melted on heating above this temperature. Values of τ were determined at different temperatures, from about 6K below the bulk melting point to 2K above it. The characteristic time of melting was found to be a well-defined function of temperature (section 5.4.5.).

5.4.5.   Temperature Dependence of the Characteristic Time.

The variation of the characteristic time of melting (τ) with temperature (T) has been plotted (on a logarithmic scale) in figure 5.4.10. for the bismuth platelet (type I) and polyhedra (type II*) particles and for the particles on molybdenite substrate.   Also drawn in the figure are the experimental graphs of Peppiatt (1973, 1975) for the platelet (type I) and polyhedra (type II) particles.   The experimental points obtained in the present experiments on the platelet (type I) and polyhedra (type II*) particles generally agree
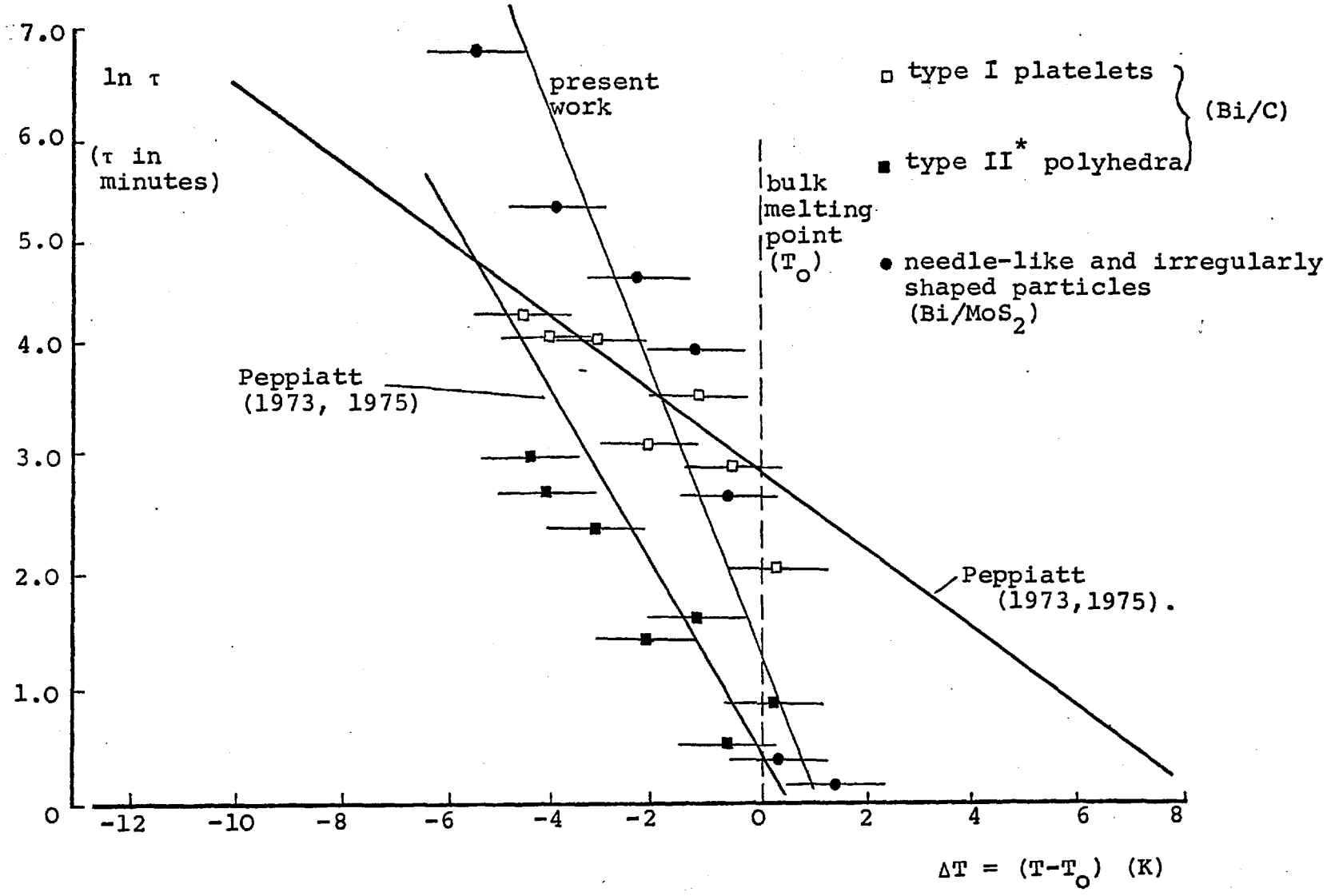
FIGURE 5.4.10.

Variation of the characteristic time (τ) with temperature (T) for the bismuth particles on carbon and molybdenite substrates (plotted on a logarithmic scale).

with the graphs of Peppiatt for the platelet (type I) and
polyhedra (type II) particles respectively.   The graph
for the particles on molybdenite substrate has been drawn
independently from those of Peppiatt.   It will be seen
that the graphs approximate to straight lines, suggesting
an exponential dependence of the characteristic time on
temperature.   This, however, is probably an artifact
due to the narrow temperature rangeover which it was
possible to investigate.

CHAPTER 6

RESULTS OF THE MELTING OF SMALL PARTICLES OF TIN.

6.1.   Introduction,

The melting of small particles of tin has been
studied by several workers who, because they were unable
to make direct observation, assumed the particles to be
spherical (see section 1. 3.).   In all cases, a depression
in the melting point from the bulk value with decreasing
particle size (given as the radii of the 'spherical' particles)
has been observed in accordance with the theories of melting
of small particles.   In particular, due to the small
scatter found in the melting temperatures of particles of
equal size,the results of Wronski (1976), (figure 1.3.2.)
suggest a definite melting temperature for each particle
size.   By treating the results theoretically, Wronski
deduced a value of the solid/liquid interfacial energy.
The present experiments, performed in the electron micro-
scope, have shown that when tin is deposited on amorphous
carbon, molybdenite or graphite substrates, the particles
were in fact in the form of thin platelets which, on
melting, form the spherical liquid droplets (figure 6.1.1.).
By assuming that these platelets melt by forming a liquid
skin along facets or curved surfaces round the platelets,
a dependence of the melting point of the individual platelets
on the respective thicknesses would be expected (see 2.3.4.).
For comparison with previous workers, the dependence of the
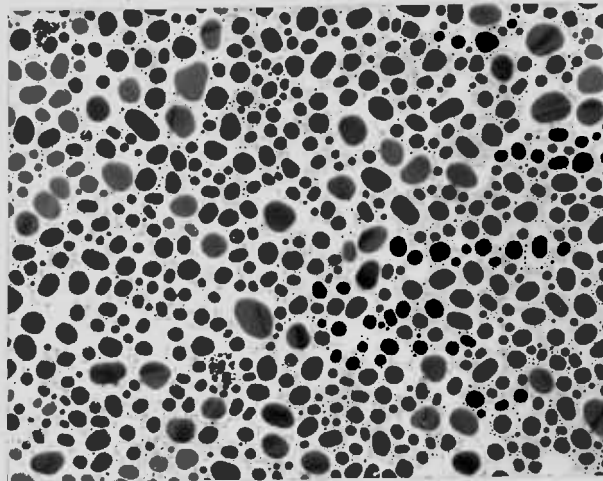
(a)

| 0.4μm |
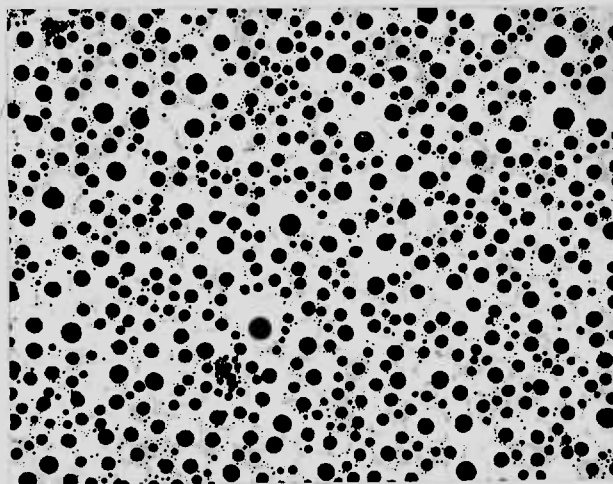
(b)

FIGURE 6.1.1.

(a) A layer (∿100Å thick) of tin on carbon substrate
     (substrate temperature ∿330K);

(b) The deposit of figure (a) when molten.

melting point on the radius of the final liquid droplet has
also been plotted, although no theoretical conclusions may
be drawn from this.

The existence of a time delay in melting as observed
for the bismuth particles (Peppiatt, 1973,1975) was also
investigated in the melting of the tin particles.   However,
no such obvious time delay effect was noticed within
experimental error (section 6.3.).   Therefore, a definite
melting point could be assigned to the individual tin
particles, which is not possible for the bismuth particles.

6.2.   The Deposition and Appearance of the Tin Particles.

Thin layers of tin, with mean thicknesses ranging
from about 100$\overset{\circ}{A}$ to 200$\overset{\circ}{A}$ were deposited on substrates,
maintained at temperatures a few degrees below the maximum
supercooling temperatures observed (see section 7.3.).   In
a majority of the experiments, substrates of amorphous
carbon were used.   Immediately after evaporation, the
deposits were quickly heated (at a rate of about 20Kmin^{-1}),
with the electron beam switched off, to 50K below the bulk
melting point.   By this method, the amount of hydrocarbon
contamination (due to the cracking of the residual oil vapour
by the electron beam) was kept to a minimum, as the layers
were only observed at temperatures well above room
temperature.   Two such layers of mean thicknesses of 100$\overset{\circ}{A}$
and 200$\overset{\circ}{A}$ on carbon substrates are shown in figures 6.2.1

and 6.2.2. respectively, together with the diffraction patterns from these deposits. The diffraction patterns are characteristic of random orientation of the polycrystalline deposits, except for figure 6.2.2. which is slightly oriented with the (010) fibre axis perpendicular to the substrate. These layers consisted of individual particles, unlike evaporated films of bismuth, which would be continuous. The tin crystallites can be grouped into two size ranges — one of 50Å and less, and the other of 100Å and above. The large crystallites are surrounded by clusters of smaller particles. For the smaller particles, it is very difficult to distinguish between the solid and liquid, and hence, only the large crystallites were analysed.

The large crystallites are in the form of thin platelets, having a variety of shapes. The platelets have linear dimensions parallel to the substrate approximately two times greater than their heights (section 6.4.1.). Although a majority of the platelets in the thicker layers (figure 6.2.2.) are irregular in shape, in the thinner layers (figure 6.2.1.) they were found, in general, to be nearly circular or elliptical. Faceting of the side faces in the platelets is much less marked (particle A, figure 6.2.1.) than in the platelets of bismuth. However, some of the platelets in the thicker layers have straight edges; occasionally a few can be seen to be square in appearance (particle A, figure 6.2.2.). With the exception of a few

O,4μm   (a)   (b)
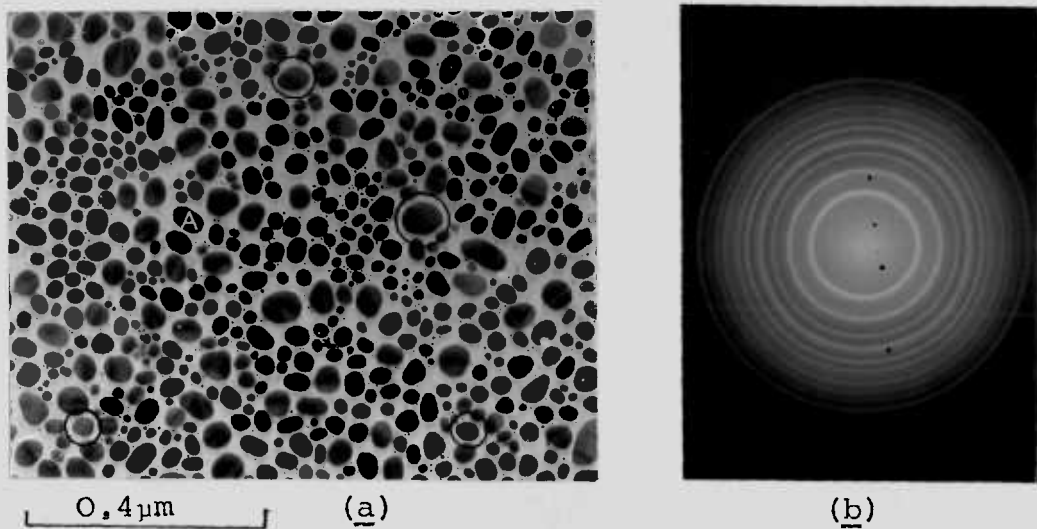
FIGURE 6,2,1,

A layer (∿100Å thick) of tin and the corresponding
diffraction pattern.

O.5μm   (a)   (b)
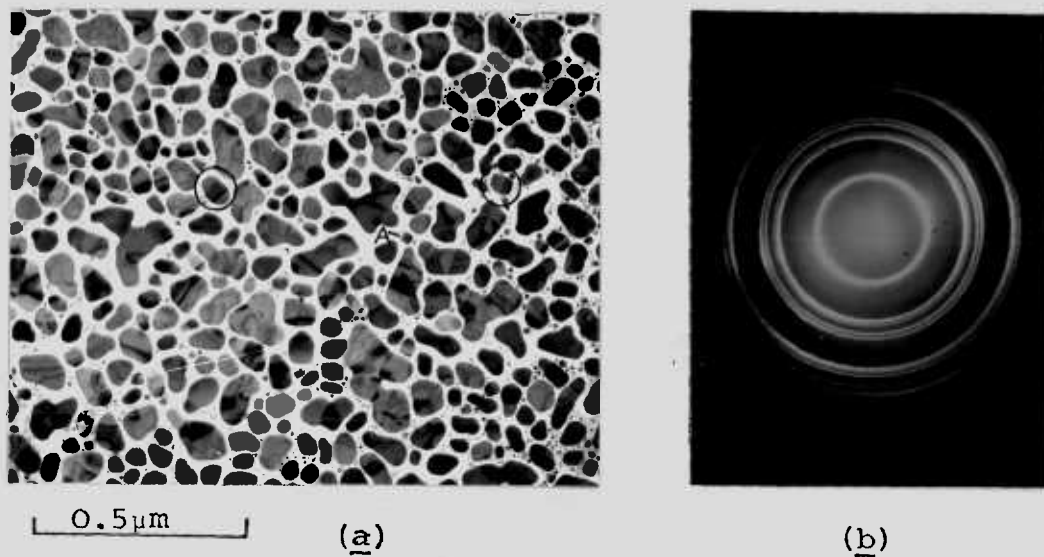
FIGURE   6,2.2,

A layer (∿200Å thick) of tin and the corresponding
diffraction pattern,

irregular particles , very little or no change in the shapes

of the platelets was observed on further heating at a

higher temperature, until melting occurred when they form

the spherical liquid droplets.   The solid platelets could

therefore be readily distinguished from the respective liquid

droplets.

Many of the platelets in the thicker layers have

grain boundaries in them, but grain boundaries are completely

absent in the platelets of the thinner layers.   These grain

boundaries are observed to disappear on heating the layers

close to the bulk melting temperature,   This is shown in

the particle A (figure 6.2.3a.) of an initially deposited

layer,   On heating at 12K below the bulk melting point, the

grain boundaries in this composite platelet (consisting of

two separate grains), have been removed.   A single

crystallite is formed, having the shape of the original

platelet (figure 6.2.3b.).   Also some of the platelets are

seen to have dark bands across them,   A few such platelets

are indicated by circles in figures 6.2.1. and 6.2.2,   These

bands are bend-contours resulting from strains in the

crystallites.   Dark bands occur whenever a part of the

crystallite is at a Bragg reflection angle to the electron

beam.   Although bend-contours are found to be already

present in the initially deposited platelets, some are

noticed to be generated on heating the platelets to higher

temperatures.   For example, particle B (figure 6.2.3a.)

has only one bend-contour in the initially deposited layer
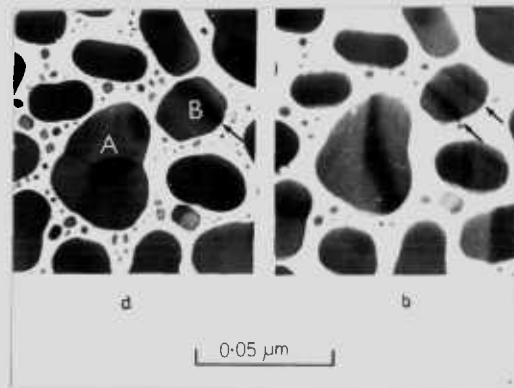
FIGURE   6.2.3.

(<u>a</u>)   Particles of tin, showing grain boundary and bend
        contour in a layer after its deposition at ∿330K;

(<u>b</u>)   The same layer after being heated for two minutes
        at 12K below the bulk melting point (505K) (the
        arrows indicate the bend contours).

on carbon substrate.   On further heating for two minutes
at 12K below the bulk melting point, another bend-contour
appears in the particle, at a distance of about 100$\overset{\circ}{A}$ from
and parallel to the first.   Still further heating of the
layer to higher temperatures did not produce any more
bend-contour in the particle.

The particles deposited on molybdenite and graphite
substrates were similar in appearance to those on carbon
substrates.   Also, no orientation of the particles on these
bases were observed despite alterations to the substrate
temperatures and rates of evaporation.   Therefore, only a
few melting experiments were performed with these substrates.

When liquid tin droplets were recrystallized by
cooling, spherical particles were formed with no apparent
faceting in the resolidified particles.   Even prolonged
heating at various temperatures below the melting point
did not produce any facet   in them.   Due to the difficulty
in distinguishing the solid from the liquid, the melting
points of the resolidified particles could not be determined
in the present experiments.

Although in a vacuum of 4×10^{-7} torr, the occurrence
of some contamination of the specimens is possible, no signs
of this were visible either in the micrographs or as extra
(oxide) rings in the diffraction pattern.

6.3. Absence of a Time Delay in the Melting of Tin Particles.

A few experiments were performed with the tin particles to investigate the existence of a time delay in melting. These were carried out by heating the particles in a layer of tin at a given temperature for various lengths of time. If it is assumed that a time delay does exist in the melting of the tin crystallites, then the number of particles remaining solid at the end of each heating period should decrease with time. Instead it was observed that although a number of the solid particles melted on heating the first time at a given temperature, very few particles or none at all melted on the second or subsequent heating of the layer to the same temperature. The result of a typical experiment is described below.

A layer of tin containing about five hundred particles, after being initially heated at 50K below the bulk melting point, was heated (with the electron beam switched off) to 10K below the bulk melting temperature. The layer was heated at this temperature for successive periods of two, five and ten minutes (being cooled down after each heating period for observation). The first period at the higher temperature caused approximately fifty solid particles to melt, the second only six and the third none at all. On increasing the temperature by 2K and by repeating the process, about thirty of the remaining solid

particles melted, but only two melted during the rest of
the heating period.   The fact that a few particles melted
on the second heating at a given temperature is probably
due to the inaccuracy in stabilizing the temperature, so
that a slightly higher temperature could have been obtained
during the second heating.

Thus the existence of a time delay in melting for
tin particles has not been observed.   If a time delay does
exist for these particles, it must have a characteristic
time of melting (τ) of several hours or less than a minute,
and would therefore not be observed in the present
experiments.   In the absence of a time delay, therefore, a
definite melting temperature can be assigned to individual
tin particle.

6.4.   Thickness Dependence of the Melting Point of Small Particles of Tin.

6.4.1.   The Thicknesses of the Tin Platelets.

The tin particles were in the form of thin platelets
with their linear dimensions parallel to the substrate a few
times greater than their thicknesses.   An estimate of the
thicknessess of the platelets can be made by comparing
the visible areas of the tin particles before and after
melting in the micrographs of figure 6.1.1. (The method to
determine the thicknesses of the individual platelets is
described in section 4.1.2.).   It was found that an
approximate linear correlation exists between the thicknesses
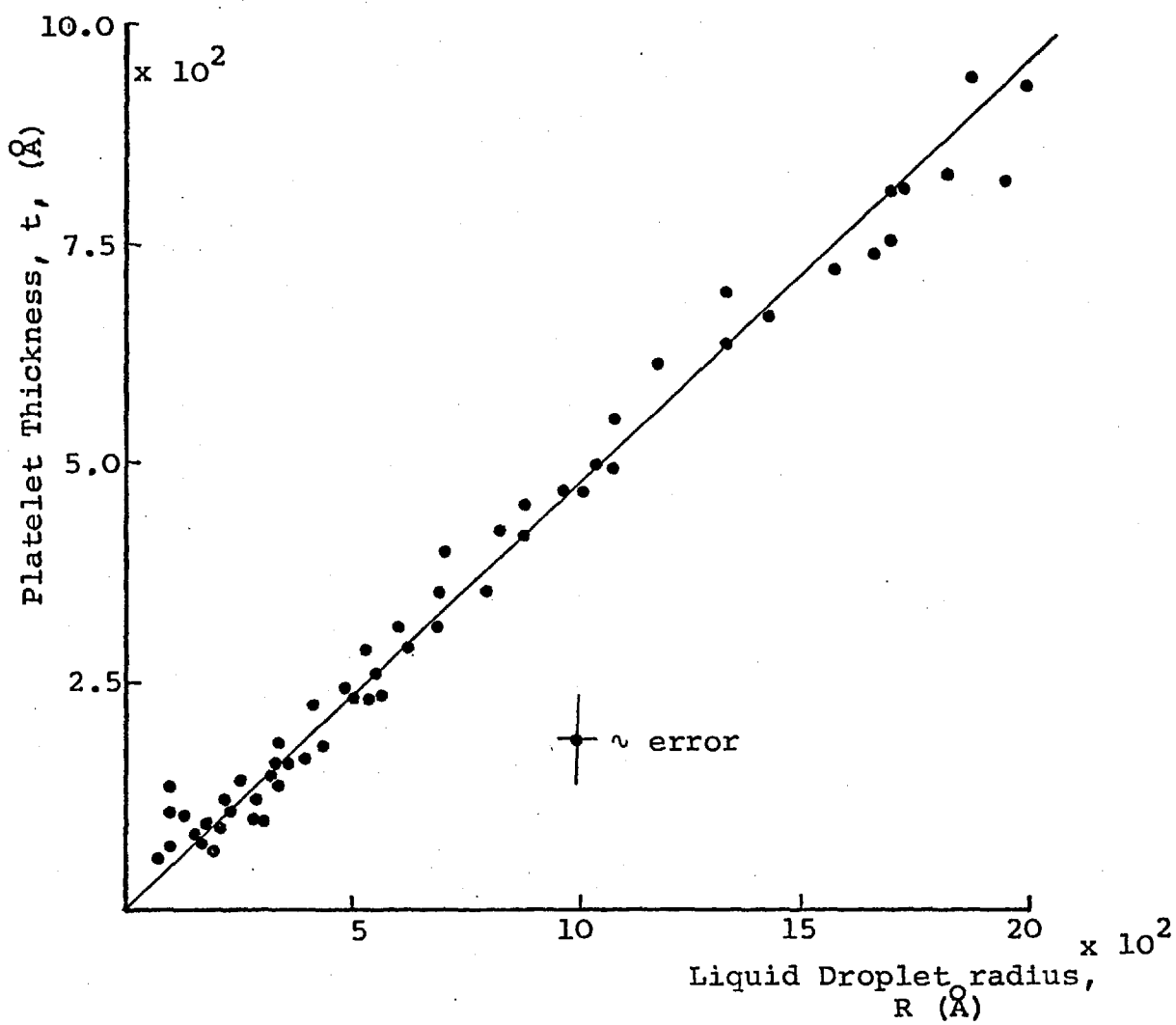
FIGURE 6.4.1.

The variation of the tin platelet thickness with
the radius of the liquid droplet.

of the platelets and the radii of the final liquid droplets
(figure 6.4.1.).   From the slope of the curve it can be
seen that for most of the crystallites

$$0.6 > \frac{t}{r} > 0.5 \qquad\qquad (6.4.1.)$$

where t is the thickness of the platelet which on melting
forms the liquid droplet of radius r.

6.4.2. The Thickness Dependence of the Melting Point
of Small Particles of Tin,

As mentioned previously, if the tin platelets are
assumed to melt by the formation of a liquid skin round
their curved edges, the melting temperature of the platelets
would be expected to depend on their thicknesses.   In figure
6.4.2., the melting point of the platelets is plotted as
a function of the platelets thickness (t), for platelet
thickness ranging from about $50\overset{o}{A}$ to $1,000\overset{o}{A}$.   The melting
temperature of the platelets on the three substrates is
included in the graph.   No significant difference between
the melting temperatures of the platelets on the three
substrates was observed.

Figure 6.4.3. is a plot of melting point depression,
$-\Delta T (= T - T_o)$ from the bulk melting temperature (T_o), of the
platelets, against the reciprocal of thickness (t) of the
platelets.   The curve is approximately a straight line
but has a slight curvature for platelet thicknesses less
than $60\overset{o}{A}$.   The slope of the straight line portion of the
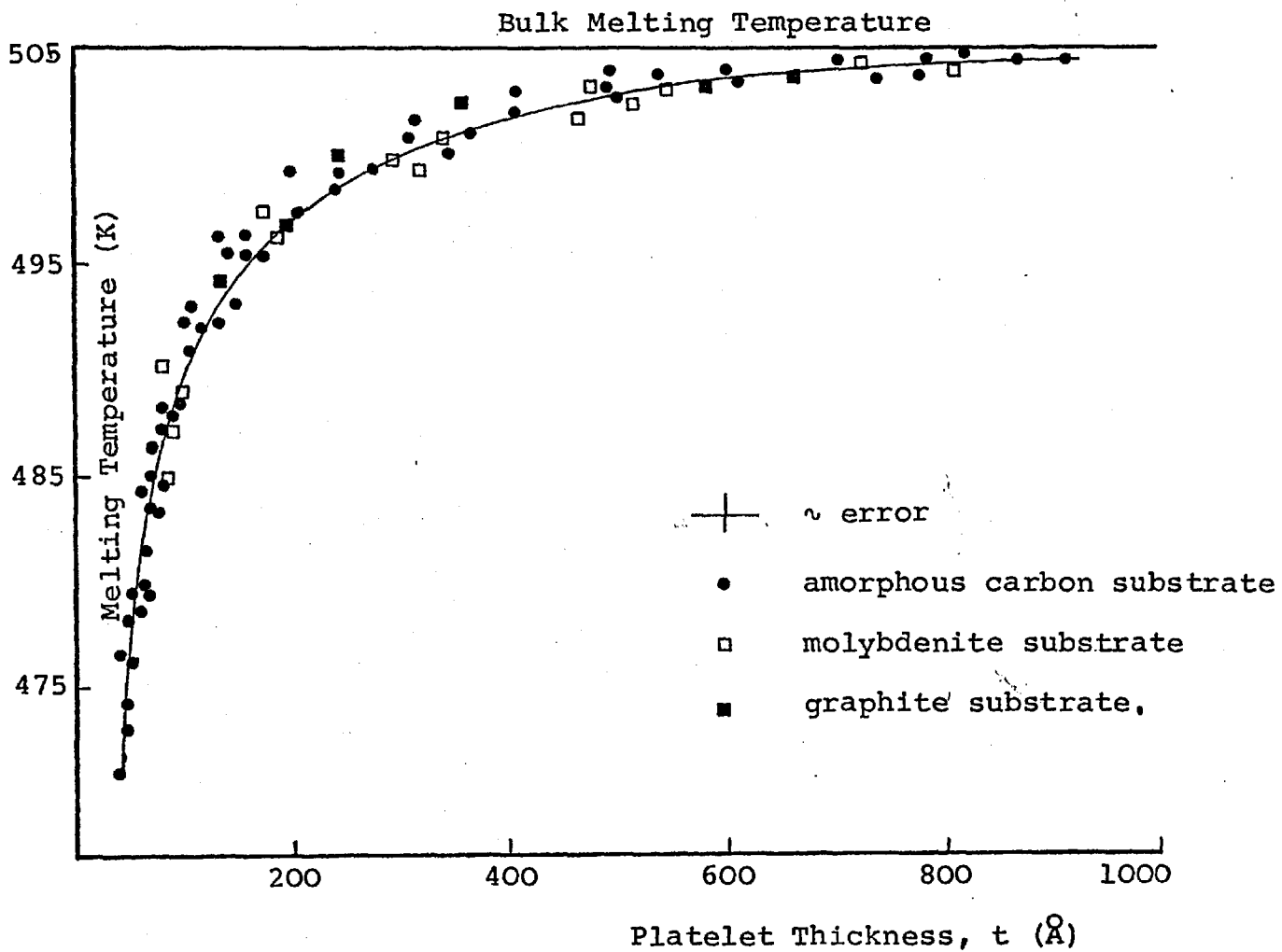
FIGURE 6.4.2.

Graph of melting temperature against thickness ,t,
for platelets of tin on amorphous carbon, and
molybdenite and graphite substrates.
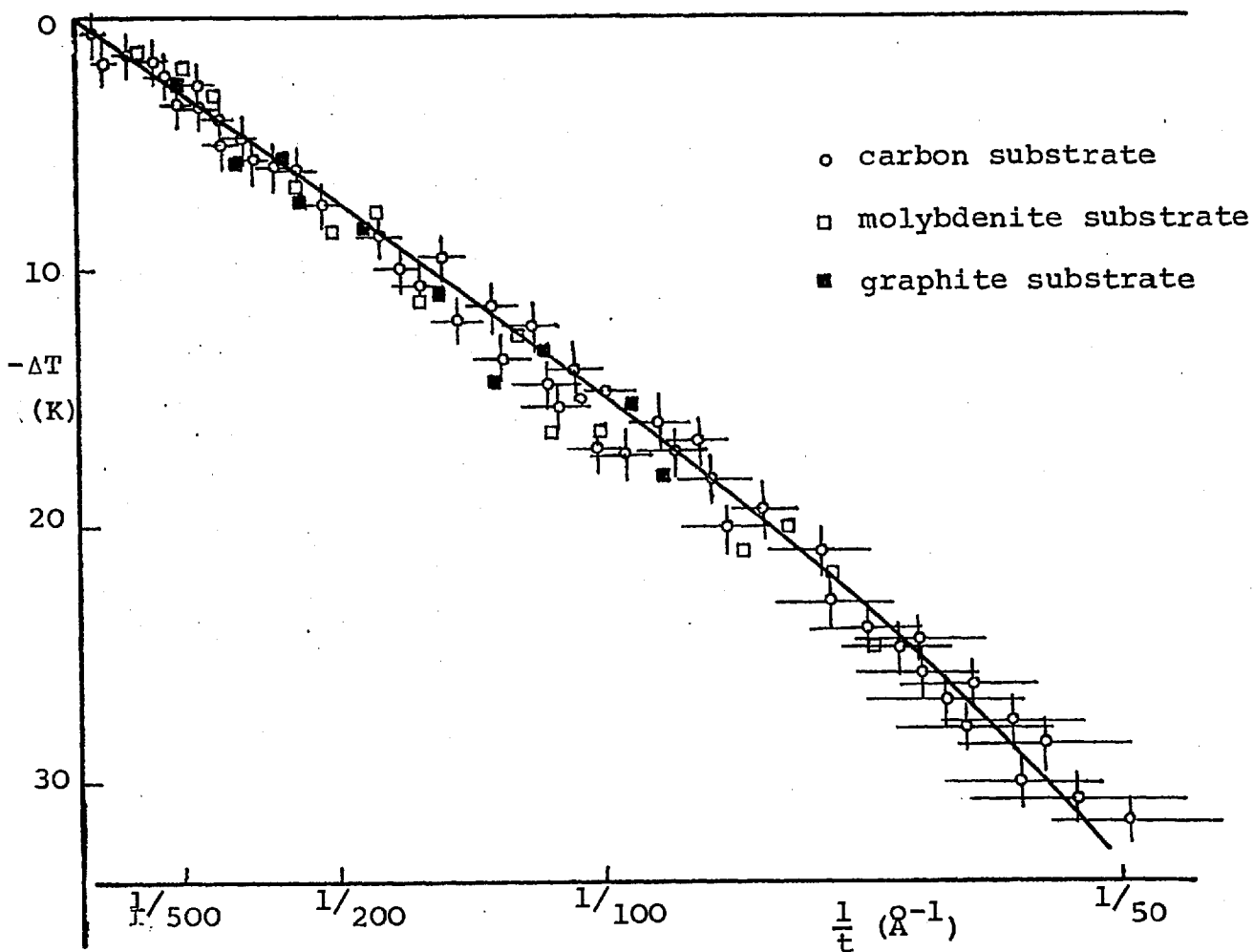
FIGURE 6.4.3.

Graph of depression of melting temperature, $-\Delta T (= T - T_O)$ from the bulk value (T_O) against the reciprocal of platelet thickness (t) for tin platelets (the errors on the points of molybdenite and graphite substrates are the same as for the points with the carbon substrates).
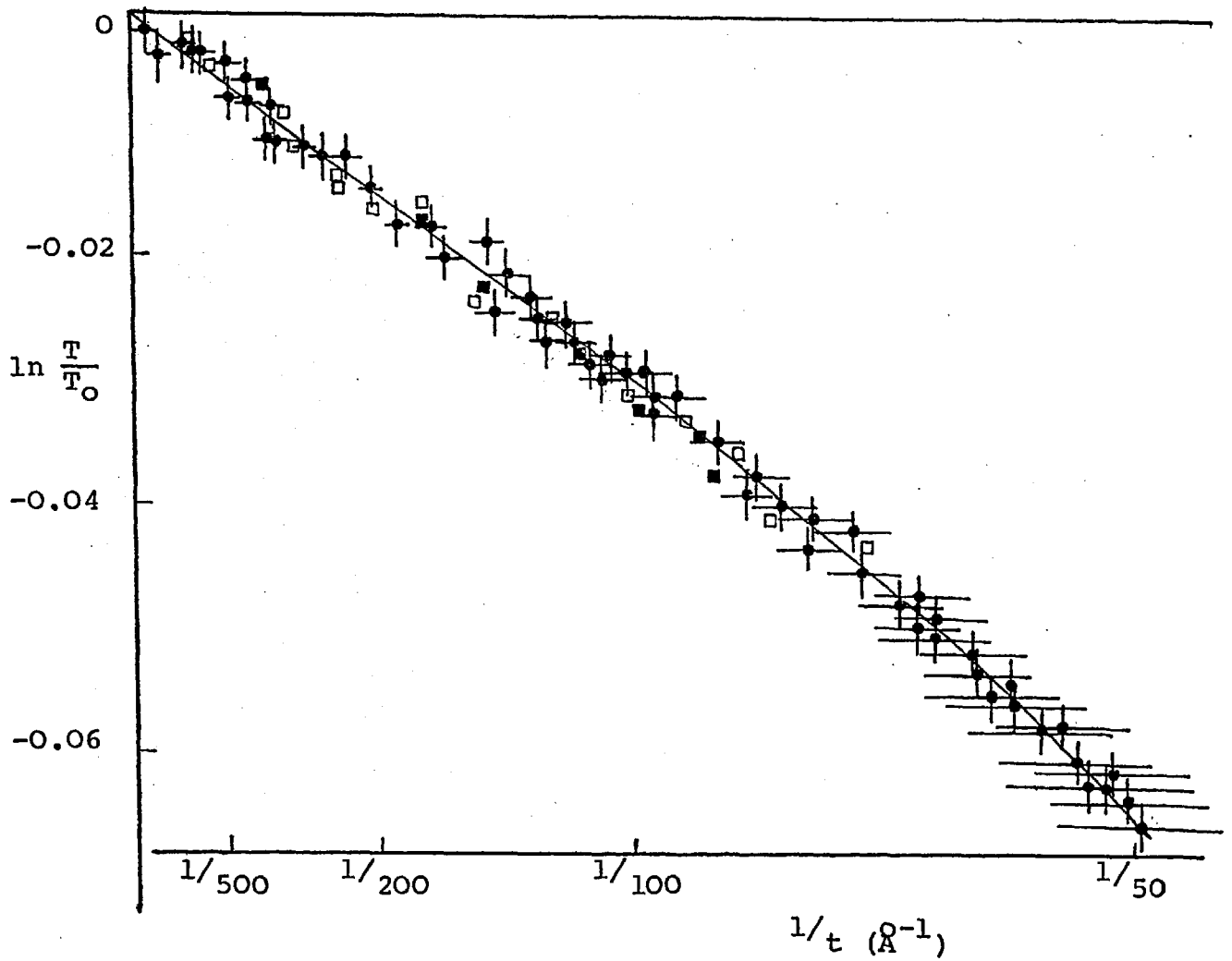
FIGURE 6.4.4.

The melting point depression ($\ln \frac{T}{T_o}$) of the tin platelets plotted as a function of the reciprocal of the platelet thickness (t).

curve is $(1.469\pm0.16) \times 10^3 K\overset{\circ}{A}$. An accurate plot, however,
would require a logarithmic plot of the depression in the
melting temperature ($\ln\frac{T}{T_o}$) from the bulk melting point (T_o)
against the reciprocal of the platelet thickness (t)
(see figure 6.4.4.). Once again the curve approximates to
a straight line in the region of platelet thicknesses
greater than $60\overset{\circ}{A}$.

For a discussion on these results, see section
8.1.

6.5. Comparison with Previous Work on the Melting of Small Particles of Tin.

For comparison with previous work, the melting
temperature of the individual tin platelets has been plotted
as a function of the liquid droplet radius (figure 6.5.1.).
Since the solid particles formed by recrystallizing the
liquid droplets were spherical, the above method of plotting
the graph would be identical to that of Curzon (1960) and
Wronski (1967). The particle sizes, as measured by these
authors were, in fact, represented the radii of the
recrystallized solid particles. In the present graph, the
melting temperature of the platelets on the three substrates,
has been shown. The smallest particles whose solid and
liquid states could be distinguished with confidence were
of the order of $60\overset{\circ}{A}$ in radius. The curves obtained by
Curzon and Wronski are also included in the graph.

The results are discussed in section 8.1.5

Bulk melting temperature (T_O)
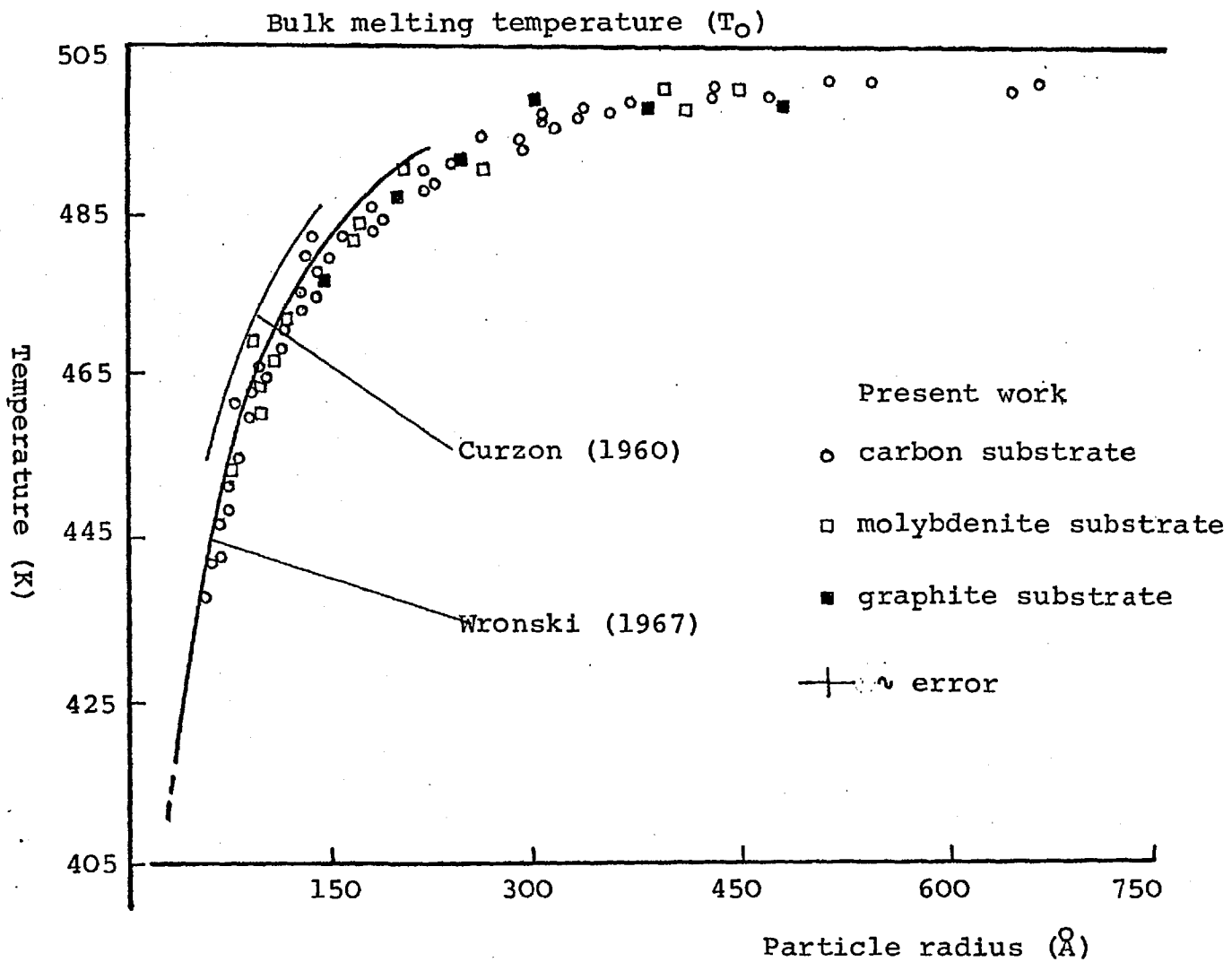
FIGURE 6.5.1.

The variation of the melting temperature with
the size of the tin particles.

CHAPTER 7

OTHER EXPERIMENTAL OBSERVATIONS.

7.1.   Diffusion in the Tin Platelets near the Melting

Point.

In a melting experiment in which the crystallites
are gradually heated from below their melting points, a
certain amount of atomic diffusion in them can occur.   This
diffusion may result in some of the crystallites changing
their shapes into more compact solid forms.

In the present experiments, the change in shape of
the tin platelets in the neighbourhood of their melting
points, has been observed by two methods.

(i) In the first method, the platelets were

heated and observed at each stage of a normal

melting experiment.   The heating and observation

was continued until all the crystallites in a layer

were seen to have melted.   The micrographs were

then analysed to see if any change in shape of the

platelets had occurred during the heating process.

(ii) In the second method, the platelets

were continuously observed while being heated near

the melting point.   For this, a layer of tin,

immediately after deposition, was heated at about

$20K \ min^{-1}$ (with the electron beam switched off) to

within $50K$ of the bulk melting point.   The heating

rate was then reduced to about $3K \ min^{-1}$ and the

layer observed continuously.   The heating rate was
further reduced to 1K min^{-1}, as soon as some of the
crystallites were seen to melt.   By using the
normal internal plate camera, a series of micrographs
was taken, usually at an interval of 5 sec. with the
photographic plates exposed to the electron beam
for about a second.   This was continued until all
the crystallites were seen to have melted.

In the normal melting experiments, the majority of the tin
crystallites once deposited did not change their shapes until
they melted.   A few irregular platelets however did display
a certain amount of atomic diffusion.   In particular, upon
heating, the re-entrant angles vanished and the platelets
assumed a more compact form (figure 7.1.1.).   The diffusion
process by which material from the side faces of the initial
platelet builds onto the top (and perhaps the bottom) surfaces,
is rather slow, often lasting up to 30 minutes, the total
time of a normal melting experiment.   However, in the second
method of heating and observing continuously, an unusually
enhanced form of diffusion (termed "snapping", see Blackman
et al., 1975) often occurred in some of the platelets by
which they changed their shapes abruptly into more compact
solid forms.   This was seen as the appearance of double
images on micrographs.   For example, in figure 7.1.2., the
initial thin form of the platelet (the larger outline) has
'snapped' into the more compact form (the inner outline),
during the exposure time ($\sim$ 1 sec) of the photographic plate.
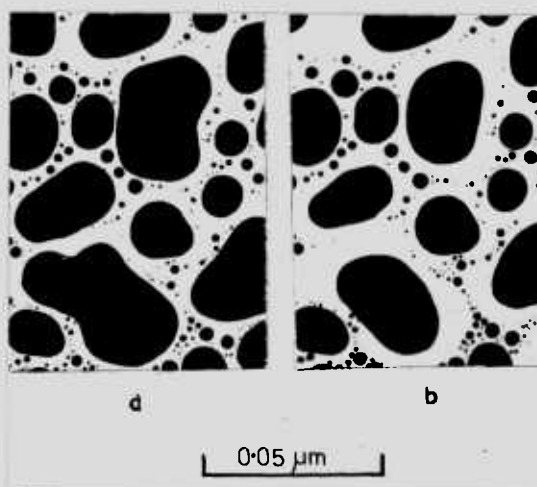
FIGURE   7.1.1.

'Slow diffusion in irregularly shaped tin particles in a normal melting experiment . (a) and (b) show the particles before and after the heating respectively.
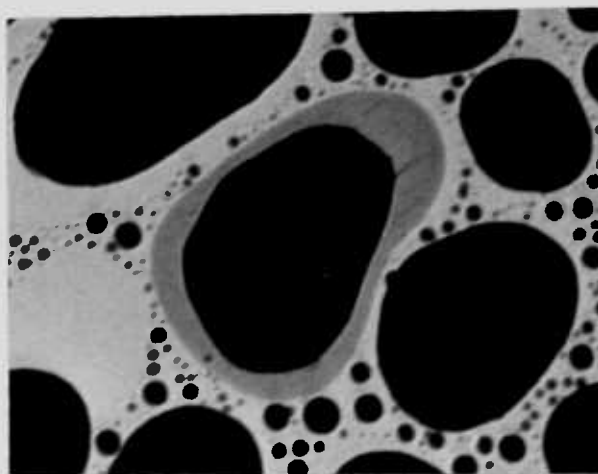
FIGURE   7.1.2.

Symmetrical 'snapping' in a tin platelet.
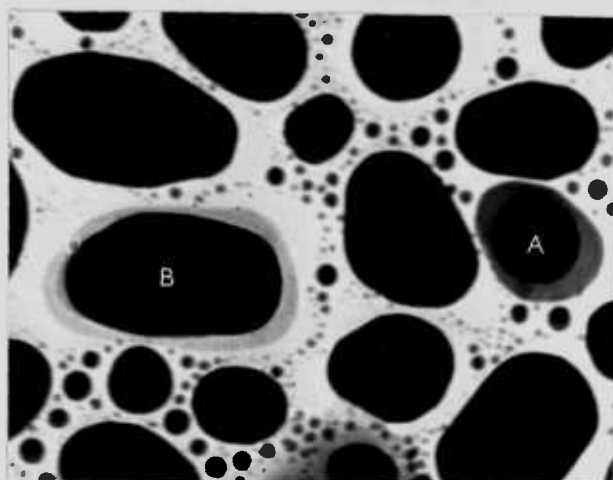
FIGURE   7.1.3.

Symmetrical 'snapping' and melting in two tin platelets.

This abrupt change in shape has occurred almost symmetrically, with material being transferred from all the side faces. The snapped platelet often retained some of the original facets, while developing some new facets (see figure 7.1.2.). The centre of mass of the platelets moved only slightly in the final particle, so that on melting, the liquid droplet formed in position with little change of the centre of mass of the original solid platelet. For example, particle A (figure 7.1.3.) has melted, while B has snapped symmetrically.

Although the snapping in the tin platelets was generally found to occur symmetrically, occasionally some of the irregular platelets were seen to snap asymmetrically. In these, more material was transferred preferentially from some sides (figure 7.1.4.). On melting, the liquid droplets in such cases were seen to be located at these sides of the original platelet. Occasionally some of the tin platelets exibited a <u>double snapping</u> in which two abrupt shape changes occurred, separated in time by approximately half a second. In figure 7.1.5., several outlines in the platelet can be seen.

Snapping in the tin platelets was seen to occur in the deposits on carbon substrates, but was absent in the platelets on the molybdenite and graphite substrates. The tin platelets on these substrates were found to become severely contaminated during the 15 minutes normally required in the continuous observation of the platelets.

The results are discussed in section 8.4.1.
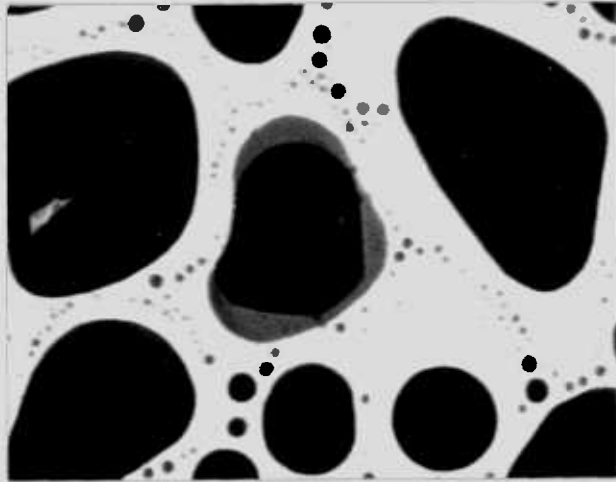
FIGURE   7.1.4.

A tin platelet which has 'snapped' asymmetrically.

0.2μm
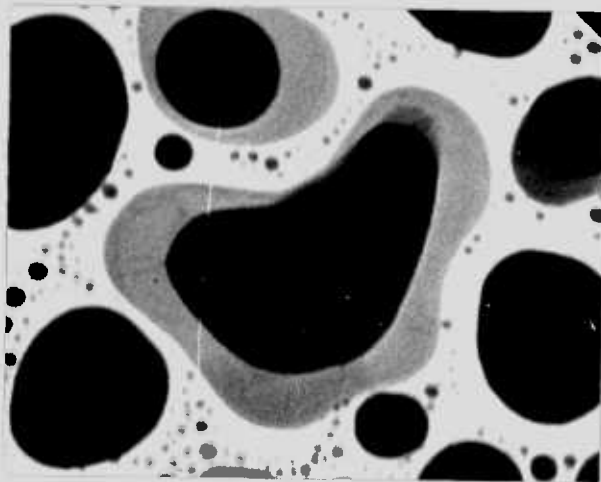
FIGURE   7.1.5.

'Double snapping' of a tin platelet.

7.2.   Diffusion in Bismuth Films on Molybdenite Substrates.

When bismuth film of thicknesses of $\sim$ 100Å were condensed onto molybdenite substrates (heated to 425K), films comprising of a network of needle-like crystallites were obtained (see figure 5.2.7a.).   On further heating (at a rate of 5K min^{-1}) these films, the network of the broke up into individual crystallites.

A different kind of behaviour was observed on similarly heating bismuth films of thicknesses greater than 100Å.   Two such films of $\sim$200Å thickness are shown in figure 7.2.1..   In each case, the layers after deposition on molybdenite substrates, maintained at 425K, consisted of many irregular holes in an otherwise continuous layer. The layers produced highly textured diffraction patterns, consistent with the basal (000.1) plane (in the hexagonal description) of the layer parallel to the substrate.   On heating (at a rate of 5K min^{-1}) to 10K below the bulk melting point, these layers did not break up into individual crystallites. unlike a similar thickness of bismuth film on carbon substrates.   Instead many of the irregular holes were observed to transform, by an atomic diffusion process, into oriented hexagonal voids with sharp edges and corners (see figure 7.2.1, a and b).   In some cases , a few triangular voids (figure 7.2.1.b) were also seen to have formed.   Small crystallites of bismuth can be noticed in some of the hexagonal voids.

(<u>a</u>)

(<u>b</u>) |___ 0.4μm ___|

<u>FIGURE 7.2.1.</u>

Oriented voids in bismuth condensed on M₀S₂.

On heating close to the bulk melting point, these layers broke up into irregular particles and eventually melted (without any 'snapping') at the bulk melting point.

7.3.   Supercooling of Small Liquid Droplets.

In addition to the experiments on melting, a few experiments were performed on the supercooling of the liquid droplets formed during the melting experiments. These experiments were also carried out with liquid droplets formed by depositing the layers as liquid on the substrates heated near the bulk melting point. As these layers were deposited at temperatures much higher than room temperature, the liquid droplets would be expected to be less contaminated by the residual gas vapours than those obtained in a melting experiment.

The amount of supercooling in the liquid droplets was determined by the methods described by other workers (Stowell, 1970; see also Peppiatt, 1973).

(i) In one method, the liquid layer was slowly cooled down (in steps of approximately 5K), and the diffraction pattern from the layer was continuously observed by using a low intensity electron beam to reduce beam heating. Also the regions of observation in the layer was frequently changed to avoid localized beam heating. The temperature at which the halo diffraction pattern

characteristic of the liquid layer changed into sharp

crystalline rings was noted.

(ii) In another method, the liquid droplets were

continuously observed with a reduced beam

intensity, while gradually cooling down the layer.

Also, as before, the regions of observation were

continuously moved.   The temperature at which

a large proportion of the liquid droplets began

to form crystal facets by solidification was

noted.

In the second method, a few liquid droplets were seen to

become solid long before the remainder; this was presumably

due to "seeding" of the liquid by specks of impurities, and

these were therefore neglected.   This method could not be

employed for the liquid droplets of tin, due to the absence

of any distinguishable faceting in the resolidified liquid

droplets.   Both of the above methods, however, produced

identical results within experimental error of a few degrees.

This suggests that the effect of electron beam heating is

negligible in this case.

For both bismuth and tin, no significant difference

was noticed between the amounts of supercooling of the liquid

droplets formed during a melting experiment and those obtained

by depositing the layer as liquid.   The normal pressure

during the experiments was $\sim 4 \times 10^{-7}$ torr.   The amount of

supercooling for liquid droplets of bismuth and tin was

Particle Size, (Å)	Substrate	Amount of Supercooling, (K)
300	Carbon	155-162
300	Molybdenite	110-115
300	Graphite	120-128

TABLE   7.3.1.

Results for the supercooling of liquid droplets of bismuth.   Bulk melting point = 544K.

Particle Size, (Å)	Substrate	Amount of Supercooling, (K)
300	Carbon	160-170
300	Molybdenite	100-115
300	Graphite	130-133

TABLE   7.3.2.

Results for the supercooling of liquid droplets of tin. Bulk melting point = 505K.

determined on carbon, molybdenite and graphite substrates

and are shown in tables 7.3.1. and 7.3.2. respectively.

The results will be discussed in section 8.3.

7.4.   Mass-spectrometer Scan of the Residual Vacuum.

Figure 7.4 shows the combined scan of the residual

vacuum both before and after the cold trap was filled with

liquid nitrogen.   The partial pressures on this graph are

only approximate.   They are given according to a unit

sensitivity for nitrogen at the spectrometer setting employed.

Because the sensitivities vary considerably with the

conditions the partial pressure values are only accurate to

within a factor of 3.   Specific consideration was given to

the partial pressure of oxygen (p.p O_2) and it was deduced

that under normal operating conditions p.p O_2 was $8 \pm 2 \times 10^{-8}$

torr.

From a comparison of the two scans it is apparent that

the cold trap has reduced considerably residual oil vapour

and water vapour, leaving the nitrogen and oxygen almost

undisturbed.
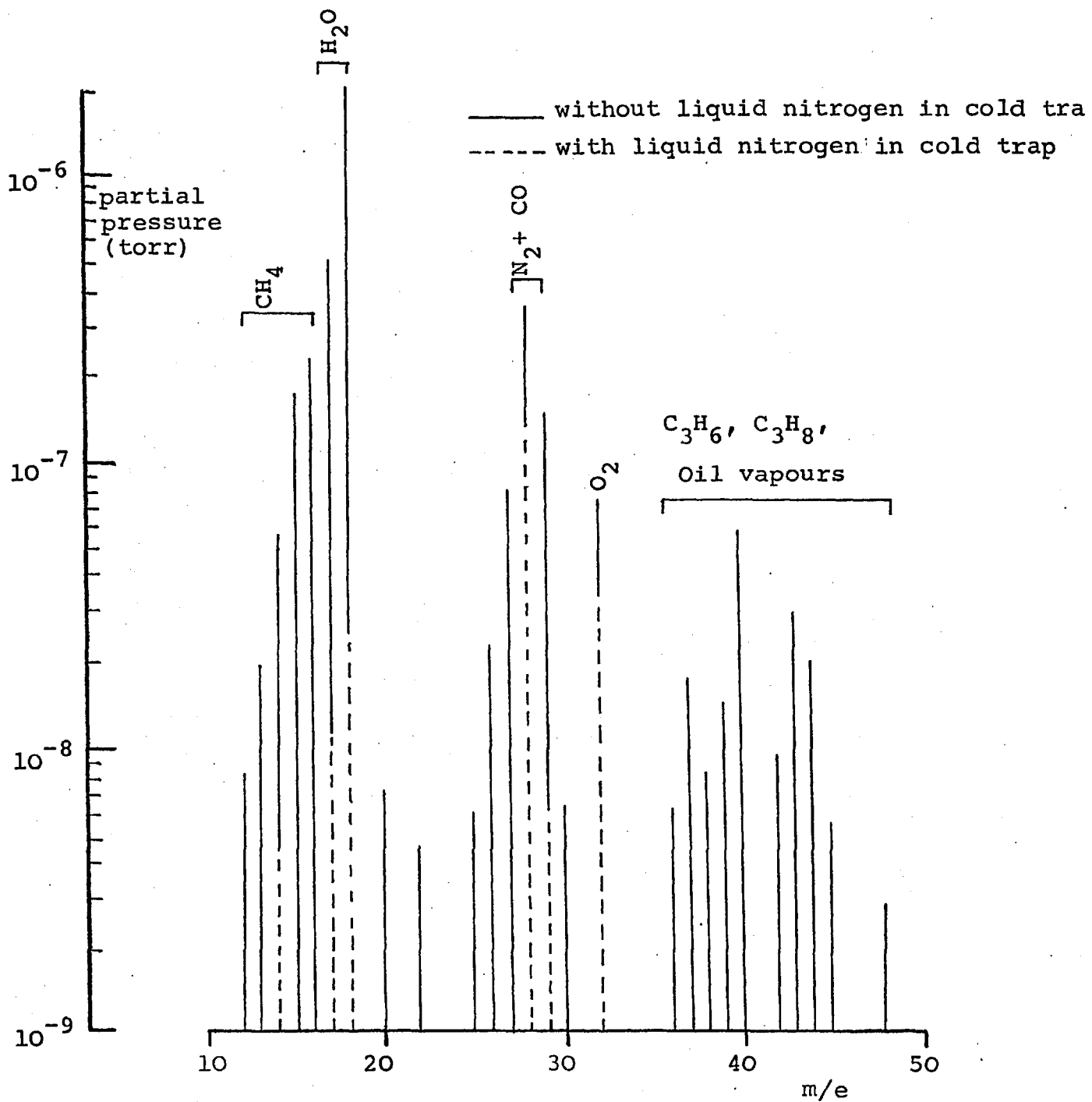
FIGURE 7.4.

"Cracking" pattern of residual vacuum in the electron microscope.

CHAPTER 8

DISCUSSION

8.1.   **The Melting of Small Particles of Tin.**

8.1.1.   **Introduction.**

The small particles of tin obtained by vapour
deposition onto substrates were in the form of thin platelets.
The diffraction pattern from layers of 100$\overset{o}{A}$ or less in
thickness were characteristic of a random orientation
of the platelets.   In the thicker layers, the platelets
were slightly oriented with (100) type planes parallel to
the substrate.   The grain boundaries observed in some of
the platelets were seen to be removed from the crystallites
upon heating to a few degrees below the respective melting
point (figure 6.2.3.).

Broad, dark contours have been observed in some
of the platelets.   These almost certainly occur when a
platelet is bent in such a way that part of the crystal is
at a Bragg angle to the electron beam.   The diffracted
beam will be removed by the objective lens aperture,
resulting in a higher contrast image for this region than
the remainder of the crystallite.   The bending in the
platelets may have resulted from the differential expansion
between the platelets and the substrate.   Upon heating the
tin platelets would have expanded to a much larger extent
than the substrate used,   If a good adhesion existed between
the tin and the substrate at some points on the platelet/

substrate interface, the bottom surface of a platelet

would not have been able to expand freely, while the top

surface would expand considerably.   The platelet would

therefore become distorted.   The effect of strain energy

due to the bending in the platelets on their melting points

has been discussed in section 8.1.3.

The results for the melting of the tin platelets

have been interpreted assuming a dependence of the melting

point of a platelet on its thickness.   This is in contrast

with the earlier work of Blackman and Curzon (1959), and

Wronski (1967) who performed the experiments in an electron

diffraction camera, and therefore had to assume that the

crystallites were roughly spherical.   A liquid skin melting

model has been used to interpret the present results; in

this the effect of the two principal radii of curvature on

the melting point of a platelet has been considered, see

section 8.1.2. below.

8.1.2.   Effect of Thickness on the Melting Point of a Platelet.

The melting point results confirm that there is a

melting point dependence on the tin platelet thickness.

The melting point of the platelets decreased from the bulk

value, T_o, (505K) with decreasing platelet thickness (see

figure 6.4.2.).   The results show that to a first

approximation, the depression in the melting point (ΔT)

varied inversely as the platelet thickness (t) (figure 6.4.3).

Also the results of a few melting experiments on molyb-
denite and graphite substrates did not differ significantly
from those experiments on amorphous carbon substrates. The
scatter in the melting point for the tin platelets of equal
thickness was of the order of 2K. Therefore, the melting
point of a platelet can be taken to be a definite function
of the platelet thickness.

As described in section 2.1.2., the theories of
melting of small particles as given by Pawlow (1908-9,
1909) and Rie (1923) cannot explain the present results.
The physical conditions defining the melting point of a
small particle (assumed spherical) in these theories are not
consistent with the present experiments. Also the melt-
ing point depressions from the bulk value are much smaller
than those given by the thermodynamic melting point of a
small particle.

It seems that the only way in which a crystallite
can melt below the bulk melting point is by the formation
of a liquid skin on the crystal surface. By assuming
that the liquid skin completely wets the surface (see
section 2.2.3.), then the liquid skin, once formed, will be
able to progress through the solid and dissolve it at the
skin melting temperature without requiring an activation
energy. However, an activation energy may be needed in
the initial nucleation of the liquid skin, as the liquid
skin must itself grow from an initial two dimensional

nucleus (section 2.2.4.) of the critical size. In the process,
a time delay in melting may result (see section 8.2.1.). Since
no time delay has been observed in the melting of the tin platelets
it seems that the liquid skin has little difficulty in forming at
the appropriate temperature.

Since the tin crystallites were in the form of thin platelets,
therefore it seems that they can melt below the bulk melting point
only by forming the liquid skin on the curved side faces of the
platelets. It is unlikely that the top or the bottom surfaces of
the platelets can melt below the bulk melting point. Since these
surfaces are flat, therefore they have an infinite radius of
curvature and will melt at the bulk melting point. Considering the
platelets to be spherical discs of thickness t and radius r_s, the
depression of the melting point from the bulk value can be given by,
to a first approximation (see section 2.3.4.):

$$T_o - T = \Delta T \simeq \frac{T_o}{L\rho_s} \left(\frac{1}{r_s} + \frac{2}{t}\right) \left[\gamma_{s\ell} + \gamma_\ell \left(1 - \frac{\rho_s}{\rho_\ell}\right)\right] \qquad (8.1.1a.)$$

Now by considering the volume of the disc before and after melting,
we have

$$\pi r_s^2 t = 0.8 \times \frac{4}{3} \pi r^3 \qquad (8.1.2.)$$

where r is the radius of the corresponding liquid droplet (Here 80%
of the volume of the droplet is considered, see section 4.1.2.). By
using $r \simeq 2t$ (equation 6.4.1.) in equation (8.1.2.) and simplifying,
gives

$$r_s \simeq 3t \qquad (8.1.3.)$$

Hence substituting equation (8.1.3.) in equation (8.1.1.) gives

$$\Delta T \simeq \frac{2.33}{L\rho_s t} \left[\gamma_{s\ell} + \gamma_\ell \left(1 - \frac{\rho_s}{\rho_\ell}\right)\right] \qquad (8.1.1b.)$$

Therefore, the slope of the linear portion of the ΔT vs. $\frac{1}{t}$

graph (figure 6.4.3.) gives the value of the surface energy
coefficient in equation (8.1.1b.).   Using the data of
appendix A.4., we have

$$\gamma_{s\ell} + \gamma_\ell \ (1- \frac{\rho_s}{\rho_\ell}) = 52 \pm 6 \ \text{ergs cm}^{-2} \qquad\qquad (8.1.4.)$$

Then with $\frac{\rho_s}{\rho_\ell} \simeq 1.029$, and $\gamma_\ell = 552 \ \text{ergs cm}^{-2}$ (Lang, 1973),
the above result gives

$$\gamma_{s\ell} = 68 \pm 6 \ \text{ergs cm}^{-2} \qquad\qquad (8.1.5.)$$

The exact form of equation (8.1.1.) requires a logarithmic
plot of the melting temperature against the reciprocal of
the platelet thickness.   This is done in figure 6.4.6., and
again the slope of the curve yields.

$$\gamma_{s\ell} = 70 \pm 7 \ \text{ergs cm}^{-2} \qquad\qquad (8.1.6.)$$

Equation (8.1.6.) gives the accurate value for the solid/
liquid interfacial energy $(\gamma_{s\ell})$ of tin.   This value will be
compared and discussed with the values obtained by other
workers by different methods, see section 8.1.4.

In order to verify that the basic assumption of
the liquid skin melting model, that is, the complete melting
of the solid surface by the liquid skin, given by

$$\gamma_s > \gamma_\ell + \gamma_{s\ell} \qquad\qquad (8.1.7.)$$

where γ_s and γ_ℓ are the interfacial energies of the solid

and the liquid in contact with the vapour, is satisfied for
the tin, crystallites, it is necessary to compare the sum
of γ_ℓ and $\gamma_{s\ell}$ with γ_s. Extrapolation of the available
data of γ_s for tin, using

$$\frac{d\gamma_s}{dT} = - 0.068 \text{ ergs cm}^{-2}K^{-1}$$

(Zadumkin, 1959), gives for γ_s of tin at the melting point

> 683.7 ergs cm^{-2} Greenhill and McDonald (1953)
>
> 679.5 ergs cm^{-2} Mykura   (1955)
>
> 671.7 ergs cm^{-2} Shebzukova et al. (1972)

For tin, $\gamma_\ell = 552$ ergs cm^{-2} (Lang, 1973). Therefore, using
the value of 70 ± 7 ergs cm^{-2} for $\gamma_{s\ell}$ obtained as above,
it can be seen that for tin

$$\gamma_s > \gamma_\ell + \gamma_{s\ell}$$

Therefore, as the wetting condition is satisfied, the
formation of the liquid skin on the curved surfaces of the
tin platelets is energetically favourable at temperatures
close to the melting point.

8.1.3.   Effect of Strain Energy due to the Bending in the Tin Platelets on the Melting Points.

The strain energy due to the bending of a tin
platelet alters the free energy of the crystallite or the
liquid skin; the platelet melts at a different temperature

lower than the normal melting temperature (section 2.4.).
If E is the strain energy per unit volume of the crystallite,
then considering the tin platelets to be discs of thickness
t and radius r, we have, as before, for the depression of
the melting point from the bulk value.

$$\Delta T' \simeq \frac{T_o}{L\rho_s} \left[\frac{2.33}{t} \left\{ \gamma_{s\ell} + \gamma_\ell (1- \frac{\rho_s}{\rho_\ell}) \right\} + E \right] \qquad (8.1.8.)$$

or,

$$\Delta T' \simeq \Delta T + \Delta T_{BEND} \qquad (8.1.9.)$$

where ΔT is given by equation (8.1.3.)

and

$$\Delta T_{BEND} = \frac{T_o}{L\rho_s} E \qquad (8.1.10.)$$

is the lowering in the melting point from the normal melting
point due to the strain energy.

By an analogy with the bending in a beam, the strain
energy per unit volume (E) in a tin platelet of thickness t,
length ℓ, which is bent through an angle of 2θ (figure
8.1.1.) can be given by

$$E = \frac{1}{6} y \theta^2 \left(\frac{t}{\ell} \right)^2 \qquad (8.1.11.)$$

where y is the Young's modulus of the material of the beam.
The angle of bending (2θ) can be determined by considering
the distance between two bend contours observed in a tin
platelet (for example, see figure 6.2.3.) as follows.

As previously noted, the broad dark contours in the

image of a platelet occurs when the platelet is bent in
such a way that a crystal plane is at the Bragg reflecting
angle, θ_B, given by

$$\theta_B = \sin^{-1} \frac{\lambda}{2d_{hkl}} \qquad (8.1.12)$$

Here, λ is the wavelength of the electron beam used and
d_{hkl} is the lattice spacing of the crystal plane having
the Miller indices (hkl).   By considering the figure 8.1.1.,
if 'a' is the distance between the two bend contours and R
is the radius of curvature of the bent beam, measured from
the centre of curvature to the 'neutral surface' in the
beam, we have

$$\theta_B \simeq \frac{1}{2} \frac{a}{R} \qquad (8.1.13)$$

The neutral surface should have the same length as the
original beam, but the top and the bottom surfaces of the
beam will be extended and compressed respectively.   From
figure 8.1.1., the angle of bending, 2θ, is given by

$$2\theta \simeq \frac{\ell}{R} \qquad (8.1.14.)$$

Therefore, substituting in equation (8.1.14) the value of R
from equation (8.1.13.) and simplifying

$$\theta \simeq \frac{\ell}{a} \theta_B \qquad (8.1.15.)$$

or, $\theta \simeq \frac{\ell}{a} \sin^{-1} \frac{\lambda}{2d_{hkl}}$ (8.1.16.)   from equation (8.1.12.)

Therefore, substituting equation (8.1.16) in equation
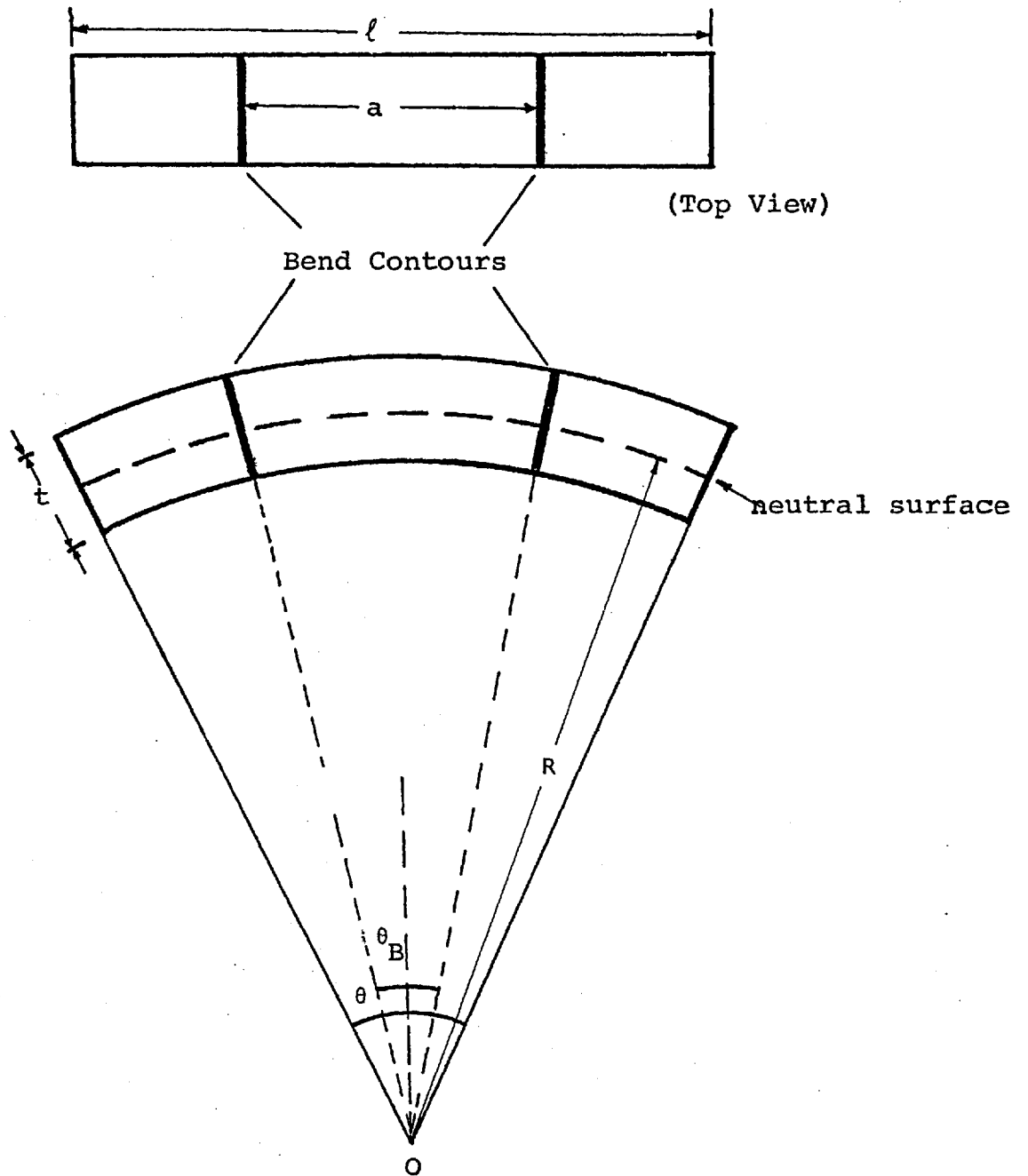
FIGURE 8.1.1.

The bending of a crystallite.

(8.1.11.), we have, for the strain energy per unit volume
of the beam

$$E = \frac{1}{6} y \left(\sin^{-1} \frac{\lambda}{2d_{hkl}}\right)^2 \left(\frac{t}{a}\right)^2 \qquad (8.1.17.)$$

Now, consider, for example, the tin platelet of figure
6.2.3. The distance between the two bend contours is
approximately 100Å and the thickness of the platelet is
approximately 300Å. Therefore, by assuming that the bend
contours are due to the reflections from one of the close
packed planes, say, (200) planes of tin, and by using
$\lambda = 0.043$Å for 80kV electron beam used, strain energy
per unit volume (E) can be estimated from equation (8.1.17.)
to be of the order of 10^7 ergs cm^{-3}. The corresponding
lowering in the melting point (ΔT_{BEND}) can be calculated
from equation (8.1.10) to be of the order of 0.3K, and is
therefore negligible. Similarly, from calculations for
reflections from the other planes in tin, it can be shown
that the effect of strain energy due to the bending in the
tin platelets on their melting points is negligible.

8.1.4.   Comparison of the $\gamma_{s\ell}$ Value of Tin with those
          of the Other Workers.

          The values of the solid/liquid interfacial energy
($\gamma_{s\ell}$) of tin have been determined by various workers either
from the melting point results of the small crystallites of
tin or from the observations of the maximum supercooling in

the liquid droplets of tin.   For comparison with the $\gamma_{s\ell}$

value of 70 ± 7 ergs cm^{-2} obtained from the present melting

point experiments, the values obtained by the other workers,

by using the melting and the supercooling results, are listed

in tables 8.1.1. and 8.1.2. respectively.   The $\gamma_{s\ell}$ values

obtained from the melting results should depend on the

crystallographic orientation of a particular plane on which

the melting is initiated.   In the absence of any knowledge

about this plane, the values of $\gamma_{s\ell}$ should refer to some

sort of an average of the $\gamma_{s\ell}$ values of the different crystal

planes.   The results obtained from the supercooling

experiments should be considered similarly .   However, in

the present experiment, the resolidified liquid droplets

were found to be spherical, and are therefore, presumably

isotropic.   The anisotropy of the solid/liquid interfacial

energy of tin is, however, yet unknown (Jones, 1974).

The values of $\gamma_{s\ell}$ obtained from the melting

experiments of small crystallites of tin differ significantly

from those obtained from the supercooling results.   These

results are based on the supposed homogeneous nucleation of

solid from a supercooled liquid.   A considerable amount of

evidence has been obtained which indicates that the values

may be in error.   In several cases, the supercooling

required to cause nucleation has been found to be substantially

larger than those reported by earlier workers (see, for

example, Stowell et al., 1970;   Takahashi and Tiller, 1969)

Reference	$\gamma_{s\ell}$ (ergs cm^{-2})
Present work	70 $\pm$7
Wronski (1967)	62 $\pm$ 10
Blackman and Curzon (1959)	73 $\pm$ 7
(see also Curzon, 1960).	
Takagi (1954)	66[*]

Table 8.1.1.   The values of the solid/liquid interfacial energy ($\gamma_{s\ell}$) of tin determined from the melting results of small crystallites of tin.

[*]This value has been calculated by Blackman and Curzon from Takagi's melting results.

Reference	$\gamma_{s\ell}$ (ergs cm^{-2})
Peppiatt (1973)	57.5
Pound and La Mer (1952)	58,5 $\pm$ 1,0
Turnbull (1950)	54.5

Table 8.1.2.   The values of the solid/liquid interfacial energy ($\gamma_{s\ell}$) of tin determined from the supercooling results of the liquid droplets of tin.

indicating heterogeneous nucleation in the earlier studies.
Therefore, the $\gamma_{s\ell}$ values obtained from the supercooling
results can only be taken to be a lower limit, rather than
an actual value even for the later results (see section 8.3.).

The $\gamma_{s\ell}$ values obtained from the melting results
of small crystallites of tin by Takagi, Blackman and Curzon,
and Wronski differ from that obtained from the present
melting experiments performed in an electron microscope.
As the above authors were unable to observe the tin
crystallites in their electron diffraction experiments, the
crystallites were assumed to be spherical for simplicity
in the theoretical treatment of the results.   In the light
of the present experiments, this assumption in the case of
the tin crystallites obtained by vapour deposition is not
justified.   It is therefore not too surprising that the
present value of $\gamma_{s\ell}$ differ from those obtained by the above
authors.

There are several other methods which have been
employed to determine the solid/liquid interfacial energy
of a material (for a review of the methods, see, Jones, 1974).
Besides the above two methods, no other method seems to
have been used for tin.   In the absence of any such
determination, the present value of $\gamma_{s\ell}$ for tin appears to
be the most reliable obtained so far.

8.1.5.   Comparison of the Melting Point Results with those
of the Other Workers.

To allow a direct comparison with the melting point
results of Blackman and Curzon (1959) (see also, Curzon, 1960),

and Wronski (1967), obtained by using the electron
diffraction method, the depression in the melting point
from the bulk value in the present experiments has been
plotted as a function of the crystallite size taken as the
liquid droplet radius (see figure 6.5.1.). As previously
noted (section 6.5.), since the recrystallized liquid
droplets were found to be spherical, the present plot would
be identical to those of the above authors. These authors
measured the particle sizes after cooling the specimens
at the end of a melting experiment (section 1.3.). The
results of neither Palatnik and Komnik (1960), nor Takagi
(1954) are included, as discussed in sections 1.1.2 and
1.3. respectively.

It can be seen that the present results are
consistent with those of Blackman and Curzon, and Wronski
in that an increasing depression in the melting point for
the smaller crystallites has been obtained. Furthermore,
Wronski's results show that the substrate has no effect on
the form of the melting curves. He obtained identical
results for tin on both carbon and silicon monoxide substrates
(see figure 1.3.2.). Also in the present experiments,
similar results were obtained on amorphous carbon, and
molybdenite and graphite substrates. The melting curves
of the above authors generally lie at the upper limit of
the experimental points in the present work. This would
be expected, as the electron diffraction method used by these
authors necessarily involved an averaging of the crystallite
size over a complete layer of crystallites, rather than an

individual crystallite in the electron microscope work.
The crystallite sizes determined by the electron diffraction
method are therefore considerably in error.

The present results generally show a scatter of
approximately 2K in the melting point for the tin crystallites
of equal size, and compares to those obtained by Wronski.
However, these results are in contrast to a scatter of
the order of 20K observed by Peppiatt (1973, 1975) in his
results of the melting point of small lead crystallites.
The scatter was attributed to the presence of imperfections,
in particular plane dislocations observed in the lead
crystallites.   Such faults are not expected to be present
in the tin crystallites which have a tetragonal structure.
No imperfections were visible in the tin platelets.   Also
as previously discussed (section 8.1.3.), the effect of
strain energy due to the bending in the tin crystallites on
their melting point is negligibly small, and therefore cannot
explain the scatter in the melting temperatures.   As the
scatter is small, this may be due to errors in the temperature
measurements.

Blackman and Curzon, and also Wronski made a
theoretical treatment of their melting results by assuming
the tin crystallites to be spherical.   This assumption is
not justified for the tin crystallites observed in the present
experiments.   Therefore, no theoretical conclusions can
be derived from the results of plotting the melting
temperatures as a function of the radius of a spherical
crystallite.

8.1.6.   Summary.

The melting temperatures have been determined for thin tin platelets ($\sim 50\text{Å}$ to $\sim 1000\text{Å}$), obtained by vapour deposition onto amorphous carbon, molybdenite and graphite substrates.   The melting temperature of a platelet was found to decrease with decreasing platelet thickness.   No significant difference was observed between the melting temperatures of the platelets on the three substrates used.   The results have been interpreted by a liquid skin melting model.   A melting temperature dependence on the platelet thickness can be obtained by considering the liquid skin to form on the curved side faces of a platelet.   From the slope of the depression in melting temperature against the reciprocal of the platelet thickness curve, a value of 70 ± 7 ergs cm^{-2} has been obtained for the solid/liquid interfacial energy ($\gamma_{s\ell}$) of tin.   This value has been compared with those of the other workers obtained by different methods.

The tin platelets were found to melt without a time delay in melting.   The melting temperatures determined were therefore a definite function of the platelet thickness.

The effect of strain energy due to the bending in the tin platelets on their melting points have been estimated. This is found to be negligibly small.

The melting point results have been compared with those of Blackman and Curzon, and Wronski, by plotting the

melting temperatures as a function of the radius of a

spherical crystallite.   However, in the light of the present

experiments on the tin crystallites obtained by vapour

deposition, no theoretical conclusions has been derived

from these results.

8.2.   The Melting of Small Particles of Bismuth.

8.2.1.   The Time Delay in the Melting of Small Particles

          of Bismuth.

          The most interesting observation made in the

experiments on bismuth was the existence of a time delay

in the melting of an aggregate of small particles (section

1.2., and Chapter 5).   The time delay phenomenon observed

strongly suggests the existence of a free energy barrier to

the production of the liquid phase.   If a particle is held

at a constant temperature, this barrier will only be over-

come by a sufficiently large statistical fluctuation.   The

fact that the bismuth particles have been observed to melt

below the bulk melting point (T_o), suggests that the theory

already discussed of melting (see for example, section

8.1.2.) by forming a liquid skin covering the whole, or

suitable parts of the solid surface must apply to the

bismuth particles.   Therefore, if a time delay exists in

the process, it must be in the formation of the initial

liquid skin.   This is possible because the liquid skin can-

not appear spontaneously, but itself must grow from an

initial liquid nucleus.   In the case of bismuth, there is

a great difference between the open structure of the solid,

and that of the liquid which is more closely packed than

the solid resulting in a volume contraction of 3% upon

melting.   Thus, for the liquid skin to form, an activation

energy will be required due to the substantial rearrangement

of atoms necessary on melting.   As suggested in section
2.2.4., the liquid may grow on the crystal surface from an
initial two dimensional liquid nucleus formed either by
activating atoms directly from the surface, or by an
aggregation of adatoms on the surface.   A small, two
dimensional liquid nucleus on the crystal surface will only
be able to grow, if it is above a critical size.   The
formation of such a liquid nucleus will require the
activation energy necessary for the rearrangement of atoms
on melting, and also an activation energy due to the edge energy
around the perimeter of the nucleus (Peppiatt, 1975).   Once
a nucleus of above critical size has formed by a statistical
fluctuation, the nucleus would be able to grow into a
liquid skin either by the absorption of adatoms, or by
activating atoms directly from the surface.   This would
result in a time delay, similar for example to that in
supercooling (Hollomon and Turnbull, 1950).   Providing
the temperature is above the 'skin melting temperature'
the liquid skin, once formed, is able to advance through the
remainder of the solid as this results in a progressive
reduction of the free energy of the system, and so dissolve
the solid.

      The absence of time delay in the melting of small
particles of lead (Peppiatt, 1973) and tin (section 6.3.)
suggests that the initial liquid nucleus had little difficulty
in forming compared to the bismuth · particles.   As adatoms

are likely to be present in all these cases, the difference
probably lies in the substantial rearrangement of atoms
necessary between the solid and liquid bismuth which does
not occur in lead and tin.   However, the adatoms are likely
to play a major part in the formation of the liquid skin.

On the basis of the above discussion, the time
delay observed in the melting of the bismuth particles would
be expected to be greatly dependent on the following
parameters.

1. The size, surface area, and the morphology
of the crystallites:

The skin melting temperature (T_{SK}) below which
the time delay cannot occur, will approach the bulk melting
point for large particles while showing a great reduction
for small particles (section 2.3.).   Also, by assuming that
the initial liquid nucleus can form at all sites on the
solid surface, an increase in the size of the particles
increases the number of possible nucleation sites.   If the
specimen is held at a constant temperature above the skin
melting temperatures of the particles in a layer, the
particles having the largest surface area would be expected
to have a shorter time delay than smaller particles (see
section 5.2.3.).   However, if the available surface area
is limited by the possibility of the liquid nucleus forming
only on certain crystal planes of a particle, the shape of
the particle would affect the time delay.

2.   Imperfections in the crystallites:

The production of the liquid nucleus will be influenced by the imperfections present in the crystallite. Given the difficulty in forming the liquid nucleus due to the rearrangment of atoms on melting, the imperfections will provide suitable nucleation sites for melting as the liquid nucleus requires less activation energy to form in these regions.   The imperfections will also act as sources of adatoms for the formation of the liquid nucleus.

3.   The temperature of the crystallites: ·

An increase in temperature favours the production of the liquid, and also increases the concentration of adatoms.   Therefore, the time delay would be expected to be lower the   higher   the temperature, section 5.4.5.

8.2.2.   Effect   of Size of the Particles on the Time Delay.

(i)   Absence of Time Delay in the Polyhedra

(Type I) Crystallites.

The polyhedra (type I) crystallites (section 5.2.1.) having sizes greater than $1400\text{\AA}$ were found to melt without a measurable time delay when heated close to the bulk melting point (section 5.4.1.),   Upon heating a layer of bismuth comprising of the type I (polyhedra) and type I (platelet) particles for various lengths of time from temperatures below the bulk melting point to near the bulk melting point, the number of the polyhedral particles

remaining solid did not decrease with time until at the bulk

melting point, all the polyhedral particles in the layer

were seen to have melted.   During this time the number of

the platelet (type I) particles decreased steadily, and

therefore a characteristic time of melting (τ) (see, section

1.2.) could be determined at each temperatue.   For the

polyhedral particles, even if a time delay does exist at

the bulk melting point, the characteristic time of melting

would be so small that it could not be determined within

the time scale of the present experiments.

As previously noted, the skin melting temperature

of a crystallite increases with the size of the crystallite;

for large crystallites it approaches the bulk melting point

(T_o).   The equation relating the skin melting temperature

(T_{SK}) of a crystallite to its size is given by (section 2.3.).

$$T_{SK} \simeq T_o - \frac{2T_o}{L\rho_s r_s} \left[\gamma_{s\ell} + \gamma_\ell (1 - \frac{\rho_s}{\rho_\ell}) \right] \qquad (8.2.1).$$

(Here the relation for the case of a spherical

crystallite having radius r_s has been used.   This seems to

be appropriate for the polyhedral particles, as these were

seen to assume a more compact spherical form on annealing

near the bulk melting point, see figure 5.4.1.a).   Then by

using the values of the physical constants of bismuth listed

in appendix A.4., the skin melting temperature for the

smallest (1400Å) and the largest (6500Å) polyhedra (type I)

particles observed in the present experiments, can be

calculated to be approximately 2K and 0.5K below the bulk

melting point (544K) respectively.   Also, as these particles

are large, it is possible that a large number of imperfections

may be present in them.   It is these imperfections which

would enable these crystallites to slowly regrow into a more

compact spherical form.   This   contrasts the platelet (type 1)

particles in the layer which remained stable despite the

heating, and therefore are presumably more perfect.   The

imperfections in the polyhedral particles provide suitable

nucleation sites for the liquid skin.   Therefore, on heating

to the bulk melting point, the polyhedral particles would

be expected to melt with the shortest time delay not

measurable in the present experiments.

(ii)   The Dependence of the Time Delay on the

Surface Area of a Particle.

The characteristic times of melting (τ) of the

polyhedra (type II) particles (section 5.2.1.) with sizes

ranging from a few hundred to a few thousand Ångstorms in

diameters were determined at a given temperature as a

function of the surface area of the particles.   The results

show that at temperatures of a few degrees below the bulk

melting point, the characteristic time of melting of the

particles in a layer vary inversely as the square of the

radii of the particles (figure 5.4.5.).   As these particles

are spherical, this gives a dependence of the characteristic

time of melting on the surface area of the particles.   At

lower temperatures a departure from the linear dependence

of the characteristic time on surface area was observed (figure 5.4.6.).

At these temperatures, only the smallest particles in the layer melt,

the specimen temperature being above the skin melting temperature of

these particles. As very few of the large particles melt at these

temperatures, the graph bends upwards at the large particle end due

to the increased time delay in the large particles (figure 5.4.6.).

Now, by considering that the liquid nucleus can form at any

position on the solid surface, let the nucleation rate per unit area

per second be I and be given by

$$I = \frac{kT}{h} \exp \left[- \frac{E(T,r)}{kT} \right] . \qquad (8.2.2.)$$

Here E is the activation energy for the formation of the liquid

nucleus and is a function of temperature (T) and size (r) of a

crystallite.

The number of nuclei formed per second on area $4\pi r^2 = 4\pi r^2 I$ (8.2.3a.)

After time τ, one particle is melted. Hence, by assuming that

the nucleation is immediately followed by melting of a particle, we

have

$$4\pi r^2 I \tau = 1 \qquad (8.2.3b.)$$

Substituting equation (8.2.2.) in equation (8.2.4.)and simplifying

$$\tau = \frac{1}{4\pi r^2} \frac{h}{kT} \exp \left[\frac{E(T,r)}{kT} \right] . \qquad (8.2.4a.)$$

Taking logarithms, we get

$$kT\ln (\tau r^2) = E (T,r) + kT\ln (\frac{h}{4\pi} \frac{1}{kT}) \qquad (8.2.4b.)$$

where the second term on the right hand side is only slowly dependent

on temperature, and can be regarded as constant. In figure 8.2.1.,

$kT\ln (\tau r^2)$ is plotted as a function of crystallite size (r) at
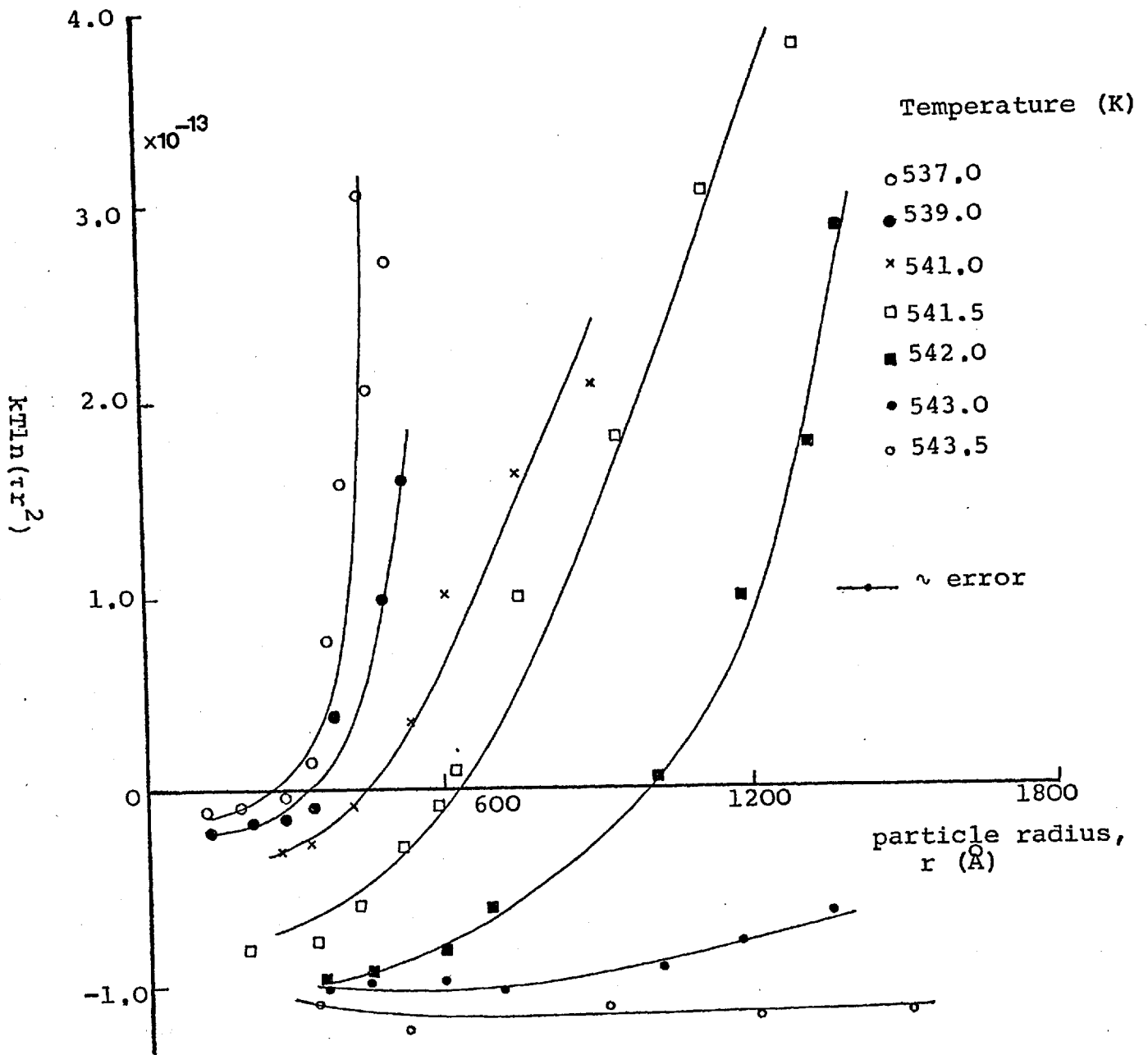
FIGURE 8.2.1.

various temperatures. By considering 500$\overset{\text{o}}{\text{A}}$ to be the average size of the crystallites studied, values of E(T,r) can be evaluated from equation (8.2.4b.) and are listed in the following table.

Temperature (K)	E(T,r) (eV)
537.0	0.801
539.0	0.792
541.0	0.753
541.5	0.710
542.0	0.680
543.0	0.665
543.5	0.626

The detailed interpretation of the results, however, must depend on a detailed nucleation theory of melting analogous to that for super-cooled droplets. Such a theory has not so far been evaluated.

8.2.3. Effect of Morphology of the Particles on the Time Delay

On heating a solid deposit of bismuth containing the type I (platelet) and the type II* (polyhedra) particles at a given temperature, it was observed that a large number of the type II* (polyhedra) particles melted within the first few minutes of heating compared to the type I (platelet) particles during the same time. This resulted in a curvature in the graph for the total of the two types of particles (figure 5.4.3.), the curvature being due to the higher melting rate of the polyhedra (type II*) particle compared to the platelet (type I) particles. If N_I and N_{II^*} are the number and τ_I and τ_{II^*} are the characteristic times of melting of the platelet (type I) and polyhedra (type II*) particles respectively, then the graph of figure 5.4.3. can be represented by the sum of the curves for the polyhedra (type II*) (fig. 5.4.4.a) and the platelet (type I) (fig. 5.4.4.b) particles as follows.

$$N = N_I \exp\left(-\frac{t}{\tau_I}\right) + N_{II*} \exp\left(-\frac{t}{\tau_{II*}}\right) \qquad (8.2.5.)$$

where N is the total number of the two types of particles
remaining solid after time t. From the curves for the two
types of particles, it can be seen that at a given
temperature

$$\tau_I > \tau_{II*} \qquad\qquad\qquad (8.2.6.).$$

In the present experiments, the characteristic time of
the polyhedra (type II*) particles at a   given temperature
was found to be similar to that obtained by Peppiatt
(1973, 1975) for the polyhedra (type II) particles. This
is presumably due to the identical shape of these two types
of particles.

The increased melting rate (the reciprocal of τ)
of the polyhedra (type II*) particles compared to the
platelet (type I) particles is possibly due to the difference
in shape between these two forms of crystallites. The
polyhedral particles are almost spherical, with side faces
consisting mostly of the $(11\bar{2}0)$ type plane (in the hexagonal
notation); the surfaces of the type I (platelet) particles
consist largely of the basal (0001) plane (Peppiatt, 1973).
The observation that the type I (platelet) particles have
a larger time delay (at a given temperature) than the type II*
(polyhedra) particles suggests that the liquid nucleus is
less likely to form on the basal plane than on the other planes.

8.2.4.   The Time Delay in the Melting of the Particles

on the Molybdenite Substrate.

The bismuth particles on the molybdenite substrates were mostly in the form of needle-like platelets, while a few were irregularly shaped (section 5.2.2.).   The needle-form of the platelets suggests that these particles had difficulty in nucleation on the side faces during the growth from the vapour phase, and possibly that a screw dislocation is present along each particle.   Nucleation is more likely to occur where the screw dislocation emerges at each end of the particle rather than on the side faces. The core of the screw dislocations would provide more suitable nucleation sites for the liquid nucleus, than the side faces which are presumably free from such imper-fections.   The liquid droplet formed on melting a particle was always located at one end of the particle.   This is possibly due to the formation of the liquid skin at one end of the particle where the screw dislocation emerges. In this case, the skin melting temperatue of the needle-like particle would be similar to that of a spherical particle (section 2.3.3.).

The crystallites on the molybdenite substrates exhibited a time delay in melting (section 5.4.4.).   The time delay was found to be lower in the initial stages of melting, resulting in a curvature in the graph (figure 5.4.8.).   A value of characteristic time (τ) was generally

determined from the later stages of heating which showed a
good exponential decay in the number of solid particles
remaining solid.   However, no correlation could be found
between the rate of melting and the morphology of the
crystallites when the graphs were drawn separately for the
needle-like and the irregularly shaped particles (figure
5.4.9.).   This is in contrast to the results obtained in
the previous section.   A similar higher initial melting
rate has been observed by Peppiatt (1973) for the platelet
(type I) particles on amorphous carbon substrates.   It is
probable that the needle-like or the irregularly shaped
particles used in the experiments were not all identical,
but had substantial differences (for example, strains,
imperfections and the shape of the particles, will probably
influence its properties).   This in turn may lead to
different processes by which the critical liquid nucleus
may form and grow.   In this case, the particles would be
expected to have a wide range of activation energies for
melting, and therefore a large spread in the time delay.
This, however, must wait the outcome of future experiments.

It was also observed that some of the particles
had a large time delay even at temperatures above the bulk
melting point, resulting in a superheating of approximately
2K (section 5.4.4.).   This is in contrast to the super-
heating of up to 7K in the platelet (type I) particles on
amorphous carbon substrates observed by Peppiatt (1973), 1975).

If there is a contact angle for the liquid on
the solid surface (section 2.2.3.), a liquid skin would
not be able to form below the bulk melting point without
a virtually impossible statistical fluctuation.   In
such a case, a small particle would not melt below the bulk
melting point, but would be superheated above the bulk
melting point.   While the particles have been observed to
melt below the bulk melting point, and therefore the wetting
condition (section 2.2.3.).must have been satisfied for a
majority of particles, it is probable that for a few
crystallites, the wetting condition is not satisfied,
perhaps because of surface contamination.   These particles
would not be able to melt without being superheated above
the bulk melting point.

8.2.5.   Effect of Temperature on the Time Delay.

An increase in temperature favours the formation
of the liquid skin, and also increases the concentration of
adatoms which are likely to play a major part in the
formation of the liquid skin.   Also an increase in temperature
reduces the activation energy needed to form the critical
nucleus.   The variation in the number of adatoms (N) with
temperature (T) can be given by

$$N = N_o \exp \left(- \frac{\Delta F}{kT}\right)$$ (8.2.7.)

where N_o is the initial number of   atoms and ΔF is the
activation energy required to activate an atom on the solid
surface.   An increase of temperature, therefore, will
increase the number of adatoms available for the formation

of the critical nucleus;   the liquid skin is therefore

more likely to form at higher temperatures than at lower

temperatures.   Therefore, the time delay would be expected

to decrease at higher temperatures.   The experimental curves

for the variation of the characteristic times of melting

with temperatures for the various types of particles

studied in the present experiments have been   redrawn,

without the experimental points, in figure 8.2.2, to allow

a direct comparison.   The curve for the type I (platelet)

particles has been extended into the regions beyond the

bulk melting point investigated by Peppiatt (1973, 1975).

These experimental plots produce a good linear relationship

between $\ln(\tau)$ and T, the temperature.   The experimental

points corresponding to the type II* (polyhedra) particles

agree well with the experimental curve for the type II

(polyhedra) particles obtained by Peppiatt.   The results

show a decreasing time delay with increasing temperature

as is expected.   The slopes of the curves for the type II*

(polyhedra) and the needle-like particles are nearly equal.

This is probably because, although the shapes of these two

forms of particles differ, their skin melting temperature

will be determined by the relation for the skin melting

temperature of a spherical particle, considering the liquid

skin forming at one end of the needle-like crystallite.

Now by assuming that

$$\tau = \tau_o \exp \left(\frac{\Delta E}{kT}\right) \qquad\qquad (8.2.8.)$$

FIGURE 8.2.2.

The variation of the characteristic time of melting (τ) with temperature. (Plotted on a logarithmic scale).
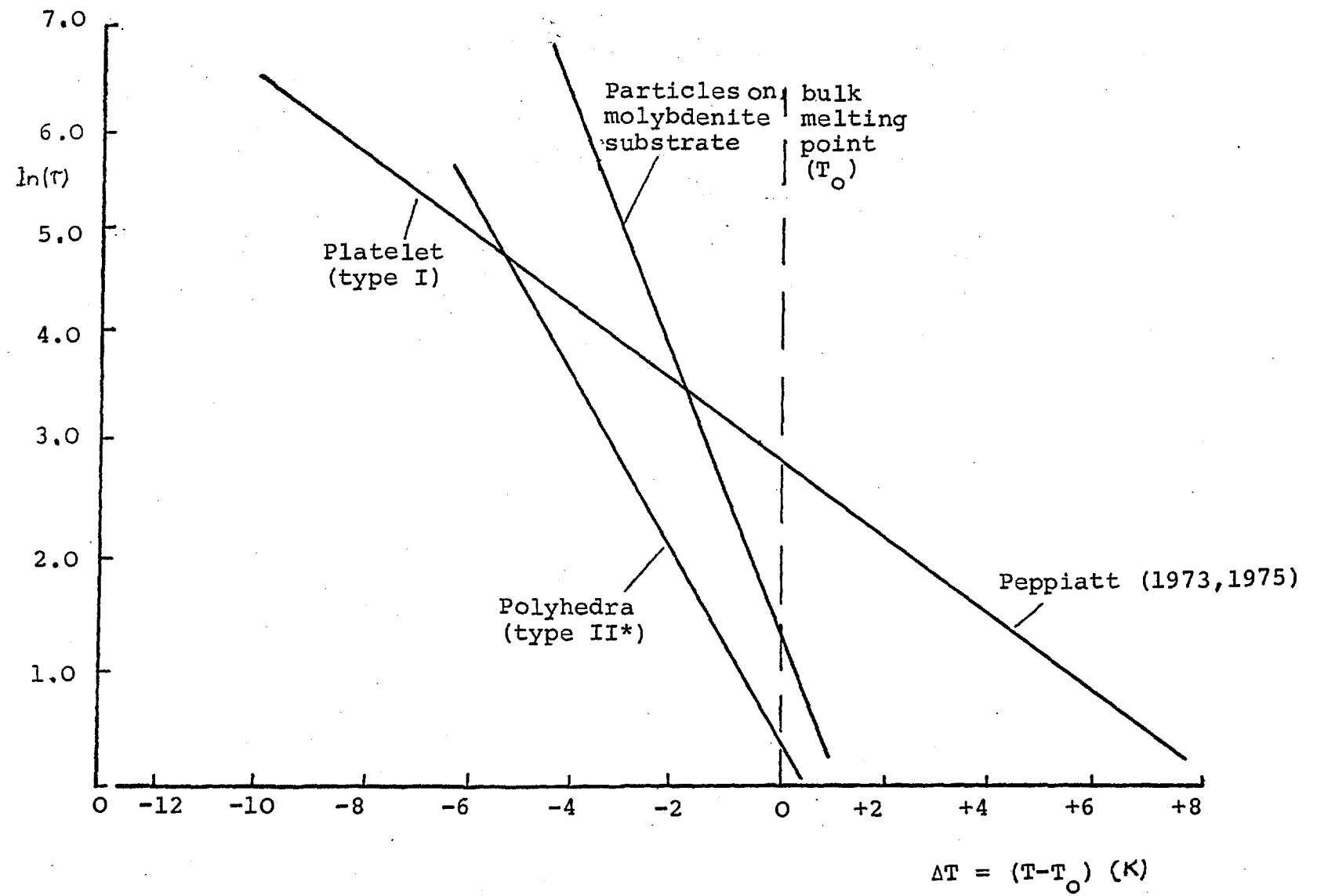
an attempt can be made to explain the variation of $\ln(\tau)$

with the temperature (T) in terms of a simple activation

energy for melting.   In the above equation, ΔE is the

activation energy, and τ_0 is independent of temperature.

Taking logarithms and differentiating equation (8.2.8.)

$$\Delta E = - kT^2 \frac{d}{dT} (\ln.\tau) \qquad (8.2.9.)$$

Therefore, by using the gradients of the experimental curves

(figure 8.2.2.), activation energies (ΔE) of 20 and 23eV

can be determined for the melting of type II* (polyhedra)

and the needle-like particles respectively.   This is in

comparison to an activation energy of 9eV obtained

similarly from the slope of the curve for the type I

(platelet) (Peppiatt, 1973).   These values are widely at

variance, for example, with a value of ΔF_a, (see section

2.2.) usually less than an electron volt, obtained by

equating it to the activation energy for viscous flow.

(Turnbull, 1950) in a supercooled liquid.   The reason for

this discrepancy, however, is not clear.

8.2.6.   Summary.

The time delay observed in the melting of small

particles of bismuth has been attributed to the difficulty

in the nucleation of the initial liquid skin.   This

difficulty is probably due to the activation energy required

for the substantial rearrangement of bismuth atoms

necessary on melting.   Also an activation energy is
needed to form the liquid skin from an initial two dimensional
liquid nucleus formed by an aggregation of adatoms.   On
this picture, the experimental results on the time delay
have been discussed to be dependent on the following
parameters:

1.   The size, surface area, and morphology of the
     particles.

2.   The imperfections present in the particles.

3.   The temperature of the particles.

8.3.   Discussion on the Supercooling Results of Small Liquid Droplets.

In the present experiments, the supercooling of bismuth and tin was observed for particles of a few hundred Ångstroms diameter, on amorphous carbon films and cleavage flakes of molybdenite and graphite (section 7.3).   Tables 8.3.1. and 8.3.2. list the maximum amount of supercooling (ΔT_{max}) observed; for comparison, the results of a few other workers are also included.   The particle size and the experimental conditions are given in each case.

The degree of supercooling on the two crystalline bases was substantially lower than that on carbon.   The effect of a crystalline base on the amount of supercooling in small liquid droplets has also been noted by other workers.   Stowell et al.(1970), in an electron microscope under a residual gas pressure of approximately 10^{-8} torr, found that small ($\sim$ 100Å - 3,000Å diameters) liquid droplets of lead could be supercooled to 237K on carbon substrates, but the supercooling was only 97K on molybdenite substrates. This indicates that the substrate helps to nucleate the liquid-solid transformation.   Also bearing in mind the method of preparation of the crystalline substrates (section 4.2.1.), it is likely that these will be more contaminated than the carbon substrates.   Consequently, with the contaminants providing additional nucleation sites, the degree of supercooling will be considerably reduced from that on the carbon substrates.   Traces of contaminants

Reference	T(K)	ΔT_{max}(K)	Particle Radius	Experimental Conditions.
Present Work	382	162	300Å	Vacuum of 4×10^{-7} torr, carbon substrate.
	429	115	300Å	Molybdenite substrate.
	416	128	300Å	Graphite substrate.
Peppiatt (1973)	400	144	300Å	Vacuum of 5×10^{-7} torr, carbon substrate.
Coombes (1967)	462	82	200Å	Vacuum of 10^{-5} torr, carbon substrate.

Table 8.3.1. Results for the supercooling of bismuth.

(T_o = 544K)

Reference	T(K)	ΔT_{max}(K)	Particle Radius	Experimental Conditions.
Present Work	335	170	300Å	Vacuum of 4×10^{-7} torr, carbon substrate.
	390	115	300Å	Molybdenite substrate.
	372	133	300Å	Graphite substrate.
Peppiatt (1973)	351	154	300Å	Vacuum of 5×10^{-7} torr, Carbon substrate.
Blackman and Curzon (1959)	415	90	50Å	Vacuum of 10^{-5} torr, Carbon substrate.
Sayama (1941)	425	80	0.1cm	Molybdenite substrate.

Table 8.3.2 Results for the supercooling of tin.

(T_o = 505K).

on the crystalline substrates have occasionally been observed in the present work.

The amount of supercooling on carbon does not differ significantly from that of Peppiatt (1973) obtained in identical conditions, but is appreciably greater than those of the other workers in a poor vacuum. The results of Coombes (1967) on bismuth and Blackman and Curzon (1959) (see also Curzon, 1960) on tin are probably dominated by the nucleating influence of gaseous and polymerized hydrocarbon contaminants in the electron diffraction camera. The fact that greater supercooling can be achieved by an improvement in the vacuum condition (see also Stowell et al., 1970) suggests that the environment has a significant effect on the results. It is therefore not clear whether homogeneous nucleation occurred in any of the cases quoted above, or even in the present experiments.

[Takagi (1954) quotes a supercooling of 192K for tin particles of 86Å average diameter on crystalline substrates. This value is much higher than that obtained presently in an improved vacuum compared to that which she could have possibly achieved in the electron diffraction camera. The reason for this discrepancy is not obvious, but is perhaps due to the use of far smaller particles than used here (see Turnbull, 1950), or an inaccuracy in the temperature measurement.]

The liquid droplets in the present experiments did not all solidify simultaneously as the crystalline diffraction pattern was observed to gradually increase in intensity over a range of temperature, quoted in tables 7.3.1. and 7.3.2.   The reason might be due to the presence of some minute specks covering parts of the substrates. Recrystallization of the droplets would be expected to occur in these parts before the droplets in the other parts due to the "seeding" effect of foreign particles.   Another cause may be a size effect on supercooling (Turnbull, 1950), which was not systematically investigated in the present work.   Blackman and Curzon (1959), by using the same criterion to determine the particle size as used in their melting experiments (see section 1.3), found that for tin particles in the size range of $60\overset{\circ}{A}$ to $200\overset{\circ}{A}$ diameter, the supercooling varied inversely with particle size.

The results of supercooling of small liquid droplets have been used by various authors to obtain an estimate of the solid/liquid interfacial energy ($\gamma_{s\ell}$) of a material.   This is based on the theoretical treatment of supercooling by Holloman and Turnbull (1950).   By assuming the nucleation to be homogeneous (see section 2.2.1.), they derived the following formula relating the amount of supercooling (ΔT) to the nucleation rate per unit volume (I)

$$I = n \left(\frac{kT}{h}\right) \exp\left(-\frac{\Delta F_a}{kT}\right) \exp\left[-\frac{16\pi\gamma_{s\ell}^3}{3\rho_s L^2} \cdot \frac{T_o^2}{(\Delta T)^2} \cdot \frac{1}{kT}\right] \qquad (8.3.1).$$

where L is the latent heat of fusion per unit mass, T_o is
the bulk melting point and n is the number of liquid atoms
per unit volume. Following Holloman and Turnbull, by
using the values of 10^{-1} sec^{-1} per particle for I and
10^{-2} for exp $- \dfrac{\Delta F_a}{kT}$, the following expressions
relating the interfacial energy $(\gamma_{s\ell})$ to the maximum amount
of supercooling (ΔT_{max}) and the average volume (v) of the
particle involved can be obtained,

$$\gamma_{s\ell}^3 = A. \ (\Delta T_{max})^2 . T . \left[\ln(v) + B \right] \qquad\qquad (8.3.2)$$

where

(i) for bismuth, $A = 4.58 \times 10^{-4}$, $B = 79.4$
and (ii) for tin, $A = 5.34 \times 10^{-4}$, $B = 79.6$

Here, v is in cubic centimetres and $\gamma_{s\ell}$ is in ergs cm^{-2}.

Thus, from the maximum amount of supercooling
observed in the present experiments, values of 58.0 ergs cm^{-2}
and 60.5 ergs cm^{-2} for $\gamma_{s\ell}$ can be obtained for bismuth
and tin respectively. These values differ from 46.0 ergs
cm^{-2} and 54.5 ergs cm^{-2} respectively obtained by Holloman
and Turnbull. Their observed values of supercooling for
5 μm size particles of bismuth and tin were 90K and 80K
respectively. The discrepancy between the values of $\gamma_{s\ell}$
is therefore due to the greater supercooling achieved in the
present experiments. As contaminantion has such a great
influence, it seems that this method of obtaining the
maximum degree of supercooling may only be used to estimate
a lower limit for the solid/liquid interfacial energy.

8.4.   Discussion on Other Observed Properties of the
          Thin Films.

8.4.1.   Diffusion in Small Particles of Tin.

(i) Introduction.

As described in section 7.1., upon heating,
changes in shape of the solid tin particles occurred in two
distinct ways.   In one, at temperatures of 10K or more
below the respective melting point, substantial changes in
shape of irregularly shaped platelets occurred continuously
over a period of several minutes during a melting
experiment (see figure 7.1.1.).   The changes were of a
gradual character, and were consistent with normal diffusion
processes, also observed by other workers (see, for example,
Pashley et al. 1964; Peppiatt, 1973).   In the second
type, at temperatures within a degree of the melting point
of the respective platelet, changes of shape occurred
abruptly by an unusually enhanced form of diffusion, termed
'snapping' (Blackman et al., 1975).   Changes of shape of
this type has also been observed by Peppiatt (1973) in
somewhat larger bismuth crystallites; the diffusion process
was termed "rapid solid diffusion".   Snapping in the
bismuth crystallites was, as a rule, asymmetric with more
material being transported from some sides of the crystallite
than others.   In the tin platelets, snapping occurred
asymmetrically and also symmetrically in which material
was transported from all sides of a crystallite (figures
7.14. and 7.13.).   Occassionally, a few tin platelets also

exhibited a "double" snapping with a sudden shape change

occurring twice in rapid succession (figure 7.1.5).

(ii)   Snapping ("Rapid Solid Diffusion").

An explanation has been proposed by Peppiatt

(1973) to interpret his observations   on the snapping

(or rapid solid diffusion) in micron size bismuth crystallites.

In this, parts of a crystallite assumed to contain more

imperfections and strains than the remainder, is expected

to melt at temperatures below the melting point of the rest

of the (less imperfect) solid particle. The speed of the

change in shape results from the rapid movement of the

liquid portion towards the solid particle to reduce the

surface energy by forming a more spherical shape. The

liquid, after covering the top solid surface, either

completly or partly, is expected to resolidify as the

solid is still below its melting point.

While the above theory might explain the

abruptness observed in snapping due to the rapid movement

possible in liquid, it does not seem to explain the

retention of the shape of certain edges of a crystallite

after snapping as observed by Peppiatt in the bismuth

crystallites. If it were to assume that the abrupt

changes in shape were due to the production and subsequent

movement of the melt, the shape of the edges after snapping

would be expected to form differently by a rearrangement

of the atoms on the surfaces of the edges. As for bismuth

crystallites, the initial shapes of the edges of the tin
crystallites were generally retained after snapping (figures
7.1.2, 7.1.3, and 7.1.4).

An explanation, therefore, is proposed in which
it is assumed that the surfaces of the edges of a tin
crystallite are strained.   Upon heating, it is likely that
strains will be introduced in the surfaces of edges of a
crystallite due to the difference in the thermal expansion
coefficients between the substrate and the crystallite.
As soon as a strained region is removed, enhanced diffusion
will occur due to the large amount of strain energy
released.   As it is likely that the crystallites are far
from their equilibrium shape, a release of the strain
energy will reduce the energy of the system and the
crystallite will assume a more compact form during the
process.   The platelet will grow in thickness and the
visible area of the crystallite will have decreased
substantially, as has been observed.   Also, in the process,
the shapes of the edges of a particle would be expected
to be retained.

As stated previously, since the snapping was
predominantly observed within a degree of the melting point
of the respective platelets, the possibility of a liquid
layer forming on the surfaces of the edges of the platelets
might not be ruled out.   The liquid layer, however, must
be assumed to be thin, possibly a few monolayers in thick-
ness in contrast to the melting of parts of a crystallite

assumed by Peppiatt in the snapping of the bismuth crystallites. The liquid layer might form on the surfaces of the strained edges, as this results in the reduction of the energy associated with such surfaces, and therefore, in an enhancement of the diffusion process.   As the liquid layer is assumed to be thin, no appreciable change in shapes of the edges would be expected to occur by the rearrangement of the atoms on the surfaces of the edges after snapping. Imperfections present on the edges may also cause the formation of such a liquid.   However, no such imperfections were seen to be present in the thin tin platelets in the present work.

The tin platelets, in the form of an ellipse or circle ,   were generally seen to snap symmetrically, while the asymmetric snapping was more common in the irregularly shaped platelets with several re-entrant angles. The elliptical or circularly shaped platelets were therefore presumably strained on all sides, whereas in the irregularly shaped platelets only a few regions were strained.   Some of these irregularly shaped particles also exhibited a 'double' snapping.   It is not understood why, after the release of the strain energy which causes the particle to snap once, the same particle should snap again, as the strain energy would be expected to dissipate at the end of the first snapping.

Snapping in the tin platelets was observed only

on carbon substrates, not on molybdenite and graphite
substrates, although the shapes of the particles were
identical on all the substrates. The tin particles on
these substrates were seen to be severely contaminated at
the end of an experiment. These contaminants might have
inhibited the movement in the particles.

(iii)   Normal Solid Diffusion.

As described previously, changes of shape in the
tin platelets at temperature of 10K or below the melting
point of the respective platelets occurred by a slow
diffusion process, consistent with normal diffusion processes.
By a removal of the re-entrant angles, the shapes of the
edges of the irregularly shaped particles were rounded
and the particles attained a more compact form. Several
minutes were required to attain a substantial change in shape.

The above rounding of edges in small crystallites
have been observed by other workers during the continuous
deposition of thin films in an electron microscope (Pashley
and Stowell, 1966; Pashley et al., 1964). The shape
changes observed were always such that the surface area of
a particle was decreased. This is presumably to reduce
the surface energy of the system. The predominant process
in such shape changes is probably surface diffusion.

8.4.2.   Diffusion in Bismuth Films on Molybdenite Substrates.

As described in section 7.2., continuous films
with misshapen holes were obtained by condensing more
bismuth onto molybdenite substrates at approximately 425K,

than was needed to obtain the films with the needle-like
crystallites (figure 5.2.7.).   On heating these layers for
a few minutes at about 10K below the bulk melting point,
the misshapen holes changed into mostly oriented hexagonal
holes (figure 7.2.1.), while in some layers a few triangular
holes (figure 7.2.2.) were also seen to have formed.

Coopersmith et al. (1966) observed the formation
of mostly oriented triangular holes, together with a few
hexagonal and circular holes in their lead films deposited
onto heated molybdenite substrates in an electron microscope.
Such films were obtained when the depositions were carried
out in the absence of the electron beam.   These films
differed significantly from those deposited in the presence
of the electron beam, when the films were composed of
globular (111) lead crystallites.   These authors attribute
the discrepancy to the irradiating effect of the electron
beam (in the present experiments the depositions were
carried out in the absence of the electron beam).   They
attribute the formation of the triangular holes to the
coalascence of the (111) lead crystallites, although in such
a process more polygonal or circular holes would be
expected than those observed.   This is because the energy
associated with the boundary of a polygonal or circular hole
will be less than that associated with the boundary of a
triangular hole.

In the present work, the transformation from the
misshapen to a hexagonal or triangular hole in the bismuth

films was always such as to reduce the boundary associated

with a given hole.   The atomic diffusion process by which

such a change occurs is therefore energetically favourable,

as the change results in a decrease of the energy associated

with the boundary of a hole.   The tendency of bismuth films

on molybdenite to form the needle-like crystallites might

explain the formation of the hexagonal holes.   On heating

these layers, needle-like crystallites with one side form-

ing the boundary of a hole, may assume the configuration

for the formation of a hole with straight edges.   Such a

growth process is likely to form the polygonal holes more

frequently than the triangular holes, as has been observed.

8.4.3.   The Shapes of the Solid Particles

(i) Tin Particles.

The majority of small tin particles near the

melting point, have almost elliptical or   circular outlines.

A few particles were also seen to be square shape in

appearance.   These particles were slightly oriented with

their (100) ($\cong$ 010) fibre axis perpendicular to the substrate.

With the exception of a few of the elliptical or circular

particles showing slight faceting on the side faces (see

figure 6.2.1.), these particles were mostly bounded by

smooth curved surfaces on the side faces.   These faceted

surfaces presumably correspond to small cusps in a polar

plot of the surface energy (Herring, 1950, 1952), the smooth

curved surfaces probably have almost equal surface energies.

(ii)   Bismuth Particles.

The bismuth particles on the carbon substrates
were obtained mainly in two distinct shapes according to
their method of production, see section 5.2.1.   A platelet
form (type I) was obtained by heating a thin   ($\sim$ 100$\overset{o}{A}$ thick-
ness) initial solid deposit; a polyhedral form (type I and
type II[*]) was produced by heating a film of over 200$\overset{o}{A}$ in
thickness, while another polyhedral form (type II) was
obtained by resolidifying the liquid droplets.   The
bismuth particles on the molybdenite substrates were generally
needle-like in appearance.

The platelet form particles displayed a variety
of shapes ranging from elongated to regular hexagons
(figure 5.2.5.).   It seems highly unlikely that these
shapes or the needle-like shapes can be the Wulff equilibrium
shapes.

The polyhedral particles have almost spherical
shapes.   The distinct faceting on the side faces give these
particles a regular hexagonal appearance.   It seems that
these particles are much closer to the Wulff equilibrium
shape.   The side faces might be the six hexagonal ($11\bar{2}.0$)
faces.

APPENDICES

A.1.   TO DERIVE $\left[f_s(T) - f_\ell(T)\right]$.

$f_s(T)$ and $f_\ell(T)$ are the Helmholtz's free energies per unit mass of the solid and liquid respectively, at a temperature T.   If the temperature of a material is raised by an amount ΔT, the resultant changes in specific free energies will be given by:

$$\Delta f_s = - s_s \Delta T - p_s \Delta v_s \qquad \text{(A.1.1.)}$$

$$\Delta f_\ell = - s_\ell \Delta T - p_\ell \Delta v_\ell \qquad \text{(A.1.2.)}$$

for the solid and liquid respectively, where s is the entropy, Δv is the corresponding change in volume each per unit mass, and p is the vapour pressure.   Since the vapour pressure in the present experiments is very small, the second terms in the above equations can be neglected:

$$\Delta f_s = - s_s \Delta T \qquad \text{(A.1.3.)}$$

$$\Delta f_\ell = - s_\ell \Delta T \qquad \text{(A.1.4.)}$$

Subtracting these, and taking the changes to be infinitesimally small

$$df_s - df_\ell = - (s_s - s_\ell) . dT \qquad \text{(A.1.5.)}$$

Now the differences in the specific entropies of the solid and liquid is given by:

$$T(S_\ell - S_s) = L \qquad \text{(A.1.6.)}$$

where the latent heat of fusion per unit mass, L, is considered constant over the temperature range involved.   Therefore,

$$df_s - df_\ell = L. \frac{dT}{T}$$ (A.1.7.)

Integrating this between T_O the bulk melting temperature and the temperature T gives

$$f_s(T) - f_\ell(T) - f_s(T_O) + f_\ell(T_O) = L.\ln\left(\frac{T}{T_O}\right)$$ (A.1.8.).

However, at the bulk melting temperature

$$f_s(T_O) = f_\ell(T_O)$$ (A.1.9.)

as this is the equilibrium temperature for the bulk material. Therefore,

$$\left[f_s(T) - f_\ell(T)\right] = L.\ln\left(\frac{T}{T_O}\right)$$ (A.1.10.)

$$\simeq L. \frac{T-T_O}{T_O}$$

A.2.   THE SKIN MELTING TEMPERATURE (T_{SK}) OF A CURVED SURFACE.

(This section is based on unpublished work by Dr.S.J. Peppiatt.).

Let R_1 and R_2 be the principal radii of curvature of a small part of a curved surface (figure A.2.1.).   The angles subtended by this "rectangular" area at the respective centres O_1 and O_2 are $d\theta_1$ and $d\theta_2$.   Thus, the sides of this rectangle are given by

$$dl_1 = R_1 d\theta_1$$
                                                        (A.2.1.)
$$dl_2 = R_2 d\theta_2$$
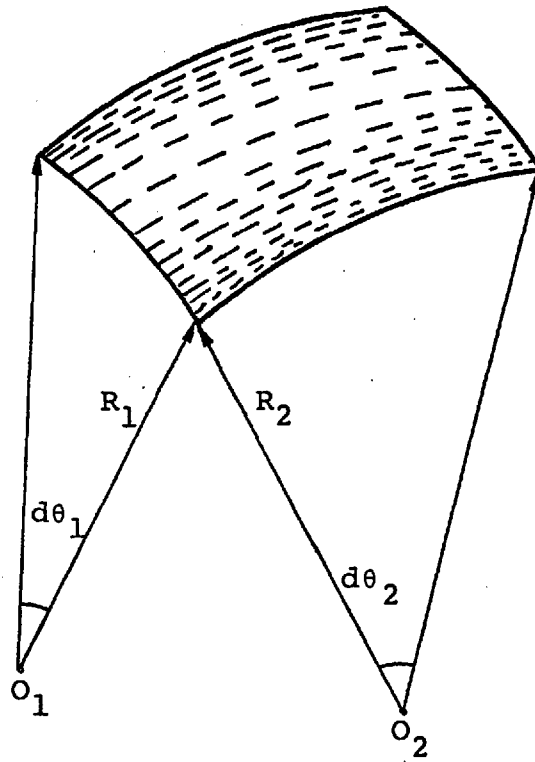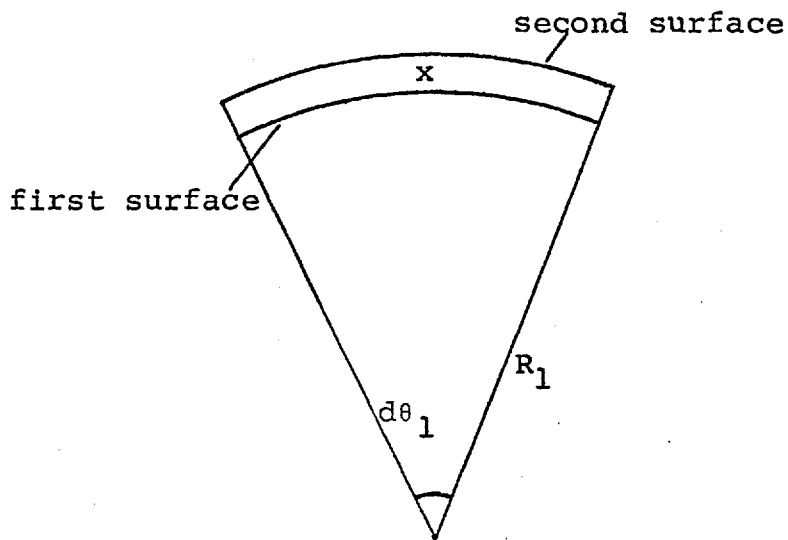
FIGURE A.2.1.

FIGURE A.2.2.

Providing $d\theta_1$ and $d\theta_2$ are small, the area of the surface is

$$dA \simeq d l_1 . d l_2$$

$$= R_1 R_2 d\theta_1 d\theta_2 \qquad \text{(A.2.2.)}$$

Now consider another surface, parallel to the first, subtending the same angles $d\theta_1$ and $d\theta_2$ at O_1 and O_2 respectively, but at a distance x outside the first surface (see figure A.2.2.). The area of this second surface will be given by,

$$dA_x = dl_{x_1} . dl_{x_2}$$

$$= (R_1 + x)(R_2 + x) . d\theta_1 d\theta_2 \qquad \text{(A.2.3.)}$$

And the volume between the two surfaces is,

$$dv = \int_0^x \left[dA_x \right] dx$$

$$\simeq \left\{ R_1 R_2 x + (R_1 + R_2) \frac{x^2}{2} \right\} d\theta_1 d\theta_2 \qquad \text{(A.2.4.)}$$

(neglecting third order terms in x)

The difference in area between the first and the second surface is,

$$dA_x - dA = \left\{ (R_1 + R_2) x + x^2 \right\} . d\theta_1 d\theta_2 \qquad \text{(A.2.5.)}$$

Now consider a solid surface to melt uniformly to a depth δ_0 (see figure A.2.3.); the thickness of the liquid

skin (δ) will be different from δ_o due to the change in density of the material on melting.

As the mass of the material remains unchanged on melting, we must have,

$$\delta_o \rho_s = \delta \rho_\ell \qquad\qquad (A.2.6.)$$

Now, the change in surface energy from an infinitesimally thin liquid skin ($\delta_o \to 0$) is,

$$\Delta F_{surf} = \left[\gamma_{s\ell} \left\{ -\delta_o(R_1+R_2) + \delta_o^2 \right\} \right.$$

$$\left. +\gamma_\ell \left\{ (\delta-\delta_o)(R_1+R_2)+(\delta-\delta_o)^2 \right\} \right] \cdot d\theta_1 d\theta_2 \qquad (A.2.7.)$$

And the change in volume energy,

$$\Delta F_{vol} = dM \left[f_\ell(T) - f_s(T) \right]$$

$$= \left[f_\ell(T) - f_s(T) \right] \left[(R_1-\delta_o)(R_2-\delta_o)\delta+(R_1+R_2-2\delta_o) \cdot \right.$$

$$\left. \frac{\delta^2}{2} \right] \cdot \rho_\ell d\theta_1 d\theta_2 \qquad (A.2.8.)$$

where dM is the mass of the material which has melted.

Therefore, the total change in free energy,

$$\Delta F_{tot} = \Delta F_{surf} + \Delta F_{vol}$$

$$= \left[C_1 \delta_o + C_2 \delta_o^2 \right] \cdot d\theta_1 d\theta_2 \qquad (A.2.9.)$$

(neglecting third order terms in δ_o)

where,

$$C_1 = (\alpha \gamma_\ell - \gamma_{s\ell})(R_1 + R_2) + \left[f_\ell(T) - f_s(T)\right] . \rho_s R_1 R_2 \qquad (A.2.10.)$$

$$C_2 = \gamma_{s\ell} + \alpha^2 \gamma_\ell - \tfrac{1}{2}(R_1 + R_2)(1-\alpha)\left[f_\ell(T) - f_s(T)\right] . \rho_s \qquad (A.2.11.)$$

and $\quad \alpha = \dfrac{\rho_s}{\rho_\ell} - 1 \qquad\qquad\qquad\qquad\qquad\qquad (A.2.12.)$

The variation of ΔF_{tot} with δ_0 at various temperatures is shown in figure A.2.4. There is a maximum for ΔF_{tot} as C_2 is negative; this maximum occurs at $\delta_0 = 0$ at the skin melting temperature (T_{SK}); at this temperature,

$$\left(\frac{\partial \Delta F}{\partial \delta_0}\right)_{\delta_0 = 0} = 0 \qquad\qquad\qquad\qquad (A.2.13.)$$

Therefore, equating the coefficients of δ_0 in equation (A.2.9.) to zero, we have from equation (A.2.10.):

$$(\alpha \gamma_\ell - \gamma_{s\ell})(R_1 + R_2) + \left[f_\ell(T) - f_s(T)\right]\rho_s R_1 R_2 = 0$$

or, $\left[f_\ell(T) - f_s(T)\right] = \dfrac{1}{\rho_s}\left(\dfrac{1}{R_1} + \dfrac{1}{R_2}\right)\left[\gamma_{s\ell} + \gamma_\ell\left(1 - \dfrac{\rho_s}{\rho_\ell}\right)\right] \qquad (A.2.14.)$

However, from equation (A.1.10.):

$$\left[f_s(T) - f_\ell(T)\right] = L . \ln\left(\frac{T}{T_0}\right)$$

Therefore, substituting T_{SK} for T at the skin melting temperature, we have from equation (A.2.14):

$$\ln\left(\frac{T_{SK}}{T_0}\right) = -\frac{1}{L\rho_s}\left(\frac{1}{R_1} + \frac{1}{R_2}\right)\left[\gamma_{s\ell} + \gamma_\ell\left(1 - \frac{\rho_s}{\rho_\ell}\right)\right] \qquad (A.2.15.)$$

$$\simeq \frac{T_{SK} - T_0}{T_0}$$

original solid surface

liquid surface

δ_0

s/l interface

δ

$d\theta_1$

FIGURE A.2.3.

$\Delta F(T)_{tot}$

T_1

$T_2 > T_1$

δ_0

$T_3 > T_2$

T_{SK}

$T < T_{SK}$
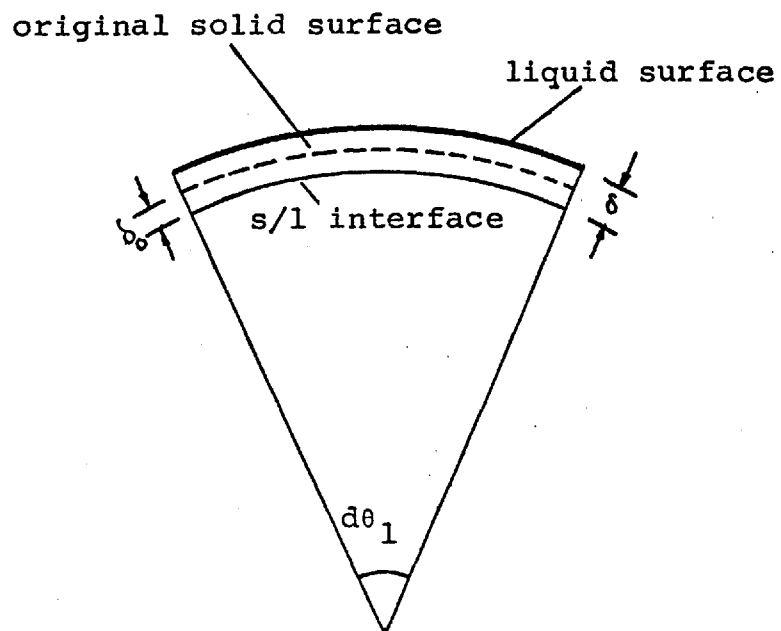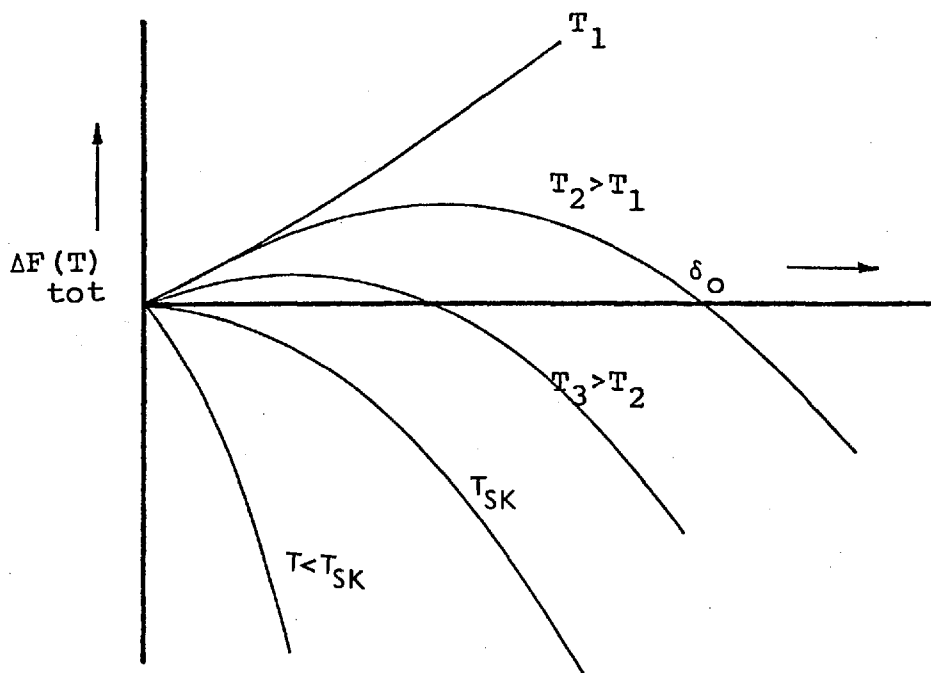
FIGURE A.2.4.

A.3.   THE STRUCTURE OF TIN AND BISMUTH.

A.3.1. The Structure of Tin.

Two different crystalline forms of tin are known:

(1) Gray or α-tin (Bijl and Kolkemeijer, 1918,1919.) has the diamond structure with unit cell of side

$$a = 6.491\text{Å}.$$

(2) White or β-tin (Wyckoff, 1963) has at room temperature (298K) a tetragonal structure with unit cell parameters

$$a = b = 5.819\text{Å}.$$
$$c = 3.174\text{Å}.$$

and four atoms at the positions.

$$000; \quad 0\tfrac{1}{2}\,\tfrac{1}{4}\,; \quad \tfrac{1}{2}\,0\,\tfrac{3}{4}\,; \quad \tfrac{1}{2}\,\tfrac{1}{2}\,\tfrac{1}{2}\,.$$

The unit cell is of such a shape that each atom is surrounded by a distorted tetrahedron of neighbours at a distance of 3.02Å. and by two more only slightly farther away at 3.17Å in the c-direction.

The temperature at which gray tin transforms to white tin is 286.2K (Hedges and Higgs, 1952). Above this temperature the white form is stable. In the present experiments, carried out at temperatures much higher than this temperature, the crystallites were found to posses the structure of white tin (see also Curzon, 1963.).

For white tin the intensities of diffraction are modified by the structure factor, S, given by,

$$S = \left[1+e^{\pi i(h+k+l)}\right]\left[1+e^{\pi i(k+\frac{1}{2})}\right] \qquad \text{(A.3.1.)}$$

where, h,k,l are the Miller indices of a lattice plane. An analysis of the diffraction obtained is given in table A.3.1. In this, the length of a vector in the reciprocal lattice (H_{hkl}) is calculated from the equation:

$$H^2_{hkl} = \frac{h^2+k^2}{a^2} + \frac{l^2}{c^2} \qquad \text{(A.3.2.)}$$

At the bulk melting point (505K), the density of solid white tin is 7.18 $gmcm^{-3}$, while that of the liquid is 6.98 $gm\ cm^{-3}$, so that on melting, the volume of the material increases by about 3%.

A.3.2. The Structure of Bismuth.

Bismuth is known to occur in eight solid phases (Strong, 1960). However, the only stable form of the material at normal pressures, has a structured rhombohedral unit cell, with two atoms per cell, and cell parameter (at 298K):

$$a = 4.746\overset{\circ}{A}. \qquad \text{(rhombohedral spacing)}$$
$$\alpha = 57^{\circ}14.5' \qquad \text{(rhombohedral angle)}$$

(see Wyckoff, 1963).

The two atoms per unit cell are situated at (uuu) and ($\bar{u}\bar{u}\bar{u}$), where

$$u = 0.237 \qquad \text{(at 298K)}.$$

h k l	$d_{hkl}(\text{Å})$	Intensity
200	2.91	S
101	2.78	S
220	2.06	S
211	2.01	S
301	1.66	W
112	1.48	S
400	1.46	S
321	1.43	S
420	1.30	S
312	1.20	S
.431 ⎱	1.09	W
501 ⎰		W
103	1.04	W
440	1.03	S

S = Strong according to structure factor.

W = Weak according to structure factor.

TABLE A.3.1.

Analysis of the diffraction pattern produced by
a thin film of tin.

This structure is, in fact, very close to a simple cubic structure, which has corresponding cell parameters of:

$$\alpha = 60^{\circ}$$
$$u = 0.25$$ (cubic lattice)

Because of this similarity with the simple cubic lattice, bismuth is often quoted as having a pseudo-cubic structure.

The structure may equally be represented as hexagonal with six atoms per unit cell and cell parameters (at 298K):

$$a' = 4.546\overset{\circ}{A}.\qquad \text{(hexagonal spacing)}$$
$$c' = 11.862\overset{\circ}{A}.$$

(see Barrett, 1960; also, Cucka and Barrett, 1962).

For thin films of bismuth, significant lattice spacing changes from the bulk value have been reported by a few workers; for example, Boswell (1951); Fujiki and Suganuma (1954); and more recently, Lisgarten et al (1974). The latter authors report a maximum decrease in a' of 0.8% and 1.3% for about 25$\overset{\circ}{A}$ thick bismuth films on carbon and formvar bases respectively. The corresponding changes in the values of c' were found to be 1-2% from the bulk value. For both substrates, however, the measured value of a' is reported to approach the bulk value for film thicknesses greater than about 100$\overset{\circ}{A}$.

The densities of solid and liquid bismuth at the bulk melting point (544K) are 9.67 gm cm^{-3} and

10.24 gm cm^{-3} respectively.   Thus when the material melts,

there is a <u>decrease</u> in volume of about 3% due to the very

open structure of the solid forming a more closely packed

liquid.

A.4.   PHYSICAL CONSTANTS OF TIN AND BISMUTH NEAR THE MELTING POINT.

(I)   TIN.

Bulk melting point	$T_o = 505K$
Density of solid	$\rho_s = 7.18$ gm cm^{-3}
Density of liquid	$\rho_\ell = 6.98$ gm cm^{-3}
Latent heat of fusion	$L = 5.8 \times 10^8$ erg gm^{-1}
Coefficient of expansion	$= 2.6 \times 10^{-5}$ K^{-1}
Young's modulus	$Y = 4 \times 10^{11}$ dynes cm^{-2}
Surface energy of liquid[1]	$\gamma_\ell = 552$ ergs cm^{-2}
Solid/liquid interfacial energy[2]	$\gamma_{s\ell} = 54.5$ ergs cm^{-2}

(II)   BISMUTH.

Bulk melting point	$T_o = 544K$
Density of solid	$\rho_s = 9.67$ gm cm^{-3}
Density of liquid	$\rho_\ell = 10.24$ gm cm^{-3}
Latent heat of fusion	$L = 4.3 \times 10^8$ erg gm^{-1}
Surface energy of liquid[1]	$\gamma_\ell = 380$ ergs cm^{-2}

(1) Lang   (1973).

(2) Turnbull (1950).

[From the maximum degree of supercooling of liquid droplets, a value for the solid/liquid interfacial energy ($\gamma_{s\ell}$) of bismuth of 58.0 ergs cm^{-2} may be inferred.   This has been used in section 8.2.   Although this value and the value for tin obtained similarly by Turnbull (1950), probably represent a lower limit of the interfacial energy, rather than the actual value.   (See section 8.3.)]

REFERENCES

Ainslie, N.G., MacKenzie, J.D. and Turnbull, D. (1961). J. Phys. Chem., 65, 1718.

Barrett, C.S. (1960). Austral. J. Phys., 13, 209.

Bijl, A.J., and Kolkemeijer, N.H. (1918). Chem.Weekblad, 15, 1264.

Bijl, A.J., and Kolkemeijer, N.H. (1919). Proc. Acad. Sci. Amsterdam, 21, 405.

Bijl, A.J., and Kolkemeijer, N.H. (1919). Proc. Acad. Sci. Amsterdam, 21, 501.

Blackman, M., and Curzon, A.E. (1959). "Structure and Properties of Thin Films". p.217. (Editors: Neugebauer, C., Newkirk, J.B., and Vermilyea, D.A., Wiley & Sons.).

Blackman, M., Peppiatt, S.J., and Sambles, J.R. (1972). Nature, 239, 61.

Blackman, M., Lisgarten, N.D., Peppiatt, S.J., and Rahman, M.S. (1975). Nature, 258, 139.

Block, R., Brings, Th., and Werner Kuhn. (1931). Z. Phys. Chem., B12, 415.

Boiko, B.T., Pugachev, A.T., and Bratsykhin, V.M., (1969). Sov. Phys. Sol. Stat., 10, 2832.

Boswell, F.W.C., (1951). Proc. Phys. Soc., A 64, 465.

Burton, W., Cabrera, N., and Frank, F.C. (1951). Phil. Trans. Roy. Soc. London, A 243, 299.

Christian, J.W., "The Theory of Transformations of Metals and Alloys". (1965). (Oxford: Pergamon).

Coombes, C.J., (1969). Ph.D. Thesis, London University.

Coombes, C.J. (1972). J. Phys. F: Metal Physics, 2, 44.

REFERENCES (contd,)

Coopersmith, B., Curzon, A.E., Kimoto, K., and Lisgarten, N.D. (1966). "Basic Problems in Thin Film Physics". p83. (Editors: Niedermayer, R. and Mayer, H.).

Cormia, R.L., MacKenzie, J.D., and Turnbull, D. (1963). J. Appl. Phys., 34, 2239.

Cotterill, R.M.J., and Pederson, L.B., (1972). Sol. Stat. Commun., 10, 439.

Cucka, P., and Barrett, C.S. (1962). Acta. Cryst., 15, 865.

Curzon, A.E. (1960). Ph.D. Thesis, London University.

Ennos, A.E. (1954). Brit. J. Appl. Phys., 5, 27.

Fisher, J.H. (1967). M.Sc. Thesis, London University.

Fisher, J.H., and Anderson, J.C. (1968). Thin Solid Films, 2, 119.

Fujiki, Y., and Suganuma, R. (1953). J. Phys. Soc. Japan, 8, 427.

Fujiki, Y., and Suganuma, R. (1954). J. Phys. Soc. Japan, 9, 144.

Gale, B., and Hale, K.F. (1961). Brit.J. Appl. Phys., 12,115.

Gladkich, N.J., Niedermayer, R., and Splegel, K. (1966). Phys. Stat. Sol, 15, 181.

Goodman, R.M., and Somorjai, G.A. (1970). J. Chem. Phys. 52, 6325.

Greenhill, E.B., and McDonald, S.R., (1953). Nature, 171, 37.

Hall, C.F. (1966), "Introduction to Electron Microscopy". p347. (New York: McGraw Hill).

Hanszen, K-J., (1960). Zeitschrift fur Physik, 157, 523.

Hanszen, K-J, (1696). 6th.Int.Congrs. for El.Micr., Kyoto,527.

REFERENCES (contd.)

Hedges, E.S. and Higgs, J.Y., (1952). Nature, 169, 621.

Henrion, J. and Rhead, G.E. (1972), Surf. Sci., 29, 20.

Herring, C. (1950). "Surface Tension as a Motivation for Sintering" in "The Physics of Powder Metallurgy" (Editor: Kingston, W.E.). (New York: McGraw Hill).

Herring, C. (1952). "The use of Macroscopic Concepts in Surface Energy Problems" in "Structure and Properties of Solid Surfaces" (Editors: Gomer, R., and Smith, C.) (Univ. of Chicago Press).

Hollomon, J.H. and Turnbull, D. (1950). "The Solidification of Metals and Alloys: Symposium". Am. Inst. Mining Met. Engnrs.

Jenkins, R.D. (1935). Proc. Roy.Sco. (London), 47, 109.

Jensen, E.J., Kristensen, W.D., and Cotterill, R.M.J. (1973). Phil.Mag., 27, 623.

Jones, D.R.H. (1974). J. Mat. Sci., 9, 1.

Khaikin, S. and Benet, N. (1939). Comptes Rendus (Doklady) de l'Academie des Sciences de l'URSS, 23, 31.

Kuhlmann-Wilsdorf, D. (1965). Phys.Rev., 140A, 1599.

Kuhns, I.E. and Mason, B.J. (1968). Proc.Roy. Soc. (London), A 302, 437.

Kürster, F.W. (1906). Lehrf. d. allg. phys. u.theorch.Chem., p189.

Lang, G. (1973). J. Inst. Metals., 101, 300.

Lennard-Jones, J.E. and Devonshire, A.F. (1939). Proc. Roy.Soc. (London), A 169, 317.

Lindemann, F.A. (1910). Phys. Z., 11, 609,

Lisgarten, N.D., Peppiatt, S.J., and Sambles, J.R. (1974). J. Phys. C: Solid State Physics, 7, 2263.

REFERENCES (contd.)

MyKura, H. (1955). Acta.Met., $\underline{3}$, 436.

Palatnik, L.S., and Komnik, Yu.F. (1960). Phys. Metal. Metalloved., $\underline{9}$, 48.

Pashley, D.W., Stowell, M.J., Jacobs, M.H., and Law, T.J. (1964). Phil. Mag., $\underline{10}$, 127.

Pashley, D.W., and Stowell, M.J. (1966). J.Vac. Sci.Technol., $\underline{3}$, 156.

Pavlovska, A., and Nenow, D. (1971). Surf. Sci., $\underline{27}$, 211.

Pawlow, P. (1908-9). Z.Phys. Chem., $\underline{65}$, 545.

Pawlow, P. (1909). Z. Phys. Chem., $\underline{65}$, 1.

Peppiatt, S.J. (1973). Ph.D. Thesis, London University.

Peppiatt, S.J., and Sambles, J.R. (1975). Proc. Roy.Soc. (London), $\underline{A}$ $\underline{345}$, 387.

Peppiatt, S.J. (1975). Proc.Roy.Soc. (London), $\underline{A}$ 345, 401.

Petrov, Yu. I. (1965), Sov.Phys. Sol.Stat., $\underline{6}$, 1701.

Pines, B. Ya., and Bublik, A.I. (1954). Zh.Tekh.Fiz., $\underline{24}$,1139.

Pocza, J.F., Barna, A., and Barna, P.B.(1969). J.Vac.Sci. Technol., $\underline{6}$, 472.

Poppa, H. (1965), J. Vac. Sci. Technol., $\underline{2}$, 42.

Pound, G.M., and La Mer, U.K. (1952). J. Am.Chem. Soc., $\underline{74}$, 2323.

Pound, G.M. (1958). "Liquid Metals and Solidifications". (Cleveland, Ohio: Am.Soc. for Metals).

Reiss, H., and Wilson, I.B. (1948). J.Coll. Sci., $\underline{3}$, 551.

Richter, H. (1943). Phys.Z., $\underline{44}$, 406.

Rie, E. (1923). Z. Phys. Chem., $\underline{104}$, 354.

Sambles, J.R. (1970). Ph.D. Thesis, London University.

REFERENCES (contd.)

Sambles, J.R. (1971). Proc. Roy. Soc. (London), A 324, 339.

Sambles, J.R. (1973). J. Phys.E: Scientific Instruments, 6, 127.

Sayama, Y. (1941), Proc.Phys.- Math. Soc. Japan, 23, 869.

Shebzukova, I.G., Khokonov, Kh.B., and Zadumkin, S.N. (1972). Fiz. Metal. Metalloved., 33, 206.

Skinner, L.M. (1969). J.Sci.Inst. (J.Phys.E), 2, 206.

Stark, J.P. (1965). Acta. Met., 13, 1181.

Stowell, M.J., Law, T.J., and Smart, J. (1970). Proc.Roy.Soc. (London), A 318, 231.

Stranski, I.N., Gans W., and Rau ,H., (1963). Ber. Bunserges. Physik Chem., 67, 965.

Strong, H.M. (1960). Am. Scientist, 48, 58.

Takagi, M. (1954), J.Phys. Soc. Japan, 9, 359.

Takahashi, T., and Tiller, W.A. (1969). Acta. Met., 17, 643.

Tamman, G. (1909-10), Z. Phys. Chem., 68, 257.

Tamman, G. (1925). "The States of Aggregation". (New York: D. Van Nostrand).

Thomson, J.J. (1888). "Application of Dynamics to Physics and Chemistry". (London: McMillan and Co.).

Turnbull, D., and Fisher, J.C. (1949). J. Chem. Phys., 17, 71.

Turnbull, D. (1950), J. Chem. Phys., 18, 198.

Turnbull, D. (1950). J. Appl. Phys., 21, 1022.

Turnbull, D. (1952). J. Chem. Phys., 20, 411.

Vladimirov, V.I. (1969). Sov. Phys. Sol.Stat., 10, 2077.

Volmer, M. (1925). Z. für Electrochemie, 35, 555.

Volmer, M., and Schmidt, O. (1937). Z. Phys. Chem., B 25, 467.

REFERENCES (contd.)

Wronski, C.R.M. (1963). Ph.D. Thesis, London University.

Wronski, C.R.M. (1967). Brit.J. Appl. Phys., $\underline{18}$, 1731.

Wyckoff, R.W.G. (1963). "Crystal Structures". Volume 1,
(2nd. edition; London, Interscience).

Zadumkin, S.N. (1959). Sov. Phys. Sol. State., $\underline{1}$, 573.

ACKNOWLEDGEMENTS